Machine learning-powered surrogate models for optimising island groundwater management: Striking a balance between cost, sustainability, and environmental impact

Weijiang Yu

A Publication format thesis submitted in partial fulfilment of the requirements for the degree of Doctor of Philosophy

Department of Civil and Structural Engineering
Faculty of Engineering
The University of Sheffield

September 2023

Declaration

I, Weijiang Yu, confirm that except where otherwise indicated, this thesis is my original work. I am aware of the University's Guidance on the Use of Unfair Means (www.sheffield.ac.uk/ssid/unfair-means), and I claim no conflicts of interest and have ensured that the research was conducted fairly and independently. This work has not previously been presented for an award at this, or any other, university.

Weijiang Yu

September 2023

Supervisors at The University of Sheffield:

Dr Domenico Baù - Department of Civil and Structural Engineering

Dr Georges Kesserwani - Department of Civil and Structural Engineering

Acknowledgements

I would like to extend my heartfelt gratitude to my primary supervisor, Dr Domenico Baù, for his unwavering guidance, mentorship, and invaluable assistance throughout my four-year PhD research. It is indisputable that without his profound expertise, generous support, and enduring patience, my research simply would not have been possible. His steadfast mentorship has not only been instrumental in the successful completion of my doctoral studies but has also served as a catalyst, igniting my enduring passion for the ongoing pursuit of research within hydrogeology and groundwater resources management.

To my second supervisor, Dr Georges Kesserwani, and the members of our seawater intrusion research group, namely Professor Alex S. Mayer (University of Texas at El Paso), Dr Yipeng Zhang (Oklahoma State University), Lauren Mancewicz (Michigan Technological University), and Dr Mohammadali Geranmehr, I warmly appreciate for your many constructive discussions and useful suggestions, which helped me address questions and challenges encountered in my research.

I would like to express my gratitude to Xitong Sun, Emma, Alovya Chowbury, Jiang Tian, Menlin Dai, Zhangjie Peng, and my office mates, both past and present, for contributing to the enriching and memorable experience of my research journey at the university. I am indebted to all the good friends I met in the Department of Civil and Structural Engineering at the University of Sheffield: Xitong Sun again, Dr Zhangjie Peng, Dr Menglin Dai, and Dr Shiyao Wang. All of you make my foreign life colourful.

My research is partially sponsored by the Grantham Centre for Sustainable Futures at the University of Sheffield. Herein, I am appreciative of the centre's support, which has enriched my scholarly journey through a myriad of beneficial training activities.

Special appreciation shows to my family members, my mom and grandmom, Meijuan Sun and Adi Liu, as well as my deceased dad, Guojian Yu, who have been a constant source of support and encouragement throughout my life, from my childhood to the present. I would like to deeply appreciate my wife, Junyu Zhou. I am fortunate to meet you and have accompanied each other over the past eleven years. Your companionship has enriched my life and enabled me to confront any challenges encountered in both life and research without trepidation. I also would like to thank my father-in-law and mother-in-law, Sen Zhou and Xiuhong Yu, for your warm care and support, particularly during the global pandemic of Covid-19. I dedicate this doctoral research to all of you.

Table of contents

Abstract

The strategy of coastal pumping optimisation is commonly used to address seawater intrusion (SWI), striking a balance between water demand and environmental protection. However, applying the popular tools, the simulation-optimisation (SO) method to solve the pumping optimisation problem formulated on a three-dimensional (3D) aquifer usually faces a computational burden, as 3D simulation models usually comprise numerous cells, causing each SWI simulation to be time-consuming. Even assisted by the surrogate-based SO (SSO) system where the SWI simulator is replaced by surrogate models during the optimisation, which has been validated more efficiently than the SO framework, solving a multi-objective groundwater management problem is still time-consuming when it comprises many decision variables. Therefore, this PhD research aims to develop a more efficient SSO framework for multi-objective groundwater management formulated on 3D coastal aquifers.

To achieve this aim, five objectives have been formed, including: 1) investigating the influence of pumping patterns on the SWI extent and groundwater supply cost; 2) exploring the efficient algorithm for offline training surrogate models; 3) exploring the efficient algorithm for online training surrogate models; 4) identifying the advantages, disadvantages of applying offline-trained and online-trained surrogate modes; 5) developing an efficient SSO framework for sustainable island groundwater management using a 3D island aquifer model based on the findings from the previous objectives. In this study, the SEAWAT model is used to simulate SWI under the pumping. The Gaussian Process (GP) modelling technique is adopted in this study to construct surrogate models, and the full enumeration method is applied to determine optimal solutions because of the inexpensiveness of the GP models.

Those research objectives have been tackled by conducting analyses through a two-objective groundwater management problem formulated on a simplified coastal aquifer created by hydrogeological conditions observed on San Salvador Island (Bahamas), minimizing groundwater supply cost and maximizing the volume of groundwater sent to the network. Key research findings indicate: 1) strengthening SWI constraints is prone to placing pumping wells closer to the shoreline or/and within deeper aquifers, leading to pumping saltier groundwater and thus enhancing the treatment cost; 2) introducing the iterative process can improve the efficiency in offline training GP models compared with the traditional offline training strategy, and the most appropriate algorithm is to select new points at each iteration by integrating information about their distances from known points and the gradients of estimates; 3) discretizing the objective space into equal sub-regions based on the obtained Pareto front and

then selecting sampling points within these sub-regions can facilitate the convergence of online-trained GP models. 4) given limitations on SWI, online-trained GP models can produce more reliable optimal pumping schemes with higher efficiency, but offline-trained GP models can offer reliable predictions across the entire input space, adaptive to variations in SWI constraint conditions. Therefore, this study develops an efficient SSO framework relying on the offline-trained GP models to investigate two-objective island groundwater management in 3D aquifers under various constraint scenarios. Results indicate the proposed SSO framework can efficiently provide trustable optimal pumping schemes.

Chapter 1

Introduction

1.1 Background of the research

1.1.1 Seawater intrusion (SWI) and its mitigation measures

In coastal aquifers bordering the sea, there exists a freshwater-saltwater interaction region where freshwater floats above saltwater due to the density difference (Coulon et al., 2022; Pinder and Cooper Jr, 1970; Qahman et al., 2005). This interaction region manifests in two structures: the saltwater wedge and the freshwater lens (Morgan and Werner, 2014; Vandenbohede et al., 2014). The former is common in regional coastal aquifers, where groundwater is recharged by precipitation and subsurface runoff, while the latter is typically found in small island aquifers, where precipitation serves as the sole source of freshwater recharge.

Figure 1.1 illustrates two types of subsurface freshwater-saltwater interaction structures. In both structures, the water table elevation gradually decreases toward the sea level as it approaches the shoreline. Due to the seaward hydraulic gradient, subsurface freshwater is driven to flow toward the sea. In natural circumstances, the interaction region formed by seaward-discharging freshwater and landward-moving seawater establishes a dynamic equilibrium.

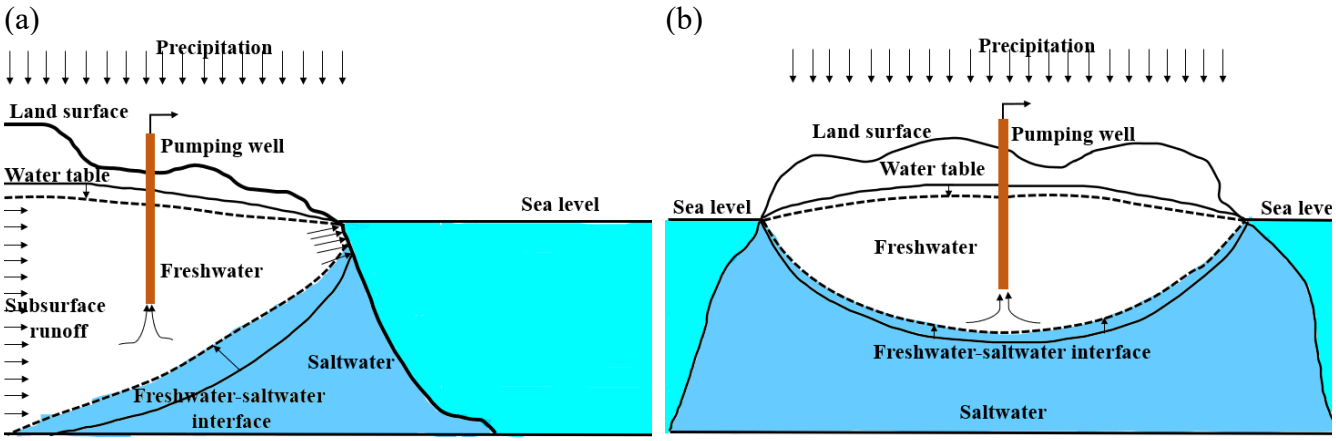

Figure 1.1. Schematic diagrams for the freshwater-saltwater interaction regions in the form of different shapes and their changes to the pumping: (a) saltwater wedge, (b) freshwater lens.

Coastal regions, hosting more than half of the world's population within 100 kilometres of a shoreline, are among the most densely populated areas globally (Kazakis et al., 2018; Tomaszkiewicz et al., 2014). In these regions, the high demand for water often compels local communities to turn to groundwater as a supplement to surface freshwater. However, when the

rate of abstraction surpasses the natural freshwater recharge, it leads to a decrease in water table elevation. Consequently, the seaward hydraulic gradient diminishes, resulting in a reduction of seaward-discharging freshwater and the encroachment of saltwater landward in aquifers, a phenomenon known as seawater intrusion (SWI).

Figure 1.1 visually depict the alterations in the water table and the freshwater-saltwater interface resulting from pumping in regional coastal aquifers and small-island aquifers, respectively. SWI elevates the salinity level of groundwater, posing a threat to the subsurface environmental system and directly jeopardizing access to subsurface freshwater for coastal communities (Jasechko et al., 2020; Agoubi, 2021). Notably, SWI presents a severe risk to the freshwater resources of islands. On small or very-low-elevation islands, the maximum thickness of the freshwater lens is typically only a few meters (Gingerich et al., 2017), so the freshwater body within the lens is highly sensitive to pumping activities and susceptible to pollution through SWI.

Additionally, the rise in sea levels due to global climate change, acknowledged by the Intergovernmental Panel on Climate Change (IPCC, 2023), further exacerbates SWI in coastal aquifers. The sea level increased by 3.7 mm per year between 2006 and 2018, with projections indicating an acceleration in the future. This phenomenon contributes to additional reductions in the seaward hydraulic gradient, compounding the challenges associated with SWI in coastal areas.

SWI has increasingly become a widespread environmental issue for most global coastal areas, and many SWI mitigation measures have been proposed. Popular ones include subsurface physical barriers, hydraulic barriers, and optimal management of groundwater pumping. Subsurface physical barriers are the impermeable or very-low-permeability walls constructed near the shoreline and orthogonally to the groundwater flow direction, retaining groundwater and blocking seawater landward movement, such as the semi-pervious full-section barrier (Sugio et al., 1987), cutoff wall (Luyun Jr et al., 2011), and subsurface dam (Luyun Jr et al., 2009). Hydraulic barriers are developed by recharging freshwater or/and extracting salt water near the coastlines to increase the seaward hydraulic gradient for repelling SWI, such as the recharging hydraulic barrier (Mahesha, 1996), saltwater abstraction barrier (Sowe et al., 2019), mixed-use of injection barrier and abstraction barrier (Abd-Elaty et al., 2020), and the abstraction-desalination-recharge method (Abd-Elhamid and Javadi, 2011).

Implementing subsurface physical and hydraulic barriers commonly encounters various challenges in practice. For example, both the cutoff wall and subsurface dam impose negligible impacts on repelling SWI in the coastal deep aquifers (Abd-Elaty and Zelenakova, 2022); both

semi-pervious full-section wall and subsurface dam require an impermeable aquifer bottom, otherwise, their effectiveness in SWI mitigation remarkably weakens (Zheng et al., 2020); subsurface physical barriers need high technically demanding excavation work and expensive construction costs (Strack et al., 2016). The efficiency of the recharge hydraulic barriers is limited by the initial saltwater wedge toe location (Mahesha, 1996; Luyun Jr et al., 2011); operating hydraulic barriers requires continuously injecting water and/or extracting saltwater, leading to huge operational and maintenance costs (Strack et al., 2016); recharging hydraulic barriers are not appropriate for the arid and hyper-arid coastal regions (Abd-Elaty et al., 2021).

Optimising coastal groundwater pumping aims to strike an acceptable balance between social development and environmental protection by adjusting pumping patterns, usually formulated by maximizing groundwater pumping rates with controlling SWI extent in a prescribed range. Compared with the subsurface physical and hydraulic barriers, the groundwater pumping optimisation strategy is easier to implement, not having as many application limitations, so it has increasingly attracted more attention and got widespread application in the field of coastal aquifer management (Christelis et al., 2019; Mostafaei-Avandari and Ketabchi, 2020; Yang et al., 2021).

1.1.2 Simulation-based optimisation (SO) framework for coastal groundwater management

Implementing a pumping optimization strategy to mitigate SWI logically comprises three stages: formulating the management problem; evaluating the aquifer response to various pumping patterns; and finally, selecting optimal pumping schemes based on the management problem and pumping evaluations. In coastal aquifer management, employing this stand-alone simulation approach is computationally infeasible, as there are typically an uncountable number of pump candidates, necessitating numerous calls to SWI simulators.

The SO framework, where SWI simulators are externally linked with an optimisation algorithm (OA), plays a pivotal role in efficiently deriving optimal pumping strategies (Christelis and Mantoglou, 2016; Kourakos and Mantoglou, 2015; Yang et al., 2018). The application of this framework typically involves a four-step process, stated as follow,

The first step is to formulate the pumping optimisation problem, encompassing the definition of management objective functions (OFs), constraint condition functions (CSs), decision variables (DVs), and state variables (SVs). Typically, the constrained management problem aims to maximize total pumping rates and minimize the economic costs of groundwater extraction, while simultaneously ensuring SWI remains within specified limits or restricting salt concentration near well sites. DVs are the pumping patterns, including well

locations, well-specific pumping rates, and the number of wells, while SVs are the response variables dependent on DVs, determined through the simulation model (SM). OFs and CSs are functions of DVs and/or SVs.

Secondly, the OA is employed to solve the optimisation problem, exploring the input variable space to identify multiple potentially optimal DVs.

Thirdly, the potentially optimal DVs searched by the OA are used as inputs for the SM, which produces corresponding SVs. These DVs and SVs form pairs of data that feed the OA.

Subsequently, guided by feedback from the simulation results, the OA decides how to adjust the DVs toward better solutions. Upon convergence, the OA returns a set of DVs, considered the optimal solutions to the management problem. The times of iterations between the SM and OA hinges on the selection and configuration of the OA, being either multiple or single. Figure 1.2 presents the flow chart for generally implementing the SO framework.

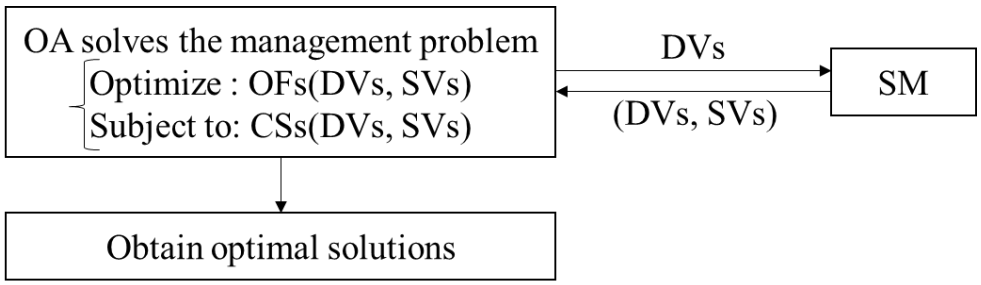

Figure 1.2. Flow chart for generally implementing the SO framework.

In coastal groundwater management, popular variable-density groundwater simulation models include SEAWAT (Kourakos and Mantoglou, 2013), SUTRA (Ketabchi and Ataie-Ashtiani, 2015), FEFLOW (Dokou and Karatzas, 2012; Karatzas, 2017) and HydroGeoSphere (Christelis et al., 2019). Compared with the approach of using stand-alone simulation, the SO method largely reduces the required number of SWI simulations during the optimisation, saving computational costs remarkably, and thus it has been successfully applied in many works of coastal aquifer management over the past decades, either single-objective (Mostafaei-Avandari and Ketabchi, 2020) or multi-objective (Yin et al., 2020) coastal groundwater management problems.

However, applying the SO method still possibly faces the computational burden as it involves repeated calls of expensive SWI simulations during the optimisation stage. In the study of Kourakos and Mantoglou (2015), the computing time required for the SO method to obtain optimal pumping patterns can be up to hundreds of hours, and in other cases, the SO method even needs to cost millions of hours to solve the management problem, regarded to be just theoretically feasible (Han et al., 2021; Yin et al., 2022). Various strategies have been implemented to allow the SO framework to be applicable to the study of coastal aquifer

management, such as adopting the analytical solution approach to simulate SWI (Ketabchi and Ataie-Ashtiani, 2015; Jamal et al., 2022), SWI simulation model developed based on the sharp-interface assumption (Coulon et al., 2022; Dey and Prakash, 2020), developing SWI simulation models with the coarse resolution (Ketabchi and Ataie-Ashtiani, 2015; Yang et al., 2021), using a simplified two-dimensional cross-section model rather than a complex three-dimensional model (Coulon et al., 2022; Javadi et al., 2015), or conducting the parallel computing strategy that uses multiple processors or computers working in parallel to simulate aquifer response under the pumping (Mostafaei-Avandari and Ketabchi, 2020; Yin et al., 2020). Overall, the effectiveness of these measures in cutting down computational costs can be attributed to approximating the physical process of SWI in coastal aquifers, sacrificing the simulation accuracy, or employing high-level computing equipment. Doing those either introduces higher uncertainties in derived optimal solutions or needs additional financial budgets to install a high-level computing system. Even taking these measures, the required time for applying the SO method is still long in some cases (Christelis et al., 2019; Dey and Prakash, 2020).

1.1.3 Surrogate-based simulation-optimisation (SSO) framework for coastal groundwater management

The computational burden associated with the SO method arises primarily from the repeated calls to expensive SWI simulations. An effective and reliable approach to alleviate runtime challenges is to implement data-driven surrogate models, replacing the time-intensive SWI simulations in the development of an SSO system.

Surrogate models are constructed by finite training data generated from the original simulators, offering statistically approximated relationships between DVs and SVs. Once the surrogate models are trained, they serve as substitutes for SWI simulation models in predicting SVs based on given DVs. This predictive capability is then integrated with the OA to determine the optimal pumping schemes. By employing surrogate models, the SSO system significantly reduces the need for computationally expensive SWI simulations, thus enhancing computational efficiency during the optimization process. In the SSO system, surrogate models are trained specifically to predict SVs, such as pumped groundwater concentration and hydraulic head at the pumping well (Fan et al., 2020; Ranjbar and Mahjouri, 2020). These predicted SVs are then utilized for calculating management objectives and constraint values.

Assisted by the SSO approach, the computational costs required for identifying optimal solutions are substantially lower compared to those incurred by the SO method. In certain instances, the runtime savings achieved through the SSO method can approach nearly 100% (Al-Maktoumi et al., 2021; Fan et al., 2020; Rajabi and Ketabchi, 2017; Ranjbar and Mahjouri,

2020; Yin et al., 2022), highlighting its significant advantage in computing efficiency. The performance of surrogate models in providing accurate and reliable estimates of SWI extent based on the pumping pattern also has been validated through various evaluation indexes (Fan et al., 2020; Yin et al., 2022).

Furthermore, in comparison with publications employing the SO method, where the number of DVs is typically less than ten (Kourakos and Mantoglou, 2013; Ketabchi and Ataie-Ashtiani, 2015), the SSO method involves a larger number of DVs, with some studies incorporating dozens of them (Fan et al., 2020; Roy and Datta, 2017; Lal and Datta, 2021). This indicates that the SSO method can be effectively applied to higher-dimensional groundwater pumping optimization problems, thereby producing more detailed and comprehensive management strategies.

Motivated by its exceptional performance in terms of computing efficiency, accuracy, and applicability to high-dimensional management problems, the SSO method has seen increasing adoption in coastal groundwater management. This application allows for achieving a balance between controlling Saltwater Intrusion (SWI) and meeting local water demand (Al-Maktoumi et al., 2021; Han et al., 2021; Lal and Datta, 2021; Yin et al., 2022).

The typical ways to create surrogate models are either offline or online training. Offline-trained surrogate models are devoted to ensuring that estimates of surrogate models are characterized with global accuracy over the entire input space. They complete the development based on simulation data before the optimisation procedure, totally substituting the expensive SWI simulators to link with the optimisation approach in the subsequent optimisation stage. Online-trained surrogate models aim to quickly identify locally optimal solutions with low computational costs (Papadopoulou et al., 2010). Online training surrogate models is an iterative process, where surrogate models built by initial training samples immediately link with the optimisation approach to search for the optimal solutions and then the obtained potentially optimal points are added into the training data set for updating the surrogate models, repeating the previous step until there are no further changes in the optimal solutions.

Figure 1.3 illustrates two flow charts for implementing the SSO framework, respectively for applying offline-trained and online-trained surrogate models. In Figure 1.3, both two types of surrogate models are trained to predict SVs given DVs.

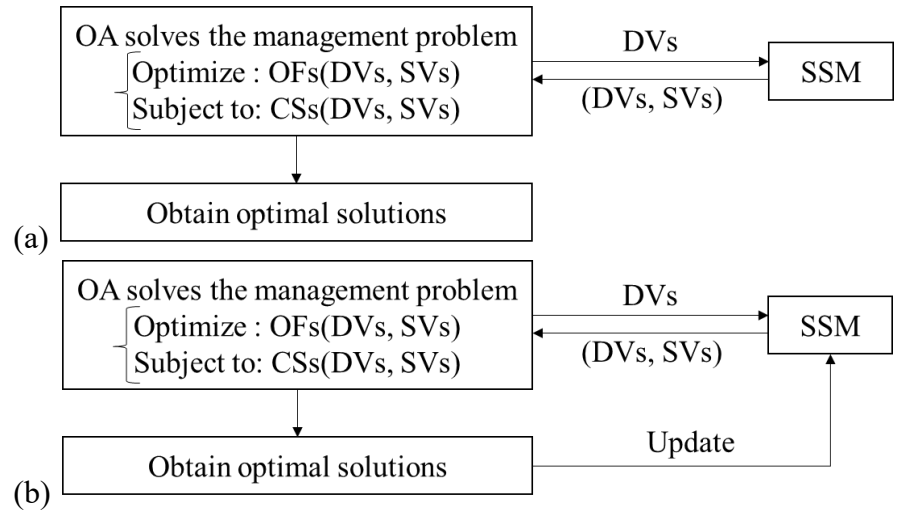

Figure 1.3. Flow charts for implementing the SSO framework with different types of surrogate models, (a) offline-trained surrogate models and (b) online-trained surrogate models. SSM represents the surrogate models built by simulation data.

Traditionally, offline training surrogate models depend on fitting a set of training samples at one time, and to ensure the global accuracy of surrogate model estimates, these training points cover the entire input space either uniformly or randomly (Fan et al., 2020; Han et al., 2021). However, since groundwater management objectives and SWI constraints are nonlinear, this traditional training approach can prove inefficient due to the potential oversampling of low-gradient areas and under-sampling of high-gradient areas. Therefore, to acquire reliable model estimates, surrogate models built by traditional offline training tend to consume more training samples than necessary, causing a certain proportion of the computational costs to be wasted. In the studies of Rajabi and Ketabchi (2017), Ranjbar and Mahjouri (2020) and Al-Maktoumi et al. (2021), offline-trained surrogate models consumed training samples that are hundreds of times the number of DVs, indicating that there is a need to design an efficient algorithm for offline training surrogate models in coastal groundwater management.

For online training, new training point identification at each iteration must indeed affect the efficiency and accuracy of the online-trained surrogates. Commonly, identified optimal solutions at each iteration serve as the new training points. That is applicable to single-objective management problems but not well-suited for multi-objective problems, where the potential optimal pumping patterns form a set of points rather than a single solution in single-objective problems. In this case, applying the traditional way to build an online-trained surrogate model needs to sample multiple points at each iteration and ultimately consumes a larger number of training samples than expected. For example, Yu et al. (2021) employed the online-trained SSO method to tackle a three-objective pumping optimisation problem in an Australian coastal area. Their surrogate models converged after two updates, but each update required the utilization

of 1,000 training samples, finally consuming a total of 3,540 training samples for addressing this eight-input-variable management problem. This highlights the necessity for proposing an efficient algorithm to develop online-trained surrogate models for addressing multi-dimensional coastal groundwater management problems.

Both offline and online-trained surrogate models bring about substantial improvements in computing efficiency because of utilizing finite training data from full-scale models, but that inevitably introduces uncertainty into the surrogate model predictions in turn (Sreekanth and Datta, 2010; Yin et al., 2022). The widely accepted way to deal with this challenge in coastal groundwater management is to adopt the strategy of using the ensemble of surrogate models.

In the ensemble approach, final predictions in SWI extent under the pumping are obtained by integrating estimates of multiple surrogate models, and the estimates of these surrogate models can be harnessed through weighted averaging (Han et al., 2020). The surrogate models involved in the ensemble approach can be either the diverse types of surrogate functions (Christelis et al., 2019; Yin et al., 2022) or a single surrogate function built multiple times using different realizations of training data (Sreekanth and Datta, 2010). Undoubtedly, building an ensemble of surrogate models, whether by training a single surrogate model using multiple groups of training samples or incorporating different types of surrogate models, inevitably increases the computational budget.

Overall, applying surrogate models in coastal groundwater management is confronted with three challenges at present, including 1) how to efficiently build surrogate models by offline training, 2) how to efficiently select new training points at each iteration when developing online-trained surrogate models to deal with multi-objective management problems, 3) how to efficiently quantify the uncertainties in derived optimal pumping solutions. To the best knowledge of the author, these challenges attract less attention and have not yet been resolved in coastal groundwater management.

1.2 Research aim and objectives

Given the research gaps mentioned in Section 1.1, this PhD research aims to explore the efficient approaches for offline and online training surrogate models to substitute computationally expensive SWI simulators in multi-objective island groundwater management. In this research, an assumed homogeneous island aquifer is developed based on hydrogeological conditions observed on San Salvador Island (Bahamas) (Gulley et al., 2016), and the SEAWAT model is applied to simulate the SWI process in the aquifer under the pumping, generating training data. Gaussian process (GP) modelling technique is adopted to

construct surrogate models for the management objective and constraint functions instead of surrogates for SWI simulators to predict SVs based on DVs. In the SSO framework developed in this study, GP models predict management objectives and constraint values for any pumping pattern, alongside quantifying associated uncertainties, while the full enumeration approach serves as the search method, identifying optimal pumping schemes. With this purpose in mind, the following research objectives have been formed to support the achievement of the aim of this research,

O1: To formulate a two-objective pumping optimisation problem, striking a balance between cost, sustainability, and environmental impact, and develop a preliminary insight into the effects of pumping patterns, and choice of SWI constraint conditions on optimal operation cost of abstracting groundwater using a 2D model.

O2: To assess the performance of proposed offline training algorithms relative to traditional offline training strategy and identify the most appropriate algorithm for offline training GP models in the two-objective coastal groundwater management using a 2D model.

O3: To assess the performance of proposed online training algorithms and identify the most efficient approaches for online training GP models in the two-objective coastal groundwater management using a 2D model.

O4: To evaluate the advantages and disadvantages of employing offline and online-trained GP models in the realm of multi-objective coastal groundwater management according to the findings from the research objectives O2 and O3.

O5: Based on the findings from O4, develop an efficient SSO framework for sustainable island groundwater management using a 3D island aquifer model, and analyse the sensitivity of optimal pumping schemes to the changes in constraint conditions.

1.3 Research questions

In line with the research aim and objectives, the crucial research questions guiding the investigation of the SSO framework in multi-objective coastal groundwater management are formulated as follows,

Q1: How do efficiently choose training samples for offline training GP models?

Q2: How do efficiently identify new training points at each iteration to update online-trained GP models?

Q3: How do ensure the GP model predictions align with the realistic, such as not producing negative economic cost estimates?

Q4: How do efficiently quantify the uncertainties in optimal pumping schemes given by the SSO method?

Q5: How do effectively evaluate the performance of surrogate models built by different training algorithms in producing reliable and accurate optimal solutions?

1.4 Thesis structure

This study is presented as a thesis in the publication format. Following the Code of Practice of The University of Sheffield, this thesis format includes submitted work and unpublished work formatted with the intention or possibility of publication. Herein, there are three publications presented across the three chapters. The last chapter of the thesis summarizes the findings obtained from this PhD research and highlights the overall contribution to knowledge. A brief description of each chapter is presented in the following.

Chapter 1: Introduction.

This chapter introduces the gaps in knowledge that shaped this research. It states the research aim and objectives and outlines how this thesis is organized in the publication format.

Chapter 2: Investigating the impact of SWI on the operation cost of groundwater supply in island aquifers.

This chapter gives the mathematical expressions for calculating the groundwater supply operation cost associated with groundwater pumping and desalination treatment and develops an insight into the effects of pumping patterns on the operation cost and SWI extent using a simplified 2D aquifer model. This chapter also assesses the interplay between optimal management costs and the choice of constraints on SWI.

Box 1. Details of publication in Chapter 2

Yu, W., Baù, D., Mayer, A.S., Mancewicz, L. and Geranmehr, M. Investigating the impact of seawater intrusion on the operation cost of groundwater supply in island aquifers.

Status: Accepted by Water Resources Research.

Acknowledgement of contribution: Weijiang Yu is the first author of this publication, and led the model conceptualisation, simulation, data analysis, manuscript writing and editing. Baù provided the overall supervision, checked the methodology, and supported manuscript proofreading. Mayer, Mancewicz, and Geranmehr provided supervision.

Chapter 3: Efficient approaches for offline and online training of GP models in multi-objective island groundwater management.

This chapter first formulates a two-objective pumping optimisation problem in a simplified 2D island aquifer model and then proposes three offline training strategies and four

online training strategies for building GP models to solve the optimisation problem, respectively. By conducting repeated Monte Carlo simulations using these GP models, it becomes possible to ascertain the probability of Pareto-optimality for each pumping scheme. Performance assessment of each training strategy involves determining the average probability of Pareto-optimality and evaluating the correlation between predictions. Based on the evaluation results, this chapter identifies the most efficient approaches for offline and online training GP models in multi-objective groundwater management, respectively, and demonstrates the advantages and disadvantages of employing offline and online-trained surrogate models in the realm of coastal groundwater management.

Box 2. Details of publication in Chapter 3

Yu, W., Baù, D., Mayer, A.S. and Geranmehr, M. Efficient approaches for offline and online training of GP models in multi-objective island groundwater management.

Status: Manuscript intended for publication.

Acknowledgement of contribution: Weijiang Yu is the first author of this publication, and led the model conceptualisation, simulation and optimisation, data analysis, manuscript writing and editing. Baù provided the overall supervision, checked the methodology, and supported manuscript proofreading. Mayer and Geranmehr provided supervision.

Chapter 4: Applying an efficient surrogate-based multi-objective optimisation framework for sustainable island groundwater management.

This chapter applies the efficient approach for offline training GP models, which is identified in Chapter 3, to solve the formulated two-objective island groundwater management in the 3D aquifer model. Moreover, this chapter analyses the effects of changing SWI constraint conditions on optimal pumping schemes.

Box 3. Details of publication in Chapter 4

Yu, W., Baù, D., Mayer, A.S. and Geranmehr, M. Applying an efficient surrogate-based multi-objective optimisation framework for sustainable island groundwater management.

Status: Manuscript intended for publication.

Acknowledgement of contribution: Weijiang Yu is the first author of this publication, and led the model conceptualisation, simulation and optimisation, data analysis, manuscript writing and editing. Baù provided the overall supervision, checked the methodology, and supported manuscript proofreading. Mayer and Geranmehr provided supervision.

Chapter 5: Discussion and Conclusion

This chapter integrates the research findings and elaborates on the contribution to knowledge and significance of the research. This chapter ends with offering suggestions for future research.

Pagination

Due to the nature of this thesis, a pagination structure has been used and is reflected in the table of contents. It consists of the chapter number followed by a period and the page number within that chapter. It can be found at the bottom right of each page. For example, page 1.5 represents the 5th page with the 1st chapter.

1.5 References

Pinder, G.F., Cooper Jr, H.H. (1970). A numerical technique for calculating the transient position of the saltwater front. *W*ater *R*esources *R*esearch, *6*(3), 875-882. https://doi.org/10.1029/WR006i003p00875

Kishi, Y., Fukuo, Y. (1977). Studies on salinization of groundwater, I: Theoretical consideration on the three-dimensional movement of the salt water interface caused by the pumpage of confined groundwater in fan-shaped alluvium. *Journal of Hydrology*, *35*(1), 1-29. https://doi.org/10.1016/0022-1694(77)90074-9

Sugio, S., Nakada, K., Urish, D.W. (1987). Subsurface seawater intrusion barrier analysis. *J*ournal of *H*ydraulic *E*ngineering, *113*(6), 767-779. https://doi.org/10.1061/(ASCE)0733-9429(1987)113:6(767)

Mahesha, A. (1996). Steady-state effect of freshwater injection on seawater intrusion. *Journal of Irrigation and Drainage Engineering*, *122*(3), 149–154. https://doi.org/10.1061/(ASCE)0733-9437(1996)122:3(149)

Qahman, K., Larabi, A., Ouazar, D., Naji, A., Cheng, A.H.-D. (2005). Optimal and sustainable extraction of groundwater in coastal aquifers. *Stochastic Environmental Research and Risk Assessment*, *19*, 99–110. https://doi.org/10.1007/s00477-004-0218-0

Luyun Jr, R., Momii, K., Nakagawa, K. (2009). Laboratory-scale saltwater behavior due to subsurface cutoff wall. *Journal of Hydrology*, *377*(3-4), 227-236. https://doi.org/10.1016/j.jhydrol.2009.08.019

Papadopoulou, M.P., Nikolos, I.K., Karatzas, G.P. (2010). Computational benefits using artificial intelligent methodologies for the solution of an environmental design problem: saltwater intrusion', *W*ater *S*cience & *T*echnology, *62*(7), 1479–1490. https://doi.org/10.2166/wst.2010.442

Sreekanth, J., Datta, B. (2010). Multi-objective management of saltwater intrusion in coastal aquifers using genetic programming and modular neural network based surrogate models. *J*ournal *of H*ydrology, 393(3-4), 245-256. https://doi.org/10.1016/j.jhydrol.2010.08.023

Abd-Elhamid, H.F., Javadi, A.A. (2011). A cost-effective method to control seawater intrusion in coastal aquifers. *W*ater *R*esources *M*anagement, *25*, 2755–2780. https://doi.org/10.1007/s11269-011-9837-7

Luyun Jr, R., Momii, K., Nakagawa, K. (2011). Effects of recharge wells and flow barriers on seawater intrusion. *Groundwater*, *49*(2), 239-249. https://doi.org/10.1111/j.1745-6584.2010.00719.x

Dokou, Z., & Karatzas, G. P. (2012). Saltwater intrusion estimation in a karstified coastal system using density-dependent modelling and comparison with the sharp-interface

approach. *Hydrological Sciences Journal*, *57*(5), 985-999. https://doi.org/10.1080/02626667.2012.690070

Kourakos, G., Mantoglou, A. (2013). Development of a multi-objective optimisation algorithm using surrogate models for coastal aquifer management. *J*ournal of *H*ydrology, *479*, 13–23. http://dx.doi.org/10.1016/j.jhydrol.2012.10.050

Morgan, L. K., Werner, A. D. (2014). Seawater intrusion vulnerability indicators for freshwater lenses in strip islands. *Journal of Hydrology*, *508*, 322-327. https://doi.org/10.1016/j.jhydrol.2013.11.002

Tomaszkiewicz, M., Abou Najm, M., El-Fadel, M. (2014). Development of a groundwater quality index for seawater intrusion in coastal aquifers. *Environmental Modelling & Software*, *57*, 13-26. https://doi.org/10.1016/j.envsoft.2014.03.010

Vandenbohede, A., Mollema, P. N., Greggio, N., & Antonellini, M. (2014). Seasonal dynamic of a shallow freshwater lens due to irrigation in the coastal plain of Ravenna, Italy. *Hydrogeology Journal*, *22*, 893–909. https://doi.org/10.1007/s10040-014-1099-z

Javadi, A., Hussain, M., Sherif, M., Farmani, R. (2015). Multi-objective optimisation of different management scenarios to control seawater intrusion in coastal aquifers. *W*ater *R*esources *M*anagement, *29*, 1843–1857. https://doi.org/10.1007/s11269-015-0914-1

Ketabchi, H., Ataie-Ashtiani B. (2015). Evolutionary algorithms for the optimal management of coastal groundwater: A comparative study toward future challenges. *J*ournal of *H*ydrology, *520*, 193-213. https://doi.org/10.1016/j.jhydrol.2014.11.043

Kourakos, G., Mantoglou, A. (2015). An efficient simulation-optimisation coupling for management of coastal aquifers. *H*ydrogeology *J*ournal, *23*, 1167–1179. https://doi.org/10.1007/s10040-015-1293-7

Christelis, V., Mantoglou, A. (2016). Coastal aquifer management based on the joint use of density-dependent and sharp interface models. *W*ater *R*esources *M*anagement, *30*, 861–876. https://doi.org/10.1007/s11269-015-1195-4

Strack, O.D.L., Stoeckl, L., Damm, K., Houben, G., Ausk, B.K., de Lange, W.J. (2016). Reduction of saltwater intrusion by modifying hydraulic conductivity. *W*ater *R*esources *R*esearch, *52*(9), 6978-6988. https://doi.org/10.1002/2016WR019037

Gingerich, S. B., Voss, C. I., Johnson, A. G. (2017). Seawater-flooding events and impact on freshwater lenses of low-lying islands: Controlling factors, basic management and mitigation. *Journal of Hydrology*, *551*, 676–688. https://doi.org/10.1016/j.jhydrol.2017.03.001

Karatzas, G. P. (2017). Developments on modeling of groundwater flow and contaminant transport. *Water Resources Management*, *31*, 3235–3244. https://doi.org/10.1007/s11269-017-1729-z

Rajabi, M.M., Ketabchi, H. (2017). Uncertainty-based simulation-optimisation using Gaussian process emulation: Application to coastal groundwater management. *J*ournal *of H*ydrology, 555, 518-534. https://doi.org/10.1016/j.jhydrol.2017.10.041

Roy, D.K., Datta, B. (2017). A surrogate based multi-objective management model to control saltwater intrusion in multilayered coastal aquifer systems. *C*ivil *E*ngineering and *E*nvironmental *S*ystems, *34*(3-4), 238-263. https://doi.org/10.1080/10286608.2018.1431777

Kazakis, N., Spiliotis, M., Voudouris, K., Pliakas, F. K., Papadopoulos, B. (2018). A fuzzy multicriteria categorization of the GALDIT method to assess seawater intrusion vulnerability of coastal aquifers. *Science of the Total Environment*, *621*, 524–534. https://doi.org/10.1016/j.scitotenv.2017.11.235

Yang, Y., Wu, J., Lin, J., Wang, J., Zhou, Z., Wu, J. (2018). An efficient simulation–optimisation approach for controlling seawater intrusion. *J*ournal of *C*oastal *R*esearch, *84*(10084), 10–18. https://doi.org/10.2112/SI84-002.1

Christelis, V., Kopsiaftis, G., Mantoglou, A. (2019). Performance comparison of multiple and single surrogate models for pumping optimisation of coastal aquifers. *H*ydrological *S*ciences *J*ournal, *64*(3), 336–349. https://doi.org/10.1080/02626667.2019.1584400

Sowe, M.A., Sadhasivam, S., Mohamed, M.M., Mohsen, S. (2019). Modeling the mitigation of seawater intrusion by pumping of brackish water from the coastal aquifer of Wadi Ham, UAE. *S*ustainable *W*ater *R*esources *M*anagement, *5*, 1435–1451. https://doi.org/10.1007/s40899-018-0271-3

Abd-Elaty, I., Abd-Elhamid, H.F., Qahman, K. (2020). Coastal aquifer protection from saltwater intrusion using abstraction of brackish water and recharge of treated wastewater: case study of the Gaza aquifer. *J*ournal of *H*ydrologic *E*ngineering, *25*(7), 05020012. https://doi.org/10.1061/(ASCE)HE.1943-5584.0001927

Dey, S., Prakash, O. (2020). Managing saltwater intrusion using conjugate sharp interface and density dependent models linked with pumping optimisation. *G*roundwater for *S*ustainable *D*evelopment, *11*, 100446. https://doi.org/10.1016/j.gsd.2020.100446

Fan, Y., Lu, W., Miao, T., Li, J., Lin, J. (2020). Multiobjective optimisation of the groundwater exploitation layout in coastal areas based on multiple surrogate models. *E*nvironmental *S*cience and *P*ollution *R*esearch, *27*, 19561–19576. https://doi.org/10.1007/s11356-020-08367-2

Han, Z., Lu, W., Fan, Y., Lin, J., Yuan, Q. (2020). A surrogate-based simulation–optimisation approach for coastal aquifer management. *W*ater *S*upply. *20*(8), 3404–3418. https://doi.org/10.2166/ws.2020.259

Jasechko, S., Perrone, D., Seybold, H., Fan, Y., Kirchner, J. W. (2020). Groundwater level observations in 250,000 coastal US wells reveal scope of potential seawater intrusion. *Nature Communications*, *11*, 3229. https://doi.org/10.1038/s41467-020-17038-2

Mostafaei-Avandari, M., Ketabchi, H. (2020). Coastal groundwater management by an uncertainty-based parallel decision model. *Journal of Water Resources Planning and Management*, *146*(6), 04020036. https://doi.org/10.1061/(ASCE)WR.1943-5452.0001227

Ranjbar, A., Mahjouri, N. (2020). Multi-objective freshwater management in coastal aquifers under uncertainty in hydraulic parameters. *N*atural *R*esources *R*esearch, *29*(4), 2347–2368. https://doi.org/10.1007/s11053-019-09585-3

Roy, D.K., Datta, B. (2020). Modelling and management of saltwater intrusion in a coastal aquifer system: A regional-scale study. *Groundwater for Sustainable Development*, *11*, 100479. https://doi.org/10.1016/j.gsd.2020.100479

Yin, J., Pham, H.V., Tsai, F.T.C. (2020). Multiobjective spatial pumping optimisation for groundwater management in a multiaquifer system. *J*ournal of *W*ater *R*esources *P*lanning and *M*anagement, *146*(4), 04020013. https://doi.org/10.1061/(ASCE)WR.1943-5452.0001180

Zheng, T., Zheng, X., Sun, Q., Wang, L., Walther, M. (2020). Insights of variable permeability full-section wall for enhanced control of seawater intrusion and nitrate contamination in unconfined aquifers. *J*ournal of *H*ydrology, *586*, 124831. https://doi.org/10.1016/j.jhydrol.2020.124831

Abd-Elaty, I., Straface, S., Kuriqi, A. (2021). Sustainable saltwater intrusion management in coastal aquifers under climatic changes for humid and hyper-arid regions. *E*cological *E*ngineering, *171*, 106382. https://doi.org/10.1016/j.ecoleng.2021.106382

Agoubi, B. (2021). A review: saltwater intrusion in North Africa's coastal areas-current state and future challenges. *Environmental Science and Pollution Research*, *8*(14), 17029-17043. https://doi.org/10.1007/s11356-021-12741-z.

Al-Maktoumi, A., Rajabi, M.M., Zekri, S., Triki, C. (2021). A probabilistic multiperiod simulation–optimisation approach for dynamic coastal aquifer management. *W*ater *R*esources *M*anagement, *35*, 3447–3462. https://doi.org/10.1007/s11269-021-02828-0

Han, Z., Lu, W., Fan, Y., Xu, J., Lin, J. (2021). Surrogate-based stochastic multiobjective optimisation for coastal aquifer management under parameter uncertainty. *W*ater *R*esources *M*anagement, *35*, 1479–1497. https://doi.org/10.1007/s11269-021-02796-5

Lal, A., Datta, B. (2021). Optimal pumping strategies for the management of coastal groundwater resources: application of Gaussian Process Regression metamodel-based simulation-optimisation methodology. *ISH J*ournal *of H*ydraulic *E*ngineering, *27*(sup1), 136-145. https://doi.org/10.1080/09715010.2019.1599304

Yang, Y., Song, J., Simmons, C.T., Ataie-Ashtiani, B., Wu, J., Wang, J., Wu, J. (2021). A conjunctive management framework for the optimal design of pumping and injection strategies to mitigate seawater intrusion. *J*ournal of *E*nvironmental *M*anagement, *282*, 111964. https://doi.org/10.1016/j.jenvman.2021.111964

Yu, X., Sreekanth, J., Cui, T., Pickett, T., Xin, P. (2021). Adaptative DNN emulator-enabled multi-objective optimisation to manage aquifer− sea flux interactions in a regional coastal aquifer. *A*gricultural *W*ater *M*anagement, *245*, 106571. https://doi.org/10.1016/j.agwat.2020.106571

Abd-Elaty, I., Zelenakova, M. (2022). Saltwater intrusion management in shallow and deep coastal aquifers for high aridity regions. *J*ournal of *H*ydrology: *R*egional *S*tudies, *40*, 101026. https://doi.org/10.1016/j.ejrh.2022.101026

Coulon, C., Lemieux, J.-M., Pryet, A., Bayer, P., Young, N. L., Molson, J. (2022). Pumping optimisation under uncertainty in an island freshwater lens using a sharp-interface seawater intrusion model. *W*ater *R*esources *R*esearch, *58*, e2021WR031793. https://doi.org/10.1029/2021WR031793

Jamal, M.S., Awotunde, A.A., Patil, S. (2022). Management of saltwater intrusion in coastal Karstic aquifers under geological uncertainties associated with shapes and locations of cave networks. *J*ournal of *W*ater *R*esources *P*lanning and *M*anagement, *148*(11), 04022053. https://doi.org/10.1061/(ASCE)WR.1943-5452.0001603

Yin, J., Tsai, F.T.C., Lu, C. (2022). Bi-objective extraction-injection optimisation modeling for saltwater intrusion control considering surrogate model uncertainty. *W*ater *R*esources *M*anagement, *36*, 6017–6042. https://doi.org/10.1007/s11269-022-03340-9

IPCC (2023). Sections. In: Climate Change 2023: Synthesis Report. Contribution of Working Groups I, II and III to the Sixth Assessment Report of the Intergovernmental Panel on Climate Change [Core Writing Team, H. Lee and J. Romero (eds.)]. IPCC, Geneva, Switzerland, pp. 35-115. https://doi.org/10.59327/IPCC/AR6-9789291691647

Chapter 2

Investigating the impact of SWI on the operation cost of groundwater supply in island aquifers

Publications included in this chapter:

Yu, W., Baù, D., Mayer, A. S., Mancewicz, L., & Geranmehr, M. (2023). Investigating the impact of seawater intrusion on the operation cost of groundwater supply in island aquifers. *Water Resources Research*, 59(10), e2023WR034798. https://doi.org/10.1029/2023WR034798

Investigating the impact of seawater intrusion on the operation cost of groundwater supply in island aquifers

Weijiang Yu[1*], Domenico Baù[1], Alex S. Mayer[2], Lauren Mancewicz[3], Mohammadali Geranmehr[1]

[1]Department of Civil and Structural Engineering, University of Sheffield, Sheffield, UK.
[2]Department of Civil Engineering, University of Texas at El Paso, TX, USA.
[3]Department of Civil, Environmental, and Geospatial Engineering, Michigan Technological University, Michigan, USA.

*Corresponding author: Weijiang Yu (wyu18@sheffield.ac.uk)

Key Points:

- Effects of pumping patterns (pump depth, rate and well location) on island groundwater supply cost and seawater intrusion (SWI) are studied.
- Shallow pumping near the island centre is cost-effective but causes more severe SWI, that is, a conflict between economic cost and SWI control.
- Controlling SWI by limiting water table drawdown usually leads to selecting more expensive groundwater supply strategies.

Abstract

Managing fragile island freshwater resources requires identifying pumping strategies that trade off the financial cost of groundwater supply against controlling the seawater intrusion (SWI) associated with aquifer pumping. In this work, these tradeoffs are investigated through a sensitivity analysis conducted in the context of an optimisation formulation of the groundwater management problem, which aims at minimizing the groundwater supply operation cost associated with groundwater pumping and desalination treatment, subject to constraints on SWI control, as quantified by the water table drawdown over the well (Δs), the reduction in freshwater volume (ΔFV) in the aquifer, or the salt mass increase (ΔSM) in the aquifer. This study focuses on a simplified two-dimensional model of the San Salvador Island aquifer (Bahamas). Pumping strategies are characterized by the distance of the pumping system from the shoreline (WL), the abstraction screen depth (D) and the overall pumping rate (Q), constituting the decision variables of the optimisation problem. We investigate the impacts of pumping strategies on the operation cost, Δs, ΔFV and ΔSM. Findings indicate increasing D or decreasing WL reduces Δs, ΔFV and ΔSM, thus preserving the aquifer hydrogeologic stability, but also leads to extracting saltier groundwater, thus increasing the water treatment requirements, which have a strong impact on the overall groundwater supply cost. From a financial perspective, groundwater abstraction near the island centre and at shallow depths seems the most convenient strategy. However, the analysis of the optimisation constraints

reveals that strategies where the pumping system approaches the island center tend to cause more severe SWI, highlighting the need to trade off groundwater supply cost against SWI control.

1 Introduction

Coastal regions are the most densely populated areas in the globe, with more than half of the world's population residing within 100 kilometres of a shoreline (Kazakis et al., 2018; Tomaszkiewicz et al., 2014). In these regions, intense water demand often forces local communities to rely on groundwater to supplement surface freshwater. Coastal aquifers are normally characterized by a freshwater-seawater contact zone, in which seaward discharging freshwater overlies the landward movement of seawater due to its lighter density (Kishi & Fukuo, 1977). When the abstraction rate exceeds the natural freshwater recharge, the seaward hydraulic gradient drops, causing the landward advancement of saltwater in aquifers, known as SWI. SWI increases the salinity level of groundwater, directly endangering access to subsurface freshwater for coastal communities (Jasechko et al., 2020; Agoubi, 2021). To protect coastal subsurface freshwater from SWI, many solutions have been proposed, including subsurface physical barriers (Abdoulhalik et al., 2017), flow barriers (Botero-Acostaa & Donado, 2015; Bray & Yeh, 2008) and surface recharge canals (Motallebian et al., 2019). Among these measures, optimal design and management of groundwater abstraction has gained much attention over the past decades, to address the conflict between groundwater abstraction and SWI control.

Simulation-optimisation (SO) frameworks have been proven to be effective tools for identifying optimal groundwater management strategies (Mayer et al., 2002; Baú & Mayer, 2006; Rajabi & Ketabchi, 2017; Christelis & Mantoglou, 2019; Dey & Prakash, 2020; Roy & Datta, 2020). A SO framework is typically characterized by three components: an optimisation formulation for the groundwater management problem, a process-based groundwater simulation model and an optimisation algorithm. The optimisation formulation requires defining the management goals as objective functions and constraints, as well as the decision variables (DVs) that identify the management policies, i.e., groundwater pumping schemes. Once DVs are selected, the simulation model is used to estimate the state variables (SVs), which define the aquifer response to pumping. DVs and SVs are then used to calculate objective functions and verify compliance with constraints. The optimisation algorithm is the mathematical tool that searches for the optimal set of DVs.

Coastal groundwater management has been most often formulated as a single-objective problem, aiming to maximize the total pumping rate from production wells subject to constraint conditions (Sedki & Ouazar, 2011; Karatzas & Dokou, 2015; Rajabi & Ketabchi, 2017; Kopsiaftis et al., 2019; Dey & Prakash, 2020; Coulon et al., 2022). Several authors have considered objective functions that relate to either the cost of or the economic revenue of groundwater supply. In Yin et al. (2020), the objective function consisted of the energy cost of groundwater pumping. Mayer et al. (2002) proposed an objective function that included capital and operation costs associated with both pumping and treatment, whereas El-Ghandour and Elbeltagi (2020) considered the objective of maximizing the revenue from groundwater supply, which accounted also for pumping costs. In Qahman et al. (2005), the objective function consisted of the benefit from groundwater supply minus the desalination cost, which accounts for potential pumping schemes that produce brackish or salt water.

When considering management goals that represent either revenue or cost, objectives result typically in complex, irregular, and potentially discontinuous functions of DVs and SVs (Mayer et al., 2002; Yin et al., 2020). Since these may pose significant challenges to identifying optimal solutions, several authors have adopted measures to simplify the objective functions. For example, Javadi et al. (2012) and Ketabchi and Ataie-Ashtiani (2015) calculated pumping costs based on extraction rates and total dynamic heads, whereas Qahman et al. (2005) formulated treatment costs as proportional to the product of abstracted volumes and desalination coefficients. Likewise, Park and Shi (2015), El-Ghandour and Elbeltagi (2020), and Yang et al. (2021) evaluated the monetary benefits of groundwater usage as linearly proportional to the pumping intensity.

In general, management constraints can be subdivided into three main groups. The first group includes limitations on ranges of the variability of DVs, such as pumping rates, well locations and screen depths (Javadi et al., 2015), and total groundwater demand (Kourakos & Mantoglou, 2011; Fan et al., 2020). A second group considers restrictions to SWI due to aquifer pumping, typically formulated about groundwater salinity. Groundwater salinity constraints have been expressed in terms of freshwater-saltwater interface location when neglecting solute dispersion effects, as at regional aquifer scales, which have allowed to adopt “sharp-interface” models (Ferreira da Silva & Haie, 2007; Christelis & Mantoglou, 2016; Kopsiaftis et al., 2019; Stratis et al., 2017; Dey & Prakash, 2020). At smaller aquifer scales, where the assumption of miscible freshwater and saltwater is needed, salinity constraints have been prescribed as salt concentration limits at control points, such as pumping wells or monitoring wells, which have required the use of variable density flow models that are more complex and computationally

more expensive than sharp-interface models (Christelis & Mantoglou, 2019). SWI constraints have also been applied indirectly to the hydraulic head, by limiting, for example, seaward hydraulic gradients or the water table drawdown at given monitoring points (Karatzas & Dokou, 2015; Pramada et al., 2018; Yang et al., 2018). A third group of SWI constraints involves the economic aspects of management. For example, Ranjbar and Mahjouri (2019) addressed groundwater management problems, in which water administrators set an expected benefit for groundwater supply by capping maximum pumping costs.

Some scholars have addressed the tradeoffs between achieving competing management objectives and complying with constraints by using multiple-objective optimisation approaches, in which constraints are transformed into additional objective functions (Park & Shi, 2015; El-Ghandour & Elbeltagi, 2020; Fan et al., 2020). Compared with the single-objective management problem, these approaches have the advantage of providing optimal management strategies under varied constraint scenarios.

In the management of groundwater in coastal aquifers that are vulnerable to SWI, the cost of groundwater supply appears to be a strong indicator of optimality as it depends significantly on the cost of desalination (McKinney & Lin, 1994; Javadi et al., 2015), which implicitly tends to exclude pumping strategies that can cause SWI. It appears, however, that the minimization of the SWI extent should be considered as an explicit objective for the stability and sustainability of water resources. In this respect, Song et al. (2018) adopted, as a main objective, the minimization of total salt mass increase in the aquifer. Zekri et al. (2015) and Triki et al. (2017) used the minimization of the mean drawdown near the shoreline, and Rajabi and Ketabchi (2017) and Fan et al. (2020) targeted the minimization of concentrations at monitoring wells. Roy et al. (2016) adopted a two-objective optimisation problem to manage the utilization of coastal groundwater, which maximized farmer benefit while minimizing SWI through a sustainability index function expressed by the water table elevation and salinity at specific monitoring locations. While this approach enables preventing local salinisation, for example at pumping wells, it may not ensure SWI alleviation on the whole aquifer.

To date, most SO applications to SWI management have considered “classic” coastal aquifers, which are typically included in larger and elongated geological formations stretching along the coastline of continents, and only a few studies have focused specifically on island aquifers (Kourakos & Mantoglou, 2015; Coulon et al., 2022), which are characterized by very particular hydrogeological settings. In this type of aquifers, fresh groundwater resources are generally lens-shaped and sustained solely by groundwater recharge from local precipitation (Figure 1). The freshwater thickness is often of the order of a few meters (Fetter, 1972), which

makes these aquifers extremely vulnerable to SWI. Excessive groundwater abstraction may thus lead to depletion of freshwater resources, aquifer salinization, and increased costs for water desalination. In these situations, curtailed pumping may ultimately result as the only viable option for maintaining or re-establishing lens aquifers.

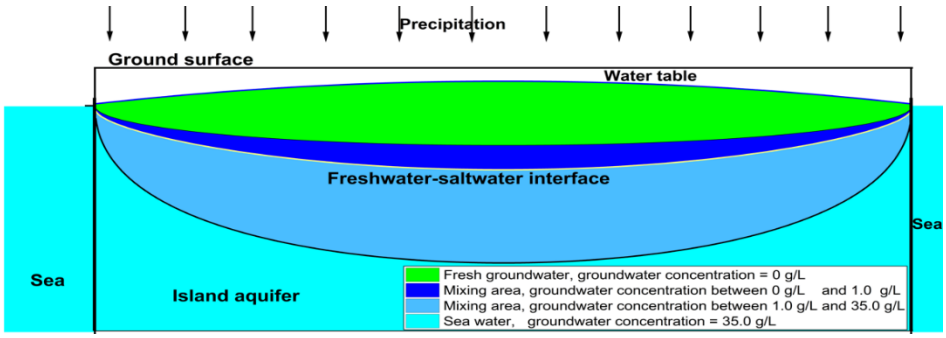

Figure 1. Cross-section diagram of a freshwater lens in an island aquifer. The thickness of the lens depends mainly on the aquifer's hydraulic conductivity and the intensity of water infiltration from precipitation.

In this study, we approach the management of groundwater in island aquifers as a single-objective optimisation problem, with the primary objective being the minimization of operating costs associated with groundwater extraction and desalination treatment. Our focus is specifically on addressing the cost increase resulting from rising groundwater demand, which is directly influenced by population density. While SWI has a direct impact on management costs due to its effect on desalination intensity, we also establish explicit constraints to control SWI.

To assess the interplay between management costs and these constraints, we adopt a SO analysis approach, considering a cost objective function and three types of SWI constraints, both individually and in combination. It is important to note that we do not adopt any specific optimisation algorithm to solve the formulated management problems. Instead, we design a large set of potential groundwater abstraction strategies (over 200), and by modelling the aquifer's responses to these strategies, we can identify the optimal pumping scheme and its associated management cost through full enumeration evaluation (e.g., Beheshti et al., 2022) within such a set when SWI control constraints are specified. Finally, by varying the variable bounds of these constraints, we can then identify various corresponding optimal pumping strategies.

This enables us to conduct, within an optimisation context, a sensitivity analysis of the optimal groundwater supply costs while aiming to minimize SWI, providing insights into sustainable island groundwater use. Such a sensitivity analysis is conducted on a simplified two-dimensional aquifer, based on hydrogeological conditions observed in the island aquifer

of San Salvador Island, Bahamas. The management cost takes into of the expenses associated with groundwater pumping and the desalination process required to ensure the salt concentration in water meets potability standards.

This paper is organized as follows. The next section presents the simulation model for SWI, the optimisation formulation of the management problem, i.e., the objective function and its constraints, and the sensitivity scenarios considered for the SWI control indicators. Simulation results and their discussion are provided in the following section. The last section presents the conclusions drawn from the investigation.

2 Methodology

The goal of this study is to investigate the effects of groundwater pumping strategies on operation cost and SWI, using the San Salvador Island aquifer as a case study. San Salvador Island is located within the Bahamian Archipelago (Figure 2), about 600 km east-southeast of Miami, and sits on a small, isolated carbonate platform (Ho et al., 2014; McGee et al., 2010). The island is about 20 km long north-to-south and has an average width west-to-east of approximately 8 km (Martin & Moore, 2008). The topography is dominated by consolidated carbonate dune ridges, with elevations between 10 and 20 meters above sea level (Davis & Johnson, 1989). Characterized by a subtropical climate, San Salvador Island has an annual temperature ranging between 22 and 28 °C (McGee et al., 2010) and annual precipitation and potential evaporation of 1000-1250 mm/yr and 1250-1375 mm/yr, respectively (Moore, 2009).

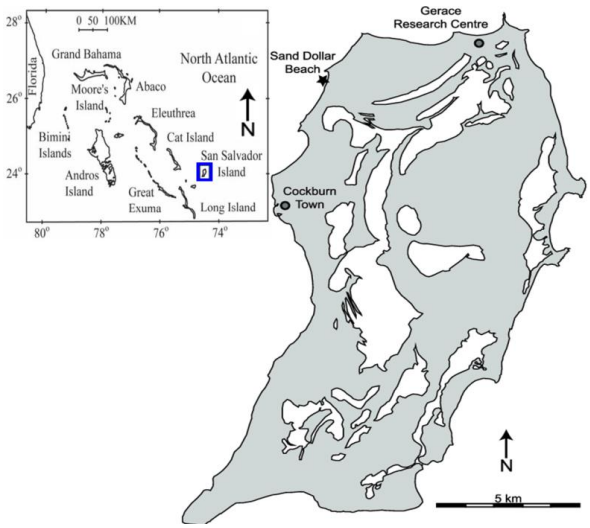

Figure 2. Location map of San Salvador Island (Moore, 2009). The dark grey and the light grey areas represent land and surface water, respectively.

2.1 Numerical simulation of SWI in the San Salvador Island aquifer

This work applies the SEAWAT model to simulate the SWI process in the island aquifer. SEAWAT couples the groundwater flow model MODFLOW and the solute transport model

MT3DMS to solve the variable-density flow equations using a finite-difference numerical approach (Langevin et al., 2008; Kourakos & Mantoglou, 2013; Yao et al., 2019). Since the SEAWAT groundwater model can account for water density variations that depend on salt concentration, it is well-suited for simulating flow in aquifers characterized by freshwater-seawater interactions.

In the investigation of the island groundwater abstraction management, a simplified two-dimensional "cross-section" model is adopted. The island cross-section model is constructed as a rectangular domain, with a length of 8,000 m, a height of 480 m, and a width of 1 m. The aquifer domain is discretized into a finite-difference regular grid with cells of size 8 m × 8 m × 1 m. Two additional grid columns are used to represent the boundary conditions at the leftmost and rightmost ends of the domain, so that the finite-difference grid is made up of 1,002 columns and 60 rows, for a total of 60,120 cells. The pumping system is represented by a point sink located at a depth *D*, a distance *WL* from the shoreline, and a pumping rate *Q*, which represents the volume of groundwater extracted per unit time and per unit aquifer width.

Figure 3 shows a conceptualization of the aquifer domain along with the numerical model grid and its boundary conditions. A no-flow boundary is prescribed at the model bottom. The model top is a specified flux boundary, reflecting the aquifer recharge from precipitation, which is assumed to be 0.2 m per year (Gulley et al., 2016). At the left and right boundaries, a constant head of 0.0 m is prescribed over the water column, which represents the sea level (at the datum). At the same boundaries, a constant concentration of 35.0 g/L is imposed, which represents the salt content in seawater.

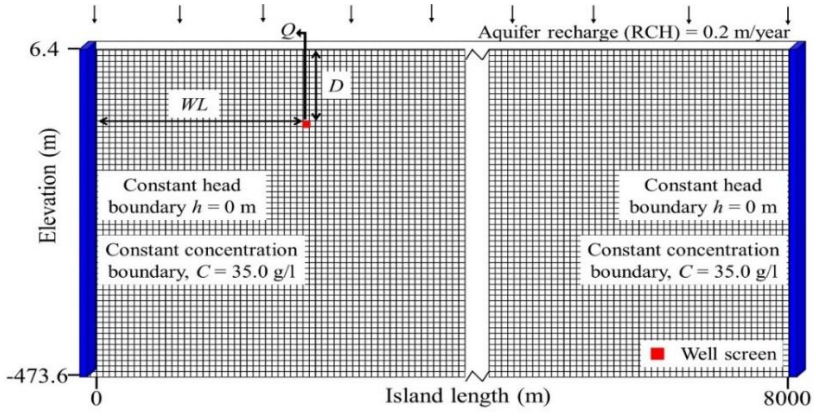

Figure 3. Island aquifer SEAWAT cross-sectional model grid along with the associated boundary conditions. The pumping system is simulated as a single cell located at depth *D* from the ground surface and distance *WL* from the shoreline.

To model SWI effects from groundwater abstraction at a steady state, the flow and solute transport are simulated as transient state processes with a sufficiently large period of constant groundwater pumping. A "baseline" scenario is first developed to simulate the island

freshwater lens under steady-state conditions of natural groundwater recharge from precipitation only. This serves as the initial condition to model the aquifer freshwater distribution under various scenarios of groundwater pumping. For the simulations involving groundwater pumping, SEAWAT is run until a steady state is reached, which is typically between 2 and 30 years depending on the simulated pumping scheme. Correspondingly, the required CPU time for each simulation varies from a minimum of about 15 minutes to a maximum of over 1 hour. Table 1 provides a list of the relevant parameters adopted in the simulation model introduced above. These parameters are drawn from published works (Gulley et al., 2016; Holding & Allen, 2015) that have used San Salvador Island or nearby island aquifers as test cases.

Table 1. *Model Parameters Used for SWI Simulation in the San Salvador Island Aquifer*

Model Component	Parameters	Units	Values
Groundwater Flow	Aquifer recharge (*RCH*)	m/year	0.2
	Effective porosity	\	0.15
	Specific elastic storage	m^{-1}	1.0×10^{-5}
	Specific yield	\	0.15
	Horizontal hydraulic conductivity (HK)	m/day	50.0
	HK transversal anisotropy ratio	\	1.0
	HK vertical anisotropy ratio	\	1.0
Solute Transport	Longitudinal dispersivity	m	1.0
	Transversal dispersivity	m	0.1
	Vertical dispersivity	m	0.01
	Molecular diffusion coefficient	m^2/s	1.0×10^{-9}
	Aquifer recharge concentration	g/l	0
Density dependence	Freshwater density	kg/m^3	1000
	Seawater density	kg/m^3	1025
	Density/concentration slope[a]	\	0.7143

[a] The water density ρ_w [kg/m^3] varies linearly with the salt concentration C [kg/m^3] through the equation $\rho_w = 1000 + 0.7143 \cdot C$.

2.2 Groundwater management formulation

The primary objective of the island groundwater management is to identify cost-optimal pumping strategies for prescribed groundwater demand levels. Pumping strategies are characterized by three DVs, the depth D [L] at which pumping occurs, the distance WL [L] of the pumping system from the shoreline, and the intensity of constant pumping Q [L^2T^{-1}]. The management cost f_{OC} accounts for two main components: the pumping operation cost f_p, and the treatment operation cost f_t, per unit aquifer width and unit time [$\$L^{-1}T^{-1}$]. The former is the

cost of energy utilization for lifting groundwater to the ground surface, whereas the latter is the cost of desalination by reverse osmosis, which is required when the salt concentration in water exceeds 1.0 g/L, in accordance with World Health Organization guidelines for drinking water (Yao et al., 2019).

The cost objective function is formulated as:

$$f_{\mathrm{OC}} = f_p(Q, h, C) + f_t(Q, C) \tag{1}$$

where h [L] and C [ML^{-3}] are state variables, which represent the hydraulic head at the well screen and the salt concentration in the extracted water, respectively. Both h and C are functions of the DVs (D, WL, Q). f_p is expressed as (Mayer et al., 2002):

$$f_p(Q, h, C) = \rho_w(C) \cdot \mathrm{g} \cdot \left(z_{\mathrm{gs}} - h\right) \cdot Q \cdot c_{\mathrm{e}} \tag{2}$$

where ρ_w is the water density, which depends on the salt concentration C (Table 1), g denotes gravitational acceleration [LT^{-2}], and z_{gs} represents the ground surface elevation [L], set equal to 15.0 m. The coefficient c_{e} represents the unit energy cost [\$M^{-1}L^{-2}T^{2}], assumed equal to 0.1848 \$/kWh. The treatment cost, f_t, is estimated as (Avlonitis et al., 2012):

$$f_t(Q, C) = \rho_w(C) \cdot SEC(C) \cdot Q \cdot c_{\mathrm{e}} \tag{3}$$

where SEC [L^{2}T^{-2}] is the specific (per unit mass) energy consumption for water desalination (Stillwell & Webber, 2016), which depends on the salt concentration C. A detailed description of SEC is presented in the Supporting Information - Appendix A.

The formulation of the island groundwater management problem is completed by two groups of constraints. The first group sets the range of variability of the DVs (D, WL, Q). The pumping depth D is subject to the inequality:

$$D_{\min} \leq D \leq D_{\max} \tag{4}$$

where $D_{\min}$ and $D_{\max}$ are the absolute depths below the groundwater surface, equal to 12.6 m and 484.6 m, respectively.

Since the model grid (Figure 3) is symmetric with respect to the island's central axis, the distance WL cannot exceed half of the island length L =8000 m. WL is thus constrained as:

$$WL_{\min} \leq WL \leq WL_{\max} \tag{5}$$

with $WL_{\min}$ equal to $0.05 \cdot L$ and $WL_{\max}$ equal to $0.5 \cdot L$. The pumping rate Q depends on the groundwater demand, which may be estimated based on the population density and the per capita water consumption and needs to be constrained in relation to the aquifer recharge rate RCH. Here, Q is assumed to be subject to:

$$Q_{\min} \leq Q \leq Q_{\max} \tag{6}$$

with $Q_{\min}$ equal to $0.05 \cdot RCH \cdot L$ and $Q_{\max}$ equal to $0.2 \cdot RCH \cdot L$. These values have been selected to cover a range of variability for Q large enough to study its effects on SWI and groundwater supply cost.

A second group of constraints is considered to minimize the extent of the SWI, thus addressing the environmental sustainability of groundwater abstraction. SWI is quantified by three indicators: the hydraulic head drawdown scaled to the water table elevation over the pumping system, the reduction in aquifer freshwater volume, and the increase in aquifer salt mass.

The drawdown at the pumping well is subject to the following constraint:

$$\Delta s \leq \Delta s_{\max} \tag{7}$$

where Δs is calculated as the percentage of water table drawdown at the well location with respect to the original water table level, and $\Delta s_{\max}$ is the maximum allowed value for Δs, which is calculated as:

$$\Delta s = \frac{H_0(WL) - H(D,WL,Q)}{H_0(WL)} \cdot 100 \leq \Delta s_{\max} \quad [\%] \tag{8}$$

where $H_0(WL)$ is the water table level over the pumping system prior to pumping (baseline scenario), and $H(D, WL, Q)$ is the corresponding steady-state water table level during pumping, which depends on the DV set.

The reduction in aquifer freshwater volume is constrained as:

$$\Delta FV \leq \Delta FV_{\max} \tag{9}$$

where $\Delta FV(D, WL, Q)$ is the percentage of the groundwater freshwater volume decrease in the aquifer:

$$\Delta FV = \frac{FV_0 - FV(D,WL,Q)}{FV_0} \cdot 100 \leq \Delta FV_{\max} \quad [\%] \tag{10}$$

where FV_0 is the freshwater volume prior to pumping (baseline scenario), and FV is the corresponding steady-state volume during pumping. $\Delta FV_{\max}$ is the maximum allowed value for ΔFV. FV is calculated by spatial integration of the pore volume in those grid cells where the simulated salt concentration is less than 1 g/l.

The aquifer salt mass increase is subject to the inequality:

$$\Delta SM \leq \Delta SM_{\max} \tag{11}$$

where ΔSM is the percentage of salt mass increase in the aquifer, given by:

$$\Delta SM = \frac{SM(D,WL,Q) - SM_0}{SM_0} \cdot 100 \leq \Delta SM_{\max} \quad [\%] \tag{12}$$

where SM_0 is the total salt mass in the aquifer prior to pumping and SM is the total salt mass at steady state during pumping. $\Delta SM_{\max}$ is the maximum allowed value for ΔSM. SM values are calculated by integrating the salt concentration multiplied by the pore volume over all model grid cells.

2.3 Optimisation Scenarios

It is worth noting that, for any given DV set (D, WL, Q), the calculations of the objective function (Equations 1-3) and the management constraints (inequalities 7, 9 and 11) require the values of the state variables, h and C, and corresponding SWI metrics Δs , ΔFV and ΔSM, which are here calculated using the SEAWAT model. Rather than relying on the solution of the optimisation problem through the application of a particular optimisation algorithm, our investigation is based on the analysis of a pre-fixed large set of groundwater abstraction strategies (i.e., SEAWAT model runs), expressed as a prescribed ensemble of DV sets, and the comparison of their "performance" in terms of management cost (Equation 1) and constraints (inequalities 7, 9 and 11). The use of a discrete set of abstraction strategies enables the analysis of the impact of both separate and combined SWI constraints, as well as the prescribed SWI bounds, on the pumping strategies that lead to the minimum management cost, and the magnitude of the cost itself.

Table 2 provides a description of the ensemble of DV sets (D, WL, Q) used in this study. The pumping system depth D varies over 14 discrete values, which meet inequality (4) and are mainly concentrated in the shallower portion of the lens aquifer, where most freshwater is found prior to pumping. As for WL, which needs to meet inequality (5), the pumping system may be positioned at 4 alternative regularly spaced locations, from the vicinity of the seashore $(0.125 \cdot L)$ to the center of the island $(0.5 \cdot L)$. The pumping rate Q is assumed to satisfy four groundwater demand levels, from a minimum of $0.05 \cdot RCH \cdot L$, to a maximum of $0.2 \cdot RCH \cdot L$. The combination of these DV values lead to an ensemble of $14 \times 4 \times 4 = 224$ alternative groundwater abstraction strategies, and thus as many SEAWAT model runs. An additional model run is also needed to simulate the baseline "no-pumping" scenario.

Table 2. *Decision Variable Values Considered for the Candidate Pumping Strategies Selected for Island Aquifer Management*

Decision Variable	Discrete Values*													
D (m)	12.6	28.6	44.6	60.6	76.6	84.6	92.6	100.6	108.6	124.6	132.6	164.6	244.6	484.6
WL (m)	$0.125 \cdot L$			$0.25 \cdot L$				$0.375 \cdot L$			$0.5 \cdot L$			
Q (m²/d)	$0.05 \cdot RCH \cdot L$			$0.1 \cdot RCH \cdot L$				$0.15 \cdot RCH \cdot L$			$0.2 \cdot RCH \cdot L$			

(*) L=8000 m and RCH=0.2 m/yr are the hypothesized aquifer length and recharge rate, respectively.

Table 3 describes constraint-bound values assigned to evaluate the trade-off between SWI restrictions and the management cost of groundwater abstraction. Both $\Delta s_{\max}$ and $\Delta FV_{\max}$ (inequalities 7 and 9) are assumed to vary from a stricter lower limit of 5% to a more relaxed upper limit of 30%, at 5% increments. $\Delta SM_{\max}$ (inequality 11) is assumed to increase from a minimum of 0.5%, up to a maximum of 5%, representing progressively larger SWI intensities.

In an initial series of tests, cost-optimal pumping strategies are identified among the alternatives presented in Table 2 as if the sole SWI constraint under consideration was represented by either of the inequalities (7), (9) or (11). These tests are designed to provide insight into the impact on the minimum-cost pumping scheme of (a) each individual SWI constraint type and (b) the selected upper bound for that constraint (Table 3).

Table 3. *Threshold Values Used in the Sensitivity Analysis of Potential SWI Constraints on the Optimal Management Cost*

Upper Bound	Values					
$\Delta s_{\max}$	5%	10%	15%	20%	25%	30%
$\Delta FV_{\max}$	5%	10%	15%	20%	25%	30%
$\Delta SM_{\max}$	0.5%	1%	2%	3%	4%	5%

Next, cost-optimal pumping strategies are investigated by assuming two concurrent SWI constraints. These combined constraint scenarios are presented in Table 4, which shows as many as 12 optimisation setups, denoted as Scenarios 1 through 12. The first four scenarios assume SWI constraints imposed on Δs and ΔFV, the second four scenarios consider constraints on Δs and ΔSM, and the remaining scenarios hypothesize constraints on ΔFV and ΔSM. These tests allow for investigating the interplay between SWI constraints and their joint impact on the groundwater lens management. Lastly, optimal pumping strategies are investigated by imposing the SWI constraints (7), (9) or (11) jointly, under various upper bound sets, with as many as 8 optimisation setups investigated. These scenarios are denoted as Scenario 13 through 20 (see Table 5).

Table 4. *Sensitivity Scenarios for Two-SWI-constraint Combinations*

Scenario	$\Delta s_{\max}$	$\Delta FV_{\max}$	$\Delta SM_{\max}$
1	10%	10%	- (*)
2	10%	30%	-
3	30%	10%	-
4	30%	30%	-
5	10%	-	1%
6	10%	-	5%
7	30%	-	1%
8	30%	-	5%
9	-	10%	1%
10	-	10%	5%
11	-	30%	1%
12	-	30%	5%

(*) The symbol '-' indicates a constraint condition not in use.

Table 5. *Sensitivity Scenarios for Three-SWI-constraint Combinations*

Scenario	$\Delta s_{\max}$	$\Delta FV_{\max}$	$\Delta SM_{\max}$
13	10%	10%	1%
14	10%	10%	5%
15	10%	30%	1%
16	10%	30%	5%
17	30%	10%	1%
18	30%	10%	5%
19	30%	30%	1%
20	30%	30%	5%

3 Results and Discussion

3.1 Impact of the DVs on pumping and desalination costs

The distribution of groundwater concentration in the baseline scenario, prior to pumping, is depicted in Figure 4. It can be observed that the freshwater lens depth varies from zero in proximity of the shoreline, to about 110 m at the centre of the island. Correspondingly, the depth at which seawater is found varies from about 40 m to approximately 165 m.

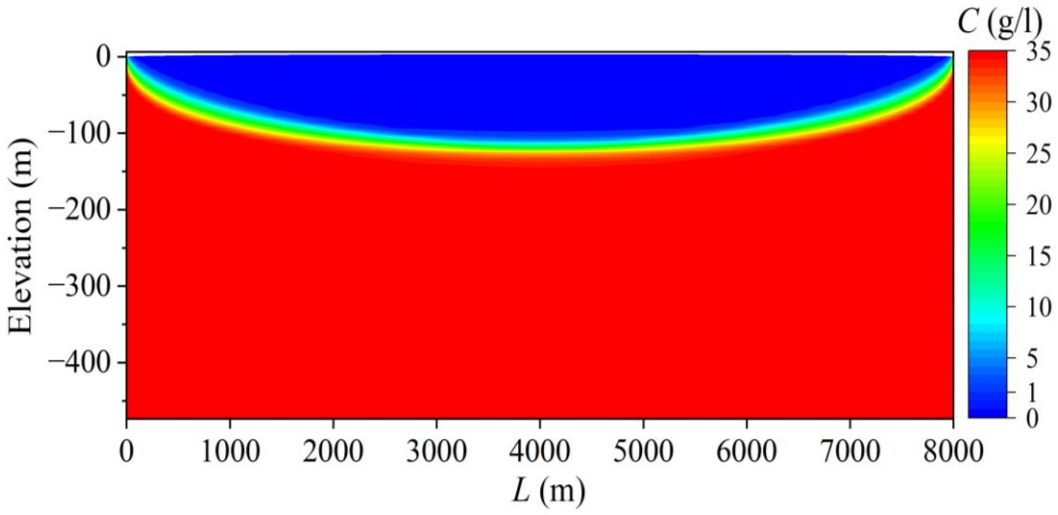

Figure 4. Distribution of groundwater concentration in the baseline scenario.

Figure 5 presents the results of an analysis of the impact of the DVs on the management cost function (Equations 1-3). The data points used for the plots in Figure 5 correspond to the 224 DV combinations (D, WL, Q) presented in Table 2. Figure 5a shows profiles of the hydraulic head h at the well screen with respect to the pumping depth D, the distance to the shoreline WL, and the abstraction rate Q. These profiles reveal that: (i) for any given combination of WL and Q, with increasing D, h tends to first slightly increase, then drops dramatically at depths around 60 m, and becomes practically constant beyond at depths below 150 m from the ground surface; (ii) h tends to increase by increasing WL, that is, by moving the well towards the centre of the island; (iii) h tends to decrease by increasing Q, that is, the hydraulic head at the well screen is lower if the pumping rate higher.

Figure 5b shows profiles of the salt concentration C of the pumped water with respect to the DVs D, WL, and Q. These profiles reveal that: (i) for D values down to 50 m, C does not exceed 5 g/l, but then increases dramatically reaching the seawater concentration of 35 g/l for D exceeding ~150 m. This is due to the groundwater abstraction being progressively shifted across the freshwater-saltwater transition zone. While the location of this transition zone depends specifically on the thickness of the freshwater lens and the hypothesized mixing conditions, qualitatively similar profiles should be expected for island aquifer settings other than those assumed here; (ii) C is seen to increase by decreasing WL, that is, by pumping closer to the shoreline, where the freshwater lens is thinner and higher salinity is found at shallower depth; (iii) C increases by increasing Q, that is, the more water is pumped, the higher the salinity, due to the upward movement of salt-rich groundwater below the pumping point (Jakovovic et al., 2011).

Figures 5c and 5d show the profiles of the pumping cost f_p and the desalination cost f_t, respectively, against the pumping depth D, and for different values of the distance WL and the abstraction rate Q. Figure 5c indicates that f_p increases quite slightly if D increases and becomes practically constant for depths exceeding ~150 m. The cost f_p is generally larger if the pumping rate Q is increased and does not seem sensitive to variations of WL. This is an apparent effect due to the logarithmic scale adopted in Figure 5c. A closer look (see Appendix B) reveals that f_p actually decreases if WL increases, that is, if the pumping system is moved closer to the island centre. These trends are explained by observing the behaviour of h in the DV space (D, WL, Q), as shown in Figure 5a, and noting the dependency of f_p on h and Q in Equation 2.

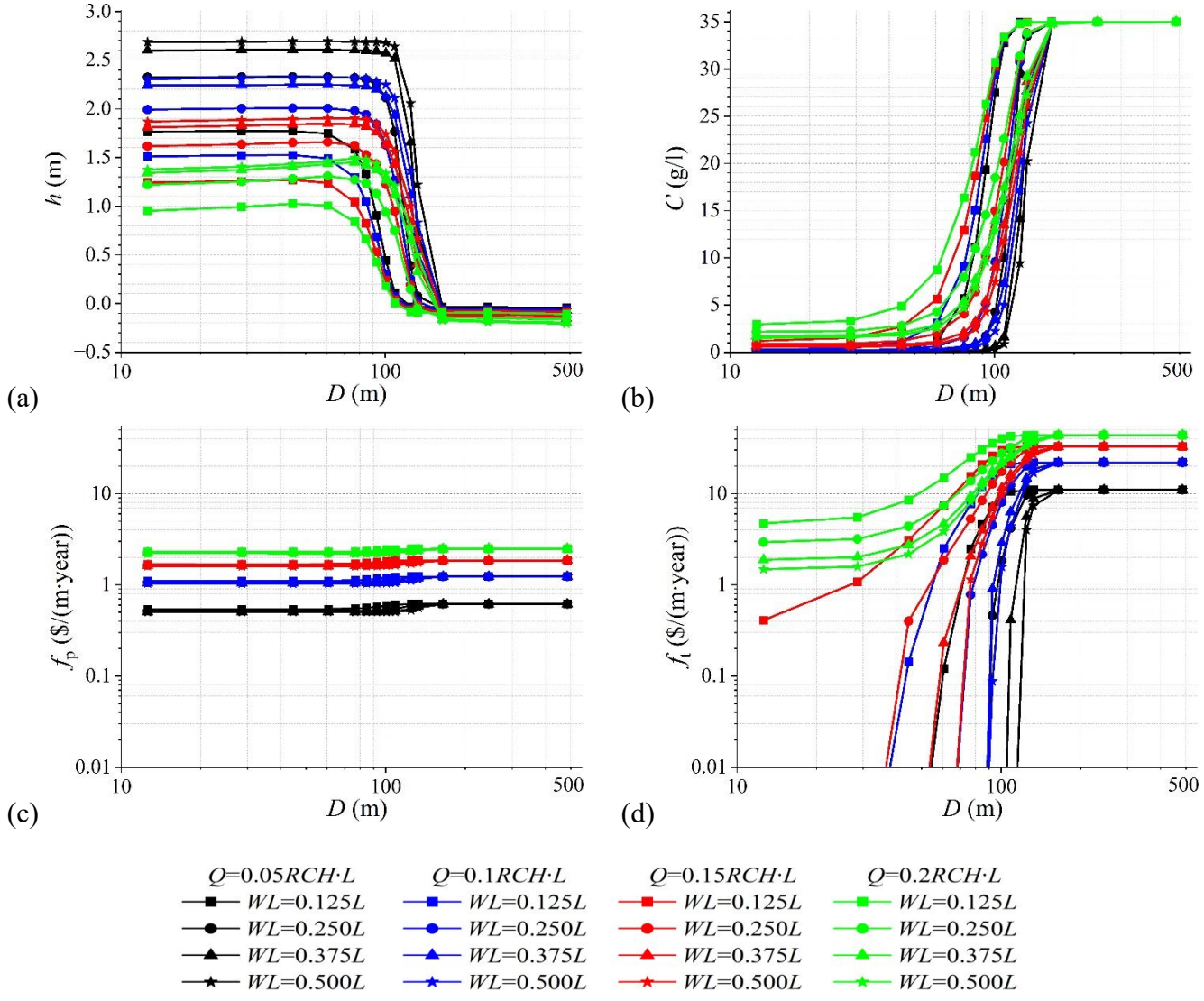

Figure 5. (a) Steady-state water table elevation over the well, *h;* (b) extracted groundwater salt concentration, *C;* (c) pump cost f_p and (d) treatment cost f_t for the proposed 224 alternative groundwater abstraction strategies (**Table 2**). f_t profiles in subpanel (d) falling

below 0.01 $/(m· year) indicate that no desalination is required (i.e., the treatment cost is zero).

Figure 5d shows that f_t increases with D and reaches horizontal asymptotes that depend mainly on the pumping rate Q. For any given combination of WL and Q, the treatment cost f_t is relatively low if the pumping system is shallower, that is, for lower D, but increases dramatically for larger D, due to the increase in concentration C, as observed in Figure 5b. However, f_t values become constant at depths larger than 150 m, as C is limited by the seawater concentration of 35 g/l (Figure 4b). The maximum values of treatment cost are observed to be practically proportional to Q, and are generally larger if the pumping system is closer to the shoreline, that is, for lower WL values, due to the reduced thickness of the freshwater lens aquifer (Figure 1).

A comparison of the profiles in Figures 5c and 5d reveals that the treatment cost f_t largely exceeds the pumping cost f_p under most circumstances. In certain pumping conditions, f_t may be up to one order of magnitude larger than f_p. On the other hand, the two cost components are comparable only for lower abstraction rates Q, and for shallow pumping systems (i.e., lower D values) situated towards the centre of the island (i.e., larger WL values). These differences are a direct consequence of the remarkably different specific energy consumptions associated with groundwater pumping and desalination.

3.2 Impact of the DVs on operation costs and SWI indicators

Figure 6a shows that, for larger WL and lower Q, f_{OC} tends to decrease with the pumping depth D until this remains within 50-100 m. This happens because groundwater abstraction occurs within the original freshwater lens, so that little or no desalination is required, and the predominant cost component is f_{p} (Figure 5c). Instead, for lower WL and larger Q, f_{OC} increases along the depth D, since the dominant cost component becomes f_{t} (Figure 5d). In general, for D larger than 50-100 m, the total cost f_{OC} increases sharply due to abstraction of groundwater with salt concentration that exceeds the treatment threshold (Figure 5b). The profiles in Figure 6a indicate that, for lower WL and larger Q, the cost-optimal pumping strategies are those with the smallest D. For larger WL and lower Q, however, the cost-optimal pumping strategies are found for intermediate values of D, between 50 and 100 m.

Figures 6b-c-d show that the drawdown percentage Δs, the percentage of the freshwater volume decrease ΔFV, and the percentage of salt mass increase ΔSM share a similar behaviour, generally decreasing with D and increasing with both WL and Q. In Figure 6b, it is interesting to observe that if D is generally over ~150 m, the drawdown is marginally affected by

groundwater abstraction and most of the pumped groundwater is resident seawater. In Figures 6c-d, the dependency of ΔFV and ΔSM on Q may be explained through simple considerations of aquifer mass balance. At steady state, the abstraction rate Q is provided in part by the freshwater recharge, and in part by the seawater inflow from the shoreline boundaries, with an overall decrease in the freshwater lens volume. If the pumping depth D is increased or the distance WL is decreased, both ΔFV and ΔSM become progressively less significant, and if D is larger than ~150 m, they become negative, which implies an overall increase of the freshwater lens volume as pumping removes salt water from underneath, thus promoting the downward flow of freshwater from recharge.

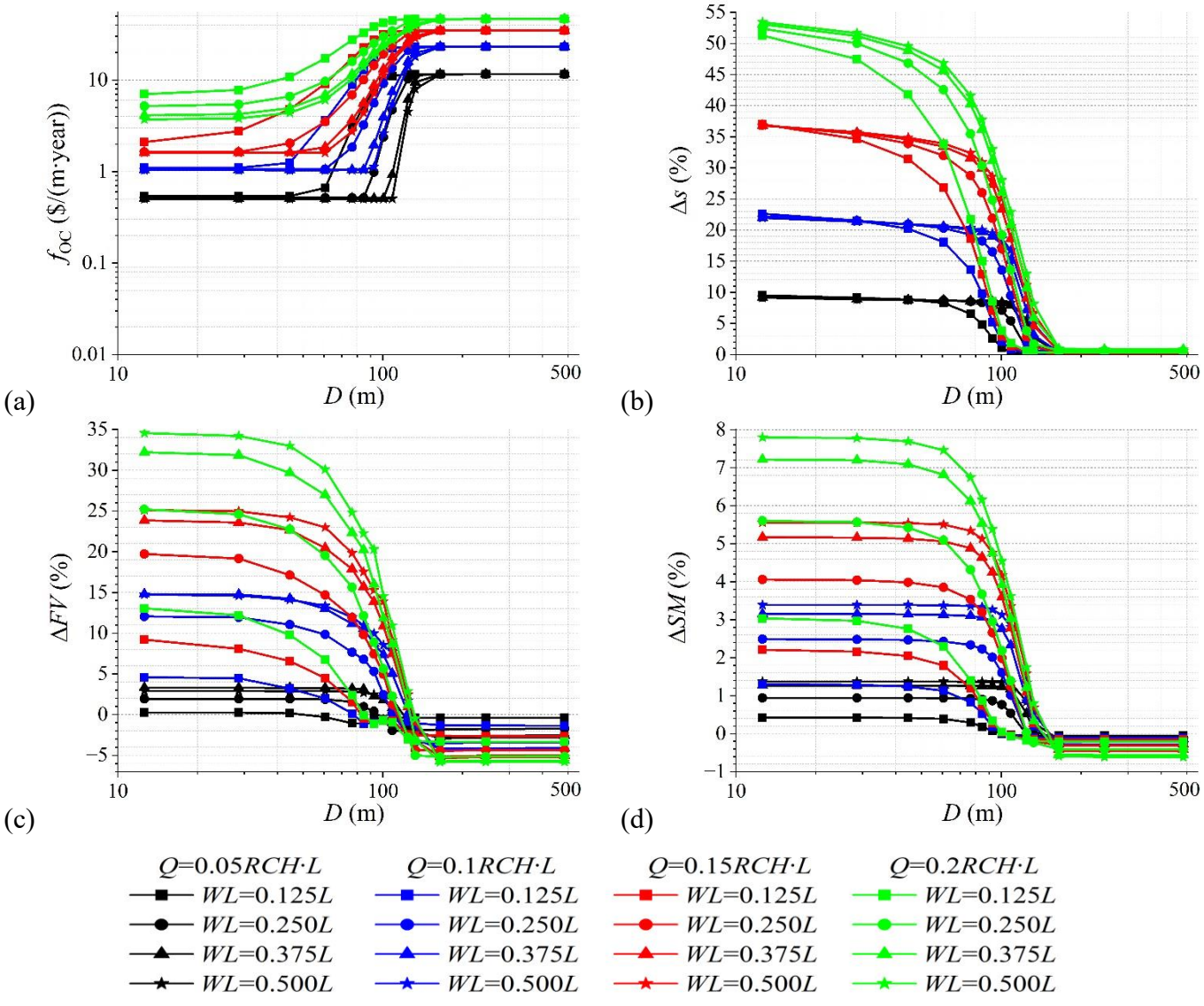

Figure 6. Profiles showing (a) the operation cost f_{OC} and the SWI indicators (b) Δs, (c) ΔFV and (d) ΔSM for 224 alternative pumping strategies. Legends for the profiles are presented at the figure bottom.

Altogether, the operating cost function f_{OC} and the SWI indicators presented in Figure 6 illustrates the inherent conflicts between the economic cost of groundwater supply and the

management SWI. On one hand, for any given demand Q, f_{OC} is minimized by selecting a shallow pumping system situated towards the centre of the island centre. On the other, to limit SWI indicators, such as Δs, ΔFV and ΔSM, it is necessary to select deeper pumping systems and closer to the shoreline, which may massively increase the operation cost due to desalination requirements.

3.3 Groundwater management under single SWI constraint scenarios

To investigate the impact of the constraints, Δs (Equation 8), ΔFV (Equation 10) and ΔSM (Equation 12), each constraint is first imposed separately. The cost-optimal pumping strategies determined by these constraints are thus selected and compared for progressively increasing (i.e., less stringent) values of the upper bounds Δs_{max}, ΔFV_{max} and ΔSM_{max}, as indicated in Table 3. For each scenario, the identification of the optimal pumping strategy requires first to determine the feasible set of pumping schemes that meet the considered SWI constraint among the pool of 224 SEAWAT model runs, and then to identify the strategy with the minimum f_{OC} value. The results of this analysis are presented in Figures 7 and 8.

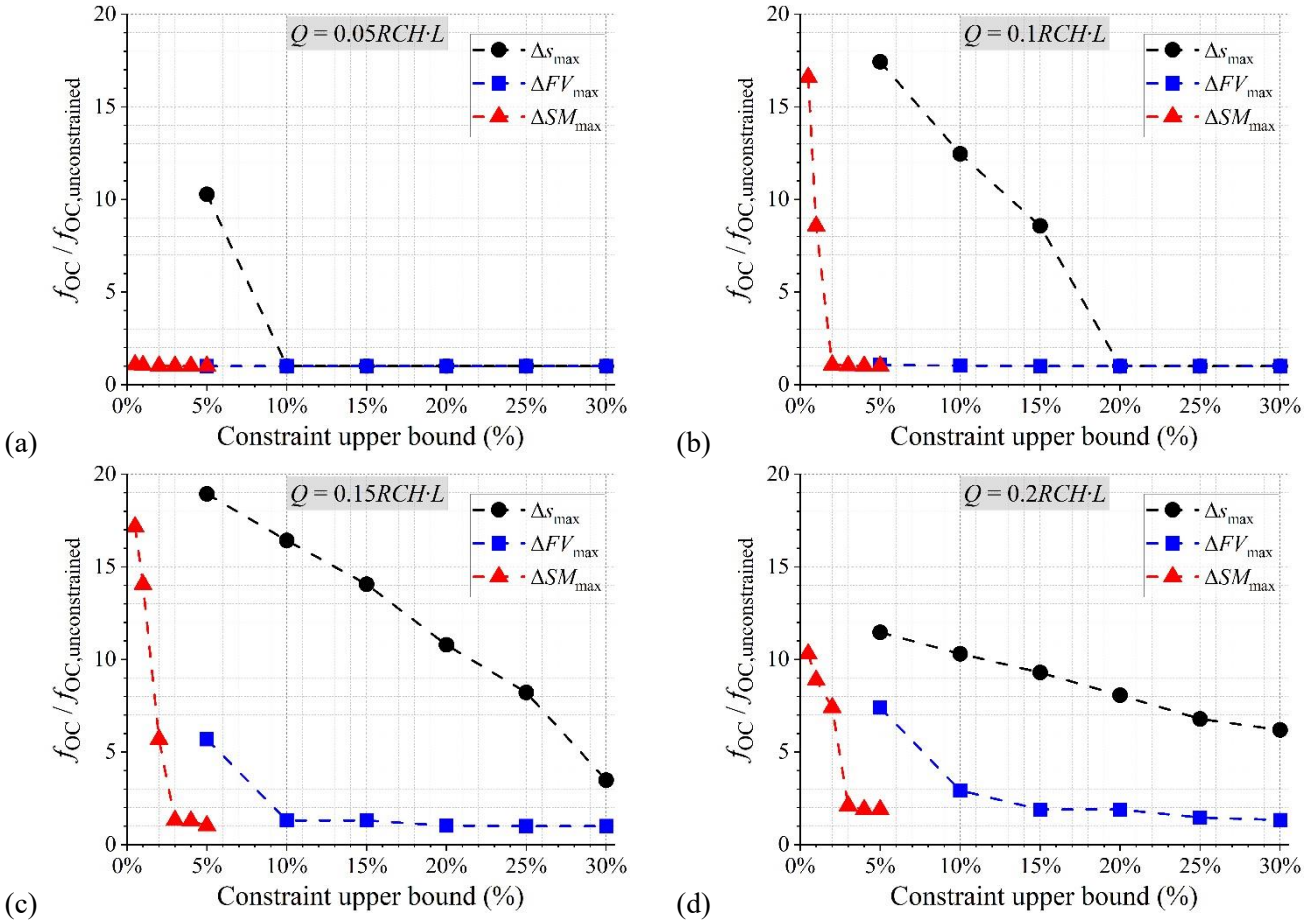

Figure 7. Trade-off profiles of the operation cost relative to unconstrained conditions vs. the upper bounds Δs_{max}, ΔFV_{max} and ΔSM_{max}, and for pumping rate ratios $Q/(RCH \cdot L)$ equal to (a) 0.05, (b) 0.1, (c) 0.15, and (d) 0.2.

Figure 7 shows profiles of the minimum operation cost under variable SWI constraints and pumping rate normalized by the recharge, that is, $Q/(RCH \cdot L)$. In each subpanel, the cost is scaled with respect to the cost under unconstrained conditions, that is, optimal-cost values calculated by imposing no limitations on SWI indicators. The unconstrained cost values, $f_{\mathrm{OC,u}}$, are 0.50, 1.04, 1.61, and 3.71 \$/(m·year) for pumping rate ratios of 0.05, 0.1, 0.15 and 0.2, respectively.

The profiles in Figure 7 illustrate the trade-offs existing between the management cost and the stringency of the SWI constraints adopted. It is worth observing that for low pumping rates (Figures 7a-b), the optimal cost may result in the same as in the unconstrained case (i.e., $f_{\mathrm{OC}}/f_{\mathrm{OC,u}} = 1$) when the constraint bound is large enough for the constraint to be "non-binding". Regardless of the selected pumping rate Q, the increase in cost due to the constraint is generally more pronounced in relation to $\Delta s_{\max}$, followed by $\Delta SM_{\max}$, and then by $\Delta FV_{\max}$, at least within the intervals of variability considered for these upper bounds (Table 3). Figure 7 shows that the relative cost $f_{\mathrm{OC}}/f_{\mathrm{OC,u}}$ is larger for $Q/(RCH \cdot L)$ values of 0.1 (subpanel b) and 0.15 (subpanel c), than for 0.2 (subpanel d), which reveals that the specific (per unit volume) cost of groundwater supply is a nonlinear function of the pumping rate. A detailed analysis of these effects is provided in Appendix C of the supporting material.

Figure 8 provides a representation of the cost-optimal pumping schemes identified in the tradeoff profiles in Figure 7 for pumping rate ratios $Q/(RCH \cdot L)$ equal to 0.1 (subpanels 8a-c-e) and 0.2 (subpanels 8b-d-f). In all subpanels, the unconstrained solution is also shown, which indicates that, with no SWI constraint, the pumping system should be positioned at the island center ($WL = 0.5 \cdot L$), and at a depth D that decreases with increasing Q.

Figures 8a-b show that when the SWI constraint (7) is made more stringent, that is, the bound for $\Delta s_{\max}$ is reduced, and the pumping rate Q is increased, the pumping system optimal location tends to shift first to a larger depth and then closer to the shoreline. As seen in Figure 7, this has a strong impact on the management cost since it strongly increases the need for desalination treatment. A quite different "pathway" is observed in Figures 8c-d. For $Q/(RCH \cdot L)$ equal to 0.1, where the optimal pumping location shifts from larger depth around the centre of the island, to shallower depth closer to the shoreline as the SWI constraint (9) is progressively tightened. A similar behaviour is observed for $Q/(RCH \cdot L)$ equal to 0.2, but when the constraint is most stringent, the optimal pumping location is found closer to the shoreline and at larger depth. This shows that to limit ΔFV, it is necessary to abstract groundwater at the fringes of the freshwater lens, where the water salinity is higher. Figures

8e-f exhibit some analogies with Figures 8c-d. If $Q/(RCH \cdot L) = 0.2$ and $\Delta SM_{\max}$ is set to 5%, or less, all cost-optimal pumping schemes are found nearby the shoreline, and at a depth D that increases with the pumping rate Q. In practice, to strongly limit ΔSM, it is convenient to extract water in regions of the aquifer where salinity is higher, that is, at the lateral and deeper fringes of the freshwater lens.

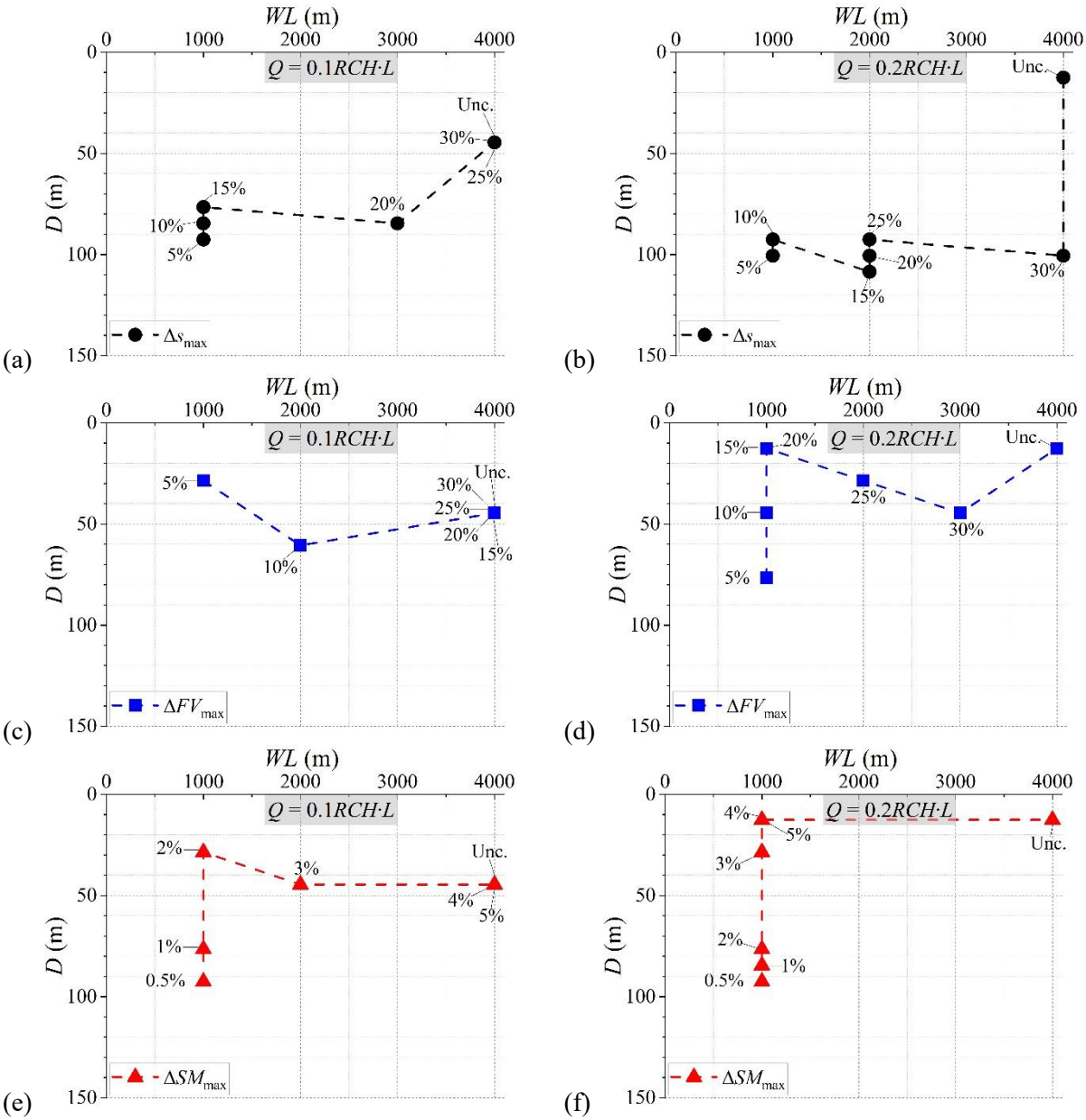

Figure 8. Representation of the location of the pumping system under the tradeoff profiles shown in Figure 7, for variable constraint scenarios for (a-b) $\Delta s_{\max}$, (c-d) $\Delta FV_{\max}$ and (e-f) $\Delta SM_{\max}$, and for pumping rate ratios $Q/(RCH \cdot L)$ equal to 0.1, and 0.2. Percentages represent the upper bounds of employed constraints while "Unc". denotes the unconstrained case.

These results underline that different SWI constraint indicators lead generally to the selection of quite different pumping schemes. As observed in the Δs, ΔFV and ΔSM profiles presented in Figures 6 and 7, SWI constraints on Δs lead to more cantered and deeper pumping

systems, whereas SWI constraints on ΔFV and/or ΔSM lead to relatively shallower pumping systems positioned towards the shoreline. The former are relatively more expensive than the latter, as they tend to produce groundwater with higher salt concentration, which has higher desalination requirements.

3.4 Investigation of optimal pumping strategies under multiple SWI constraints

This section investigates the solutions to the management problem subject to multiple SWI constraints. For each constraint indicator, three threshold values of $\Delta s_{\max}$, $\Delta FV_{\max}$ and $\Delta SM_{\max}$ are investigated. For combinations of two SWI constraints 12 scenarios are considered (Table 4), and for combinations of three SWI constraints 8 scenarios are considered (Table 5). Tables 6 and 7 summarize the cost-optimal management schemes under two and three concurrent SWI constraints, respectively.

In Table 6, Scenarios 1-4 report optimal cost values subject to concurrent constraints on Δs and ΔFV (inequalities 7 and 9). It is observed that constraints are generally non-binding if $Q = 0.05 \cdot RCH \cdot L$, and may affect the cost only for larger pumping rates. In these instances, for smaller values of $\Delta s_{\max}$ (10%), the constraint (7) is "binding", that is, satisfied with equality at the optimal solution ($\Delta s = \Delta s_{\max}$), whereas constraint (9) has no impact on the optimal cost (i.e., $\Delta FV < \Delta FV_{\max}$). Indeed, it should be noticed that if the optimal solution is driven exclusively by one constraint (e.g., Scenario 1), then any other scenario in which the other constraint bound is increased (e.g., Scenario 2) will provide the same optimal solution. For larger values of $\Delta s_{\max}$ (30%), constraint (9) is binding and affects the optimal cost jointly with constraint (7) if $\Delta FV_{\max}$ is set to 10% (Scenario 3) but has otherwise no impact if this is relaxed to 30% (Scenario 4).

Scenarios 5-8 report the optimal f_{OC} in the presence of constraints on Δs and ΔSM (inequalities 7 and 11). For $Q = 0.05 \cdot RCH \cdot L$, the optimal cost is affected only when $\Delta SM_{\max}$ is set to 1% (Scenarios 5 and 7), otherwise, the optimal solution is the unconstrained, that is, the constraints result non-binding. For larger values of Q, some of the SWI constraints may have an impact on the optimal cost. For example, for smaller values of $\Delta s_{\max}$ (10%), the constraint (7) results in binding (Scenarios 5 and 6), and for $Q = 0.15 \cdot RCH \cdot L$, it affects the optimal cost jointly with constraint (11) if $\Delta SM_{\max}$=1%. For larger values of $\Delta s_{\max}$ (30%), constraint (11) has an impact on the cost only if $\Delta SM_{\max}$ is set to 1% (Scenario 7). If $\Delta SM_{\max}$ equals 5%, the optimal cost depends only on the constraint (7) (Scenario 8).

Scenarios 9-12 report optimal f_{OC} values subject to joint constraints on ΔFV and ΔSM (inequalities 9 and 11). Although constraints result generally non-binding if Q is equal to $0.05 \cdot RCH \cdot L$, and affect the management cost only for larger pumping rates, it is observed that the constraint (11) results in binding if $\Delta SM_{\max}$ is set equal to 1% (Scenarios 9 and 11). For lower values of $\Delta FV_{\max}$ (10%), constraint (9) results in non-binding when $\Delta SM_{\max}$ equal to 1% (Scenario 9) and binding if $\Delta SM_{\max}$ equal to 5% (Scenario 10). Finally, for larger values of $\Delta FV_{\max}$ (30%), constraint (9) does not affect the cost, which depends only on constraint (11), that is, $\Delta SM_{\max}$ (Scenarios 11-12).

Table 6. *Optimal f_{OC} under the Different Combinations of Two Types of Constraint Conditions. (Cost values are provided with a superscript that represents the SWI constraints that result in binding for the optimal pumping scheme (e.g., "(7)" for constraint (7), "(7-9)" for constraints (7) and (9)). The "(U)" superscript denotes conditions in which none of the constraints is binding. The symbol "-" indicates an inactive constraint.)*

Scenario	$\Delta s_{\max}$ (7)	$\Delta FV_{\max}$ (9)	$\Delta SM_{\max}$ (11)	Optimal f_{OC} (\$/(m·year))			
				$\frac{Q}{RCH \cdot L} = 0.05$	$\frac{Q}{RCH \cdot L} = 0.1$	$\frac{Q}{RCH \cdot L} = 0.15$	$\frac{Q}{RCH \cdot L} = 0.2$
1	10%	10%	-	$0.50^{(U)}$	$12.91^{(7)}$	$26.36^{(7)}$	$38.17^{(7)}$
2	10%	30%	-	$0.50^{(U)}$	$12.91^{(7)}$	$26.36^{(7)}$	$38.17^{(7)}$
3	30%	10%	-	$0.50^{(U)}$	$1.06^{(9)}$	$9.13^{(7-9)}$	$25.15^{(7-9)}$
4	30%	30%	-	$0.50^{(U)}$	$1.04^{(U)}$	$5.59^{(7)}$	$22.93^{(7)}$
5	10%	-	1%	$0.52^{(11)}$	$12.91^{(7)}$	$27.54^{(7-11)}$	$38.17^{(7)}$
6	10%	-	5%	$0.50^{(U)}$	$12.91^{(7)}$	$26.36^{(7)}$	$38.17^{(7)}$
7	30%	-	1%	$0.52^{(11)}$	$8.88^{(11)}$	$22.56^{(11)}$	$32.94^{(11)}$
8	30%	-	5%	$0.50^{(U)}$	$1.04^{(U)}$	$5.59^{(7)}$	$22.93^{(7)}$
9	-	10%	1%	$0.52^{(11)}$	$8.88^{(11)}$	$22.56^{(11)}$	$32.94^{(11)}$
10	-	10%	5%	$0.50^{(U)}$	$1.06^{(9)}$	$2.09^{(9)}$	$10.83^{(9)}$
11	-	30%	1%	$0.52^{(11)}$	$8.88^{(11)}$	$22.56^{(11)}$	$32.94^{(11)}$
12	-	30%	5%	$0.50^{(U)}$	$1.04^{(U)}$	$1.64^{(11)}$	$7.02^{(11)}$

Table 6 reveals that, in most scenarios, the optimal f_{OC} and the corresponding feasible pumping scheme under two types of SWI constraints primarily hinge upon one dominant constraint, while the other remains ineffective. There exist, however, combinations of SWI constraints that result in joint binding of constraints (Scenarios 3 and 5). In these situations, the optimal solution needs to be "conservatively" within the intersection of the feasibility sets associated with the single constraints, which causes the minimum cost to increase.

Table 7 reports optimal cost values for the 12 combinations of the upper bounds $\Delta s_{\max}$, $\Delta FV_{\max}$ and $\Delta SM_{\max}$ associated with the SWI constraints (7), (9) and (11), respectively. It can be noticed that for lower pumping rates, that is, $Q = 0.05 \cdot RCH \cdot L$, the constraints have an impact on the cost only if $\Delta SM_{\max}$ is prescribed to be 1%, otherwise the unconstrained solution

holds (Table 6). For pumping rates of $0.1 \cdot RCH \cdot L$, or larger, the optimal cost is consistently driven by the constraint (7) if $\Delta s_{\max}$ is set to 10% (Scenarios 13-16) and may also depend on constraint (11) if $\Delta SM_{\max}$ is set to 1% (Scenarios 13 and 15). For $\Delta s_{\max}$ equal to 30% (Scenarios 17-20), the constraint (11) is consistently dominant if $\Delta SM_{\max}$ is set to 1% (Scenarios 17, 19). Otherwise, if $\Delta FV_{\max}$ is set to 10%, the constraint (9) is binding (Scenario 18). In cases where $\Delta FV_{\max}$ is set to 30% (Scenarios 19-20), the constraint (9) becomes non-binding, and the optimal cost depends either on constraints (7) or (11).

Table 7. *Optimal f_{OC} under the Different Combinations of Three Types of Constraint Conditions. (Optimal f_{OC} values are provided with a superscript that represents the SWI constraints that result in binding for the optimal pumping scheme (e.g., "(7)" for constraint (7), "(7-9)" for constraints (7) and (9)). The "(U)" superscript is used for the cost values in which none of the constraints is binding.)*

Scenario	$\Delta s_{\max}$ (7)	$\Delta FV_{\max}$ (9)	$\Delta SM_{\max}$ (11)	Optimal f_{OC} (\$/(m·year))			
				$\frac{Q}{RCH \cdot L} = 0.05$	$\frac{Q}{RCH \cdot L} = 0.1$	$\frac{Q}{RCH \cdot L} = 0.15$	$\frac{Q}{RCH \cdot L} = 0.2$
13	10%	10%	1%	$0.52^{(11)}$	$12.91^{(7)}$	$27.54^{(7\text{-}11)}$	$38.17^{(7)}$
14	10%	10%	5%	$0.50^{(U)}$	$12.91^{(7)}$	$26.36^{(7)}$	$38.17^{(7)}$
15	10%	30%	1%	$0.52^{(11)}$	$12.91^{(7)}$	$27.54^{(7\text{-}11)}$	$38.17^{(7)}$
16	10%	30%	5%	$0.50^{(U)}$	$12.91^{(7)}$	$26.36^{(7)}$	$38.17^{(7)}$
17	30%	10%	1%	$0.52^{(11)}$	$8.88^{(11)}$	$22.56^{(11)}$	$32.94^{(11)}$
18	30%	10%	5%	$0.50^{(U)}$	$1.06^{(9)}$	$9.13^{(7\text{-}9)}$	$25.15^{(7\text{-}9)}$
19	30%	30%	1%	$0.52^{(11)}$	$8.88^{(11)}$	$22.56^{(11)}$	$32.94^{(11)}$
20	30%	30%	5%	$0.50^{(U)}$	$1.04^{(U)}$	$5.59^{(7)}$	$22.93^{(7)}$

The comparison of the results in Tables 6 and 7, indicates that the scenarios limited by three types of constraint conditions often lead to the same optimal cost f_{OC} as those only constrained by only two of them. For example, the optimal strategies in Scenarios 13 and 15 are the same as those in Scenario 5, and Scenario 14 yields the same optimal solution as Scenarios 1 and 6. This shows that the optimal f_{OC} is still driven by a predominant constraint or jointly by two constraints, whereas the third constraint has no impact on the optimal pumping strategy. This can be generally attributed to the large upper bound for that constraint, which has little impact on the set of feasible pumping schemes. In some instances, however, a constraint may reduce SWI in a similar mode to another constraint, so that adding it has a limited impact on the optimal solution.

It is finally worth remarking that, based on the profiles in Figures 6b-6d, (a) constraint (7) tends to exclude shallow pumping and select pumping wells deeper into the freshwater lens; (b) both constraints (9) and (11) tend to exclude pumping near the island centre and favour well locations closer to the shoreline. As shown in Figure 8, optimal solutions under the constraint

$\Delta FV_{\max}$=20% are equivalent to those constrained with $\Delta SM_{\max}$=5%. Likewise, both cost-optimal pumping strategies and the feasible pumping schemes are nearly the same with constraints $\Delta FV_{\max}$=15% and $\Delta SM_{\max}$=4%. Therefore, the impact of constraint (9) on SWI control is practically equivalent to that of constraint (11). To reduce the complexity of management problems, the two constraints should not be adopted together. And if the SWI management is conducted with constraints on both Δs and ΔFV, the value of $\Delta FV_{\max}$ needs to be small enough to affect the selection of a pumping strategy.

4 Conclusions

This study investigated the trade-offs between the operational cost of groundwater supply and the sustainability of freshwater resources in island aquifers, considering a hydrogeological setting representative of San Salvador Island, Bahamas. Groundwater abstraction strategies have been characterized through three decision variables, the distance *WL* from the shoreline, the pumping depth *D*, and the pumping rate *Q*. The analysis has relied on the formulation of an optimisation problem, aiming to minimize the operation cost, given by the sum of the pumping cost and the desalination cost, subject to SWI constraints on aquifer drawdown above the pumping system, Δs, decrease of freshwater volume, ΔFV, and increase in salt mass within the aquifer, ΔSM. The investigation has been based on the analysis of a large set groundwater abstraction strategies, which has required as many as 224 steady-state SEAWAT model runs to calculate the optimal operation cost and the corresponding constraint variables.

Our investigation demonstrated that, in general, pumping at larger depth *D* leads to a reduced drawdown Δs, but also to an increased salt concentration *C* in the abstracted groundwater. As both the water table elevation and the freshwater lens thickness under natural conditions increase towards the island centre, pumping schemes with increasing *WL* led to an increased aquifer drawdown Δs and to a reduced salt concentration *C*. Accordingly, for any given *Q* and *D*, placing the pumping well system towards the island centre represents the best strategy to minimize the operation cost.

However, the formulated SWI indicators show that pumping in proximity to the island centre has a negative impact on the availability of freshwater resources in the aquifer, when compared to the effect of "decentralized" pumping strategies. This highlights an inherent conflict between SWI control and the economic cost of groundwater supply. When *Q* is a small fraction of the natural groundwater recharge, pumping does not violate limitations on SWI, and the optimal pumping strategy is the same as under unconstrained conditions. However, if *Q* is increased or constraints on SWI are tightened, the optimal pumping strategies are characterized

by larger pumping depth values and smaller distances from the shoreline to limit SWI, leading to higher operation costs.

In terms of SWI control, the impact of constraints on Δs on cost-optimal pumping strategies is quite different than that of constraints on ΔFV and ΔSM. Constraints on Δs are observed to lead to selecting deeper pumping systems located towards the island centre, whereas both the constraints on ΔFV and ΔSM favour the choice of shallower pumping systems closer to the shoreline. As a result, the pumping strategies under Δs constraints result generally more expensive than those under ΔFV and ΔSM constraints, as they involve extraction of groundwater with higher salinity that require more intense desalination treatment.

When the investigated SWI constraints are imposed concurrently, optimal pumping strategies are often driven by the most stringent of them. However, there may exist combinations of SWI bounds in which the most cost-effective pumping strategy depends jointly on more constraints, in which case the groundwater supply cost is higher than it would be if either constraint was selected separately. Our analysis has shown also that constraints on ΔFV and ΔSM exhibit a practical equivalence in terms of SWI control, and to reduce the complexity of management problems, they should not be adopted simultaneously in the optimisation formulation of the groundwater management problem.

One needs to be aware of potential limitations in the methods adopted in this study. First, the operation cost of groundwater supply is assumed to be driven exclusively by the energy required for the pumping and the desalination of groundwater by reverse osmosis but does not account for other processes of water resource management, for example, brine disposal, water distribution and wastewater treatment. While the economic impact of processes that have been overlooked may be significant, the cost of groundwater desalination typically constitutes the most important component on which groundwater management depends, and this provides a firm basis for the transferability of the results of this study to most common island aquifer settings.

In this paper, we focused on exploring the trade-offs between the operation cost of groundwater supply and different formulations of SWI constraints using a simplified 2D representation. Although we are aware that a 2D model may not fully capture the complexity of real-world 3D systems with multiple pumping wells, we intentionally chose this approach to ensure computational viability and feasibility within the scope of our study. We simplified the pumping system by conceptualizing it as a horizontal sink, assuming a uniform distribution of groundwater abstraction along it. While this approach may underestimate aquifer drawdown

in individual wells, it allowed us to consider fewer decision variables and conduct a reasonably simplified analysis of management cost and constraint formulation. As a result, our findings are intended to be generic to island aquifers, even though they are based on the general characteristics of a specific site. As such, this analysis serves as a crucial initial step towards developing more sophisticated models that can effectively address the optimisation challenges associated with groundwater management in real-world island aquifers, such as the one of San Salvador Island.

APPENDIX A. Energy consumption for water desalination by reverse-osmosis.

As reverse osmosis (RO) is the most popular technique for desalinating brackish water and seawater in coastal groundwater management (Abd-Elhamid & Javadi, 2011; Hussain et al., 2019) it is the method considered in this work to treat groundwater whose salt concentration exceeds accepted potability standards. The specific (per unit mass) energy consumption for desalination SEC [L^2T^{-2}] by RO is estimated as (Stillwell & Webber, 2016):

$$SEC(C) = \frac{R \cdot T_s}{M_w} \cdot \left\{ \frac{x_{sF} - x_{sP}}{x_{sB} - x_{sF}} \cdot \left[x_{sB} \cdot \ln\left(\frac{x_{sB}}{x_{sF}}\right) + x_{wB} \cdot \ln\left(\frac{x_{wB}}{x_{wF}}\right) \right] + \left[x_{sP} \cdot \ln\left(\frac{x_{sP}}{x_{sF}}\right) + x_{wP} \cdot \ln\left(\frac{x_{wP}}{x_{wF}}\right) \right] \right\} \quad \text{(A1)}$$

where R is the universal gas constant, T_s is the saturation absolute temperature [K], and M_w is the water molecular weight [e.g., M/mole]. The symbols x represents mole fractions [/], with the subscripts "s" and "w" referring to salt and water, respectively. The subscript F indicates the "feed", that is, the water abstracted that undergoes desalination; the subscript P stands for "permeate", that is, the water distributed to users after desalination; and the subscript B denotes "brine", that is, the by-product high salinity water produced by RO, which is typically disposed.

The salt mole fraction of the feed, x_{sF}, can be calculated from the feed water concentration C as (Avlonitis et al., 2012):

$$x_{sF} = \frac{C/M_s}{C/M_s + [\rho_w(C) - C]/M_w} \quad \text{(A2)}$$

where M_s is the salt molecular weight [M/mole]. The water mole fraction of the feed x_{wF} is:

$$x_{wF} = 1 - x_{sF} \quad \text{(A3)}$$

The mole fractions of the permeate, x_{sP} and x_{wP}, are obtained using Equations (A2-A3) with C equal to the target concentration C_d in the permeate, assumed to be 1.0 g/l. Likewise, the mole fractions for the brine, x_{sB} and x_{wB}, are calculated using Equations (A2-A3), with C equal to the brine concentration C_b, whose value varies depending on the adopted desalination system. If this is designed to provide a fixed recovery ratio r between the flow rate Q_d sent to water users and the feed flow rate Q ($r = Q_d/Q$), then the brine mole fractions can be derived by combining the mass balance equations of water and salt for the treatment plant (Avlonitis et al., 2012):

$$x_{sB} = \frac{x_{sF} - r x_{sP}}{1 - r} \quad \text{(A4)}$$

$$x_{wB} = \frac{1 - x_{sF} - r x_{wP}}{1 - r} \quad \text{(A5)}$$

The resulting brine concentration can then be calculated as:

$$C_b = \frac{1}{1-r} \cdot C - \frac{r}{1-r} \cdot C_d \quad \text{(A6)}$$

Equation (A6) shows that C_b may result in excessively large for high recovery ratios (e.g., $r >$ 0.8) and large feed concentrations C, which ultimately leads to cost-ineffective energy consumption (Squire, 2000). On the other hand, if the feed concentration C is slightly above the target C_d, large quantities of brine with relatively low concentration are discarded, which may result in cost-ineffective as well.

If the desalination system is designed to achieve a fixed brine concentration C_b, Equations (A2-A3) with C=C_b are still valid, but the recovery ratio r results in a function of the feed concentrations C, which is obtained from Equation (A6) as:

$$r = \frac{C_b - C}{C_b - C_d} \quad \text{(A7)}$$

In this work, we adopt the latter approach, and select a fixed brine concentration value C_b of 150.0 g/l (Ahunbay, 2019; Azerrad et al., 2019). For $C_d = 1$ g/l, and C ranging from 1 to 35 g/l, r values vary between 0.77 and 1 (Equation A7).

APPENDIX B. Pump costs associated with various pumping intensities.

To distinguish the effects of DVs on f_p, Figure B1 presents the profiles of f_p for Q values equal to $0.05RCH \cdot L$ (subpanel B1a), $0.1RCH \cdot L$ (subpanel B1b), $0.15RCH \cdot L$ (subpanel B1c) and $0.2RCH \cdot L$ (subpanel B1d). In general, the pumping cost f_p is larger if the pumping rate Q increases, and smaller if WL increases. These profiles show that with the pumping depth D increasing, f_p first drops slightly before increasing dramatically and then keeps nearly constant. The behaviour of f_p reducing at the lower D, between 12.6 m and ~100 m, becomes more obvious with Q increasing (e.g., Figures B1c and B1d). These trends are explained by observing the behaviour of h in the DV space (D, WL, Q), as shown in Figure 5a, and noting the dependency of f_p on h and Q in Equation 2.

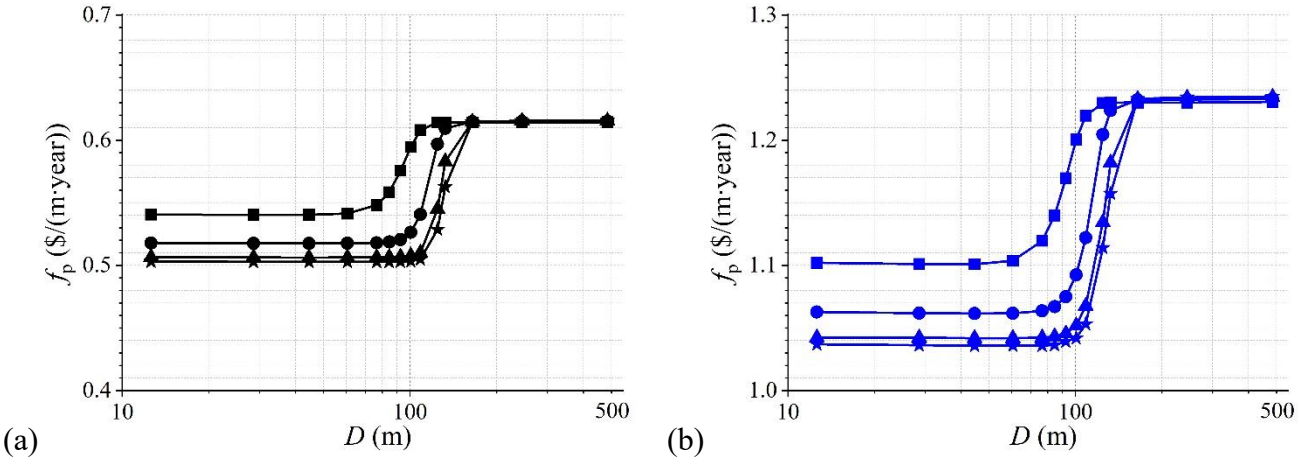

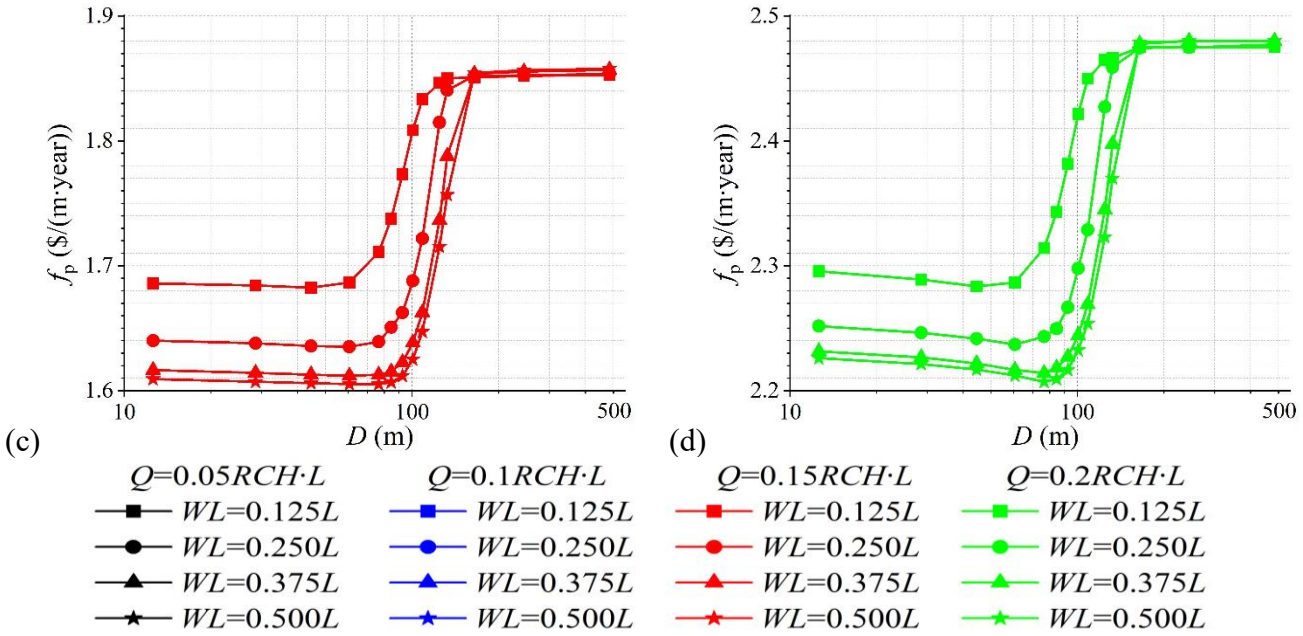

Figure B1. Profiles of f_p under variable Q for (a) $0.05RCH \cdot L$, (b) $0.1RCH \cdot L$, (c) $0.15RCH \cdot L$ and (d) $0.2RCH \cdot L$.

APPENDIX C. Cost per unit water under variable constraint scenarios.

It is worth highlighting that, in Figure 7, since the overall groundwater supply cost increases nonlinearly depending on the stringency of the adopted SWI constraints, and since the recovery ratio r (Equation A7) depends on the solute concentration C, the cost per unit water volume delivered to users, that is, $\bar{f}_{OC}=f_{OC}/(r \cdot Q)$ ($/m^3), results in a complex nonlinear function of constraint bounds Δs_{max}, ΔFV_{max} and ΔSM_{max}.

Figure C1 presents the profiles of $\bar{f}_{OC}$ calculated for each selected Q and for variable constraint bounds Δs_{max} (subpanel C1a), ΔFV_{max} (subpanel C1b) and ΔSM_{max} (subpanel C1c). These profiles show that, for any given Q, the optimal $\bar{f}_{OC}$ generally increases from unconstrained conditions to more and more stringent SWI bounds Δs_{max}, ΔFV_{max} and ΔSM_{max}. For smaller values of Q, the set constraints result in non-binding and $\bar{f}_{OC}$ remains the same as in the unconstrained case. However, if the SWI bounds are prescribed below a certain threshold, then the constraints become binding and the optimal pumping strategy inevitably involves the abstraction of groundwater with a salt concentration C that requires treatment, which has a major impact on f_{OC} (Equation 3) and also implies a reduced recovery ratio r (Equation A7), which further increases $\bar{f}_{OC}$. Comparison of the profiles in Figures C1a, C1b and C1c also confirm that $\bar{f}_{OC}$ is generally more sensitive to constraints on Δs, than it is to constraints on ΔSM, or ΔFV.

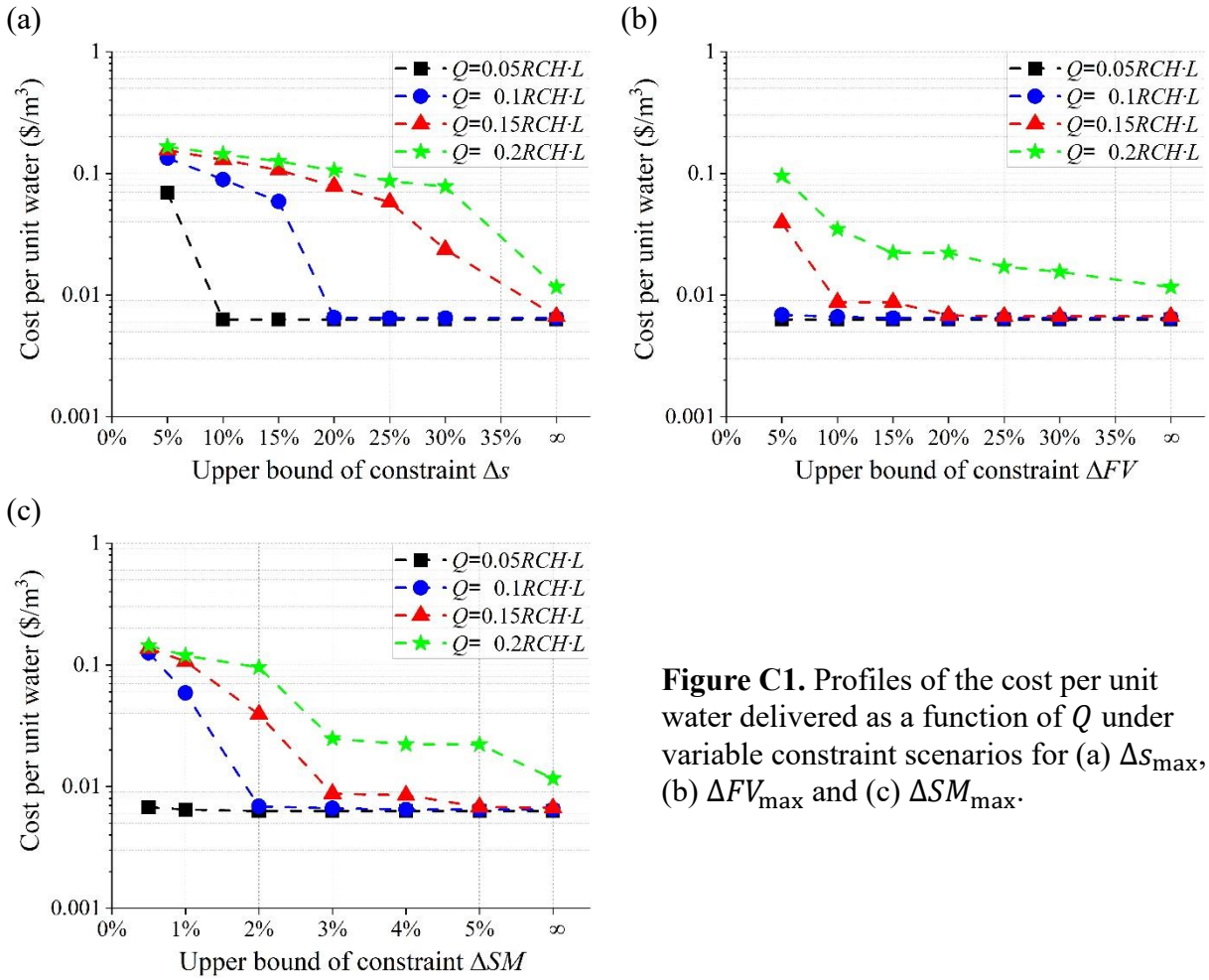

Figure C1. Profiles of the cost per unit water delivered as a function of Q under variable constraint scenarios for (a) $\Delta s_{\max}$, (b) $\Delta FV_{\max}$ and (c) $\Delta SM_{\max}$.

Acknowledgements

The authors have no relevant financial or non-financial interests to declare that are relevant to the content of this article. This work was partially supported by the EPSRC grant no. EP/T018542/1, and the NSF under grant agreement CBET-EPSRC 2022278. The authors also would like to thank the editor, Dr. Georgios Kourakos and two other anonymous reviewers for their kind feedback and insightful comments, which helped improve the clarity of this paper.

Open Research

Data – The input file for modelling SWI in the 2D simplified San Salvador Island aquifer can be found in Yu et al. (2023).

Software – Salinity distribution in the island aquifer during pumping was simulated using version 4 of the SEAWAT groundwater software (United States Geological Survey, 2012).

References

Fetter, C. W. (1972). Position of the saline water interface beneath oceanic islands. *Water Resources Research*, *8*(5), 1307–1315. https://doi.org/10.1029/WR008i005p01307

Kishi, Y., & Fukuo, Y. (1977). Studies on salinization of groundwater, I: Theoretical consideration on the three-dimensional movement of the salt water interface caused by the pumpage of confined groundwater in fanshaped alluvium. *Journal of Hydrology*, *35*(1), 1-29. https://doi.org/10.1016/0022-1694(77)90074-9

Davis, R. L. & Johnson, C. R. (1989). Karst Hydrology of San Salvador. In Mylroie, J.E. (Ed.), Proceedings of the Fourth Symposium on the Geology of the Bahamas. Bahamian Field Station, San Salvador Island, Bahamas, pp. 118–135.

McKinney, D. C., & Lin, M. D. (1994). Genetic algorithm solution of groundwater management models. *Water Resources Research*, *30*(6), 1897-1906. https://doi.org/10.1029/94WR00554

Squire, D. (2000). Reverse osmosis concentrate disposal in the UK. *Desalination*, *132*(1), 47-54. https://doi.org/10.1016/S0011-9164(00)00134-X

Mayer, A. S., Kelley, C. T., & Miller, C. T. (2002). Optimal design for problems involving flow and transport phenomena in saturated subsurface systems. *Advances in Water Resources*, *25*(8), 1233–1256. https://doi.org/10.1016/S0309-1708(02)00054-4

Qahman, K., Larabi, A., Ouazar, D., Naji, A., & Cheng, A. H. D. (2005). Optimal and sustainable extraction of groundwater in coastal aquifers. *Stochastic Environmental Research and Risk Assessment*, *19*(2), 99-110. https://doi.org/10.1007/s00477-004-0218-0

Baú, D. A., & Mayer, A. S. (2006). Stochastic management of pump-and-treat strategies using surrogate functions. *Advances in Water Resources*, *29*(12), 1901–1917. https://doi.org/10.1016/j.advwatres.2006.01.008

Ferreira da Silva, J. F., & Haie, N. (2007). Optimal locations of groundwater extractions in coastal aquifers. *Water Resources Management*, *21*(8), 1299-1311. https://doi.org/10.1007/s11269-006-9082-7

Langevin, C. D., Thorne, D. T., Jr. Dausman, A. M., Sukop, M. C., & Guo, W. (2007). SEAWAT Version 4: A Computer Program for Simulation of Multi-Species Solute and Heat Transport: U.S. Geological Survey Techniques and Methods Book 6, Chapter A22, 39 p., https://doi.org/10.3133/tm6A22

Bray, B. S., & Yeh, W. W. G. (2008). Improving seawater barrier operation with simulation optimisation in southern California. *Journal of Water Resources Planning and Management*, *134*(2), 171–180. https://doi.org/10.1061/(ASCE)0733-9496(2008)134:2(171)

Martin, J. B., & Moore, P. J. (2008). Sr concentrations and isotope ratios as tracers of ground-water circulation in carbonate platforms: Examples from San Salvador Island and Long Island, Bahamas. *Chemical Geology*, *249*(1), 52-65. https://doi.org/10.1016/j.chemgeo.2007.11.009

Moore, P. J. (2009). Controls on the generation of secondary porosity ineogenetic karst: examples from San Salvador Island, Bahamas and north-central Florida, USA, (Doctoral dissertation). Gainesville, FL: University of Florida.

McGee, D. K., Wynn, J. G., Onac, B. P., Harries, P. J., & Rothfus, E. A. (2010). Tracing groundwater geochemistry using $\delta^{13}C$ on San Salvador Island (southeastern Bahamas): implications for carbonate island hydrogeology and dissolution. *Carbonates Evaporites*, *25*(2), 91–105. https://doi.org/10.1007/s13146-010-0013-6

Abd-Elhamid, H. F., & Javadi, A. A. (2011). A cost-effective method to control seawater intrusion in coastal aquifers. *Water Resources Management*, *25*, 2755–2780. https://doi.org/10.1007/s11269-011-9837-7

Jakovovic, D., Post, V. E. A., Werner, A. D., Männicke, O., Hutson, J. L., & Simmons, C. T. (2011). Tracer adsorption in sand-tank experiments of saltwater up-coning. *Journal of Hydrology*, *414-415*, 476-481. https://doi.org/10.1016/j.jhydrol.2011.11.024

Kourakos, G., & Mantoglou, A. (2011). Simulation and multi-objective management of coastal aquifers in semi-arid regions. *Water Resources Management*, *25*(4), 1063-1074. https://doi.org/10.1007/s11269-010-9677-x

Sedki, A., & Ouazar, D. (2011). Simulation-optimisation modeling for sustainable groundwater development: a Moroccan Coastal aquifer case study. *Water Resources Management*, *25*(11), 2855-2875. https://doi.org/10.1007/s11269-011-9843-9

Avlonitis, S. A., Avlonitis, D. A., & Panagiotidis, Th. (2012). Experimental study of the specific energy consumption for brackish water desalination by reverse osmosis. *International Journal of Energy Research*, *36*, 36-45. https://doi.org/10.1002/er.1780

Javadi, A. A., Abd-Elhamid, H. F., & Farmani, R. (2012). A simulation-optimisation model to control seawater intrusion in coastal aquifers using abstraction/recharge wells. *International Journal for Numerical and Analytical Methods in Geomechanics*, *36*(16), 1757-1779. https://doi.org/10.1002/nag.1068

United States Geological Survey (2012). SEAWAT: A Computer Program for Simulation of Three-Dimensional Variable-Density Ground-Water Flow and Transport [software]. U.S. Geological Survey Software Release, https://www.usgs.gov/software/seawat-computer-program-simulation-three-dimensional-variable-density-ground-water-flow

Kourakos, G., & Mantoglou, A. (2013). Development of a multi-objective optimisation algorithm using surrogate models for coastal aquifer management. *Journal of Hydrology*, *479*, 13-23. https://doi.org/10.1016/j.jhydrol.2012.10.050

Ho, H. C., Mylroie, J. E., Infante, L. R., & Rodgers, J. C. (2014). Fuzzy-based spatial modeling approach to predict island karst distribution: a conceptual model. *Environmental Earth Sciences*, *71*(3), 1369–1377. https://doi.org/10.1007/s12665-013-2543-4

Tomaszkiewicz, M., Abou Najm, M., & El-Fadel, M. (2014). Development of a groundwater quality index for seawater intrusion in coastal aquifers. *Environmental Modelling & Software*, *57*, 13-26. https://doi.org/10.1016/j.envsoft.2014.03.010

Botero-Acosta, A., & Donado, L. D. (2015). Laboratory scale simulation of hydraulic barriers to seawater intrusion in confined coastal aquifers considering the effects of stratification. *Procedia Environmental Sciences*, *25*, 36-43. https://doi.org/10.1016/j.proenv.2015.04.006

Holding, S., & Allen, D. M. (2015). From days to decades: numerical modelling of freshwater lens response to climate change stressors on small low-lying islands. *Hydrology and Earth System Sciences*, *19*(2), 933–949. https://doi.org/10.5194/hess-19-933-2015

Javadi, A., Hussain, M., Sherif, M., & Farmani, R. (2015). Multi-objective optimisation of different management scenarios to control seawater intrusion in coastal aquifers. *Water Resources Management*, *29*(6), 1843-1857. https://doi.org/10.1007/s11269-015-0914-1

Karatzas, G. P., & Dokou, Z. (2015). Optimal management of saltwater intrusion in the coastal aquifer of Malia, Crete (Greece), using particle swarm optimisation. *Hydrogeology Journal*, *23*(6), 1181–1194. https://doi.org/10.1007/s10040-015-1286-6

Ketabchi, H., & Ataie-Ashtiani, B. (2015). Evolutionary algorithms for the optimal management of coastal groundwater: A comparative study toward future challenges. *Journal of Hydrology*, *520*, 193-213. https://doi.org/10.1016/j.jhydrol.2014.11.043

Kourakos, G., & Mantoglou, A. (2015). An efficient simulation-optimisation coupling for management of coastal aquifers. *Hydrogeology Journal*, *23*, 1167–1179. https://doi.org/10.1007/s10040-015-1293-7

Park, N., & Shi, L. (2015). A comprehensive sharp-interface simulation-optimisation model for fresh and saline groundwater management in coastal areas. *Hydrogeology Journal*, *23*(6), 1195–1204. https://doi.org/10.1007/s10040-015-1268-8

Zekri, S., Triki, C., Al-Maktoumi, A., & Bazargan-Lari, M. R. (2015). An optimisation-simulation approach for groundwater abstraction under recharge uncertainty. *Water Resources Management*, *29*(10), 3681-3695. https://doi.org/10.1007/s11269-015-1023-x

Christelis, V., & Mantoglou, A. (2016). Pumping optimisation of coastal aquifers assisted by adaptive metamodelling methods and radial basis functions. *Water Resources Management*, *30*(15), 5845-5859. https://doi.org/10.1007/s11269-016-1337-3

Gulley, J. D., Mayer, A. S., Martin, J. B., & Bedekar, V. (2016). Sea level rise and inundation of island interiors: Assessingimpacts of lake formation and evaporationon water resources in arid climates. *Geophysical Research Letters*, *43*(18), 9712-9719. https://doi.org/10.1002/2016GL070667

Roy, T., Schütze, N., Grundmann, J., Brettschneider, M., & Jain, A. (2016). Optimal groundwater management using state-space surrogate models: a case study for an arid coastal region. *Journal of Hydroinformatics*, *18*(4), 666-686. https://doi.org/10.2166/hydro.2016.086

Stillwell, A. S., & Webber, M. E. (2016). Predicting the specific energy consumption of reverse osmosis desalination. *Water*, *8*(12), 601. https://doi.org/10.3390/w8120601

Abdoulhalik, A., Ahmed, A., & Hamill, G. A. (2017). A new physical barrier system for seawater intrusion control. *Journal of Hydrology*, *549*, 416-427. https://doi.org/10.1016/j.jhydrol.2017.04.005

Rajabi, M. M., & Ketabchi, H. (2017). Uncertainty-based simulation-optimisation using Gaussian process emulation: Application to coastal groundwater management. *Journal of Hydrology*, *555*, 518-534. https://doi.org/10.1016/j.jhydrol.2017.10.041

Stratis, P. N., Dokou, Z. A., Karatzas, G. P., Papadopoulou, E. P., & Saridakis, Y. G. (2017). PTC simulations, stochastic optimisation and safety strategies for groundwater pumping management: case study of the Hersonissos Coastal Aquifer in Crete. *Applied Water Science*, *7*(5), 2425-2435. https://doi.org/10.1007/s13201-016-0438-8

Triki, C., Zekri, S., Al-Maktoumi, A., & Fallahnia, M. (2017). An artificial intelligence approach for the stochastic management of coastal aquifers. *Water Resources Management*, *31*(15), 4925-4939. https://doi.org/10.1007/s11269-017-1786-3

Kazakis, N., Spiliotis, M., Voudouris, K., Pliakas, F. K., & Papadopoulos, B. (2018). A fuzzy multicriteria categorization of the GALDIT method to assess seawater intrusion vulnerability of coastal aquifers. *Science of the Total Environment*, *621*, 524–534. https://doi.org/10.1016/j.scitotenv.2017.11.235

Pramada, S. K., Mohan, S., & Sreejith, P. K. (2018). Application of genetic algorithm for the groundwater management of a coastal aquifer. *ISH Journal of Hydraulic Engineering*, *24*(2), 124-130. https://doi.org/10.1080/09715010.2017.1378597

Song, J., Yang, Y., Wu, J., Wu, J., Sun, X., & Lin, J. (2018). Adaptive surrogate model based multiobjective optimisation for coastal aquifer management. *Journal of Hydrology*, *561*, 98-111. https://doi.org/10.1016/j.jhydrol.2018.03.063

Yang, Y., Wu, J., Lin, J., Wang, J., Zhou, Z., & Wu, J. (2018). An efficient simulation–optimisation approach for controlling seawater intrusion. *Journal of Coastal Research*, *84*(sp1), 10-18. https://doi.org/10.2112/SI84-002.1

Ahunbay, M. G. (2019). Achieving high water recovery at low pressure in reverse osmosis processes for seawater desalination. *Desalination*, *465*, 58–68. https://doi.org/10.1016/j.desal.2019.04.023

Azerrad, S. P., Isaacs, M., & Dosoretz, C. G. (2019). Integrated treatment of reverse osmosis brines coupling electrocoagulation with advanced oxidation processes. *Chemical Engineering Journal*, *356*, 771–780. https://doi.org/10.1016/j.cej.2018.09.068

Christelis, V., & Mantoglou, A. (2019). Pumping optimisation of coastal aquifers using seawater intrusion models of variable-fidelity and evolutionary algorithms. *Water Resources Management*, *33*(2), 555-568. https://doi.org/10.1007/s11269-018-2116-0

Hussain, M. S., Abd-Elhamid, H. F., Javadi, A. A., & Sherif, M. M. (2019). Management of seawater intrusion in coastal aquifers: a review. *Water*, *11*(12), 2467. https://doi.org/10.3390/w11122467

Kopsiaftis, G., Christelis, V., & Mantoglou, A. (2019). Comparison of sharp interface to variable density models in pumping optimisation of coastal aquifers. *Water Resources Management*, *33*(4), 1397-1409. https://doi.org/10.1007/s11269-019-2194-7

Motallebian, M., Ahmadia, H., Raoof, A., & Cartwright, N. (2019). An alternative approach to control saltwater intrusion in coastal aquifers using a freshwater surface recharge canal. *Journal of Contaminant Hydrology*, *222*, 56–64. https://doi.org/10.1016/j.jconhyd.2019.02.007

Ranjbar, A., & Mahjouri, N. (2019). Multi-objective freshwater management in coastal aquifers under uncertainty in hydraulic parameters. *Natural Resources Research*, *29*(4), 2347-2368. https://doi.org/10.1007/s11053-019-09585-3

Yao, Y., Andrews, C., Zheng, Y., He, X., Babovic, V., & Zheng, C. (2019). Development of fresh groundwater lens in coastal reclaimed islands. *Journal of Hydrology*, *573*, 365–375. https://doi.org/10.1016/j.jhydrol.2019.03.062

Dey, S., & Prakash, O. (2020). Managing saltwater intrusion using conjugate sharp interface and density dependent models linked with pumping optimisation. *Groundwater for Sustainable Development*, *11*, 100446. https://doi.org/10.1016/j.gsd.2020.100446

El-Ghandour, H. A., & Elbeltagi, E. (2020). Pumping optimisation of coastal aquifers using probabilistic search – case study: Quaternary aquifer of El-Arish Rafah, Egypt. *Hydrology Research*, *51*(1), 90-104. https://doi.org/10.2166/nh.2019.093

Fan, Y., Lu, W., Miao, T., Li, J., & Lin, J. (2020). Multiobjective optimisation of the groundwater exploitation layout in coastal areas based on multiple surrogate models. *Environmental Science and Pollution Research*, *27*(16), 19561-19576. https://doi.org/10.1007/s11356-020-08367-2

Jasechko, S., Perrone, D., Seybold, H., Fan, Y., & Kirchner, J. W. (2020). Groundwater level observations in 250,000 coastal US wells reveal scope of potential seawater intrusion. *Nature Communications*, *11*, 3229. https://doi.org/10.1038/s41467-020-17038-2

Roy, D. K., & Datta, B. (2020). Modelling and management of saltwater intrusion in a coastal aquifer system: A regional-scale study. *Groundwater for Sustainable Development*, *11*, 100479. https://doi.org/10.1016/j.gsd.2020.100479

Yin, J., Pham, H. V., & Tsai, F. T. C. (2020). Multiobjective spatial pumping optimisation for groundwater management in a multiaquifer system. *Journal of Water Resources Planning and Management*, *146*(4), 04020013. https://doi.org/10.1061/(ASCE)WR.1943-5452.0001180

Agoubi B. (2021) A review: saltwater intrusion in North Africa's coastal areas-current state and future challenges. *Environmental Science and Pollution Research*, 8(14), 17029-17043. https://doi.org/10.1007/s11356-021-12741-z

Yang, Y., Song, J., Simmons, C. T., Ataie-Ashtiani, B., Wu, J., Wang, J., & Wu, J. (2021). A conjunctive management framework for the optimal design of pumping and injection strategies to mitigate seawater intrusion. *Journal of Environmental Management*, *282*, 111964. https://doi.org/10.1016/j.jenvman.2021.111964

Beheshti, J., Javadi, S., Hosseini, S. A., & Moghaddam, H. K. (2022). Evaluation of strategies for pumping optimisation of coastal aquifers using numerical simulation and game theory. *Environmental Earth Sciences*, *81*, 340. doi: https://doi.org/10.1007/s12665-022-10459-w

Coulon, C., Lemieux, J.-M., Pryet, A., Bayer, P., Young, N. L., & Molson, J. (2022) Pumping optimisation under uncertainty in an island freshwater lens using a sharp-interface seawater intrusion model. *Water Resources Research*, *58*(8), e2021WR031793. https://doi.org/10.1029/2021WR031793

Yu, W., Baù, D., Mayer, A. S., Mancewicz, L. & Geranmehr, M. (2023). Dataset for 'Investigating the impact of seawater intrusion on the operation cost of groundwater supply in island aquifers' [Dataset]. Figshare. https://doi.org/10.6084/m9.figshare.23862975.v1

Chapter 3

Efficient approaches for offline and online training of Gaussian Process models in multi-objective island groundwater management

Publications included in this chapter:

Yu, W., Baù, D., Mayer, A.S. and Geranmehr, M. Efficient approaches for offline and online training of GP models in multi-objective island groundwater management (intended for publication).

Efficient approaches for offline and online training of Gaussian Process models in multi-objective island groundwater management

Weijiang Yu[1*], Domenico Baù[1], Alex S. Mayer[2], Mohammadali Geranmehr[1]

[1]Department of Civil and Structural Engineering, University of Sheffield, Sheffield, UK.
[2]Department of Civil Engineering, University of Texas at El Paso, USA.
*Corresponding author: Weijiang Yu (wyu18@sheffield.ac.uk)

Abstract

Coastal groundwater management presents challenges that can be addressed through the integration of optimisation algorithms and computationally intensive groundwater flow simulators. However, these simulators, although accurate, often demand significant computational resources, prompting the exploration of surrogate models. These surrogates, which stem from the original simulators using a set of training points, balance the dual requirements of accuracy and computational efficiency. The selection of an appropriate sampling method is pivotal to this process, ensuring the desired accuracy while ensuring computational efficiency. Both offline and online training approaches have been proposed. Offline training involves developing surrogates before optimisation, often using training datasets that cover the input space either uniformly or randomly, which can prove inefficient due to potential oversampling of low-gradient areas and under sampling of high-gradient areas. In contrast, online training updates surrogates iteratively during optimisation, which may become a challenge in groundwater management scenarios involving multiple objectives that involve multiple non-dominated solutions. This study aims to explore efficient strategies for training surrogates in the context of coastal groundwater management. To this end, a two-objective pumping optimisation problem is initially formulated based on hydrogeological conditions observed on San Salvador Island, Bahamas. Gaussian Process (GP) techniques are employed to construct model surrogates, and three offline training strategies, as well as four online training strategies, for building GP models to solve the optimisation problem, are respectively proposed. For any given pumping scheme, GP models predict its management objectives and constraint values, alongside quantifying associated uncertainties. By conducting repeated Monte Carlo simulations using these GP models, it becomes possible to ascertain the probability of Pareto-optimality for each pumping scheme. Performance assessment of each training strategy involves determining the average probability of Pareto-optimality and evaluating the correlation between predictions. The findings of this study highlight the effectiveness of both offline and online training strategies in constructing GP models that yield reliable Pareto-optimal solutions. Furthermore, the study sheds light on the advantages and

disadvantages of employing offline and online-trained surrogate models in the realm of coastal groundwater management.

Key words: offline training; online training; Gaussian process models; Pareto-optimal pumping schemes; groundwater pumping optimisation.

1 Introduction

Seawater intrusion (SWI), a global environmental issue, is a phenomenon of subsurface freshwater-seawater interface migrating landward and the subsequent salinization of coastal aquifers. It is widely acknowledged that SWI is driven by excessive groundwater extraction and climate change, which result in the recession in the hydraulic gradient between seaward-discharging freshwater and landward-moving seawater (Kishi & Fukuo, 1977). The adverse effects of SWI are serious, contaminating coastal aquifer ecosystems and endangering access to subsurface freshwater for coastal communities (Jasechko et al., 2020; Agoubi, 2021). To strike a trade-off between SWI control and satisfying local water demand, the strategy of groundwater pumping optimisation serves as an effective approach, in which all environmental and economic concerns are incorporated as objectives or constraints in a non-linear groundwater management problem. Optimal pumping schemes can be obtained after solving the formulated groundwater management problem, and that calculation usually depends on the simulation-optimisation (SO) method (Kourakos & Mantoglou, 2011; Coulon et al., 2022). Figure 1 shows the flow chart for generally implementing the SO framework.

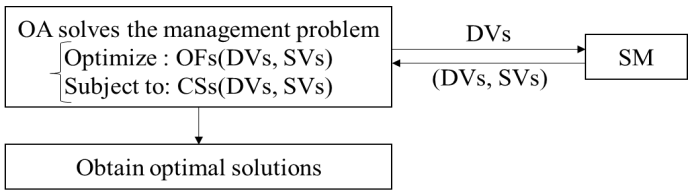

Figure 1. Flow chart for generally implementing the SO framework. OFs and CSs are respectively the objectives and constraint functions. DVs and SVs represent decision variables and state variables, respectively. OA denotes the optimisation algorithm, while SM represents the simulation model.

In the SO framework, the first step is to formulate the pumping optimisation problem, encompassing the definition of OFs, CSs, DVs, and SVs. Typically, the constrained management problem aims to maximize total pumping rates, minimize the economic costs of pumping, while simultaneously ensuring SWI remains within specified limits or restricting salt concentration near well sites. DVs are the pumping patterns, while SVs are the response variables dependent on DVs, determined through the SM. OFs and CSs are functions of DVs and/or SVs. Second, the OA is employed to solve the optimisation problem, exploring the input variable space to identify multiple potentially optimal DVs. Next, the potentially optimal DVs

searched by the OA are used as inputs for the SM, producing corresponding SVs. These DVs and SVs form pairs of data that feed the OA. Subsequently, guided by feedback from the simulation results, the OA decides how to adjust the DVs toward better solutions. Upon convergence, the OA returns a set of DVs, considered the optimal solutions to the management problem.

In coastal groundwater management, popular variable-density groundwater simulation models include SEAWAT (Kourakos & Mantoglou, 2013), SUTRA (Ketabchi & Ataie-Ashtiani, 2015) and HydroGeoSphere (Christelis et al., 2019). Compared with the full enumeration method, the SO method largely reduces the required number of SWI simulations during the optimisation, saving computational costs remarkably. Over the past decades, the SO method has been successfully applied in many works of coastal aquifer management, either single-objective (Mantoglou, 2003; Coulon et al., 2022; Dey & Prakash, 2022) or multi-objective (Kourakos & Mantoglou, 2011; Javadi et al., 2015; Wang et al., 2022) groundwater pumping optimisation problems. However, the fact is that the computational advantage of the SO method usually disappears in practical applications, attributed to the characteristic of the SO method, requiring repeated calls of SWI simulation models. In cases where the times of calling simulation model are numerous or/and each call is time-consuming, employing that to determine optimal pumping schemes certainly turns into computationally intractable or just theoretically viable (Han et al., 2021; Yin et al., 2022).

As the computational burden resulting from the SO method is due to the intensive SWI simulations, an effective and reliable route for saving runtime is to employ the data-driven surrogate models, replacing the time-consuming SWI simulations for developing a surrogate simulation-optimisation (SSO) framework. Surrogate models are built by training data generated from the original simulators, and then provide statistically approximated relationships between input and output variables. In the SSO system, surrogate models can be trained to predict SVs (e.g., pumped groundwater concentration, hydraulic head at the pumping well), which are then used for calculating management objectives and constraint values. After surrogate models are trained, they substitute SWI simulation models to predict aquifer response under the pumping and link with the OA to determine the optimal pumping schemes.

Assisted by the surrogate modelling technique, the required computational costs for identifying the optimal solutions of coastal groundwater pumping can be much lower than those consumed by the SO method. In some cases, savings in runtime can be nearly up to 100% by the SSO method (Al-Maktoumi et al., 2021; Fan et al., 2020; Rajabi & Ketabchi, 2017; Ranjbar & Mahjouri, 2020; Yin et al., 2022), exhibiting a noticeable improvement in computing

efficiency. Their capabilities in providing accurate and reliable SWI extent estimates given the pumping pattern and in deriving trustable optimal pumping solutions are validated in many publications (Fan et al., 2020; Yin et al., 2022). Moreover, the SSO method is widely accepted to solve high-dimensional management problems where the number of decision variables can be up to dozens (Fan et al., 2020; Lal & Datta, 2021), while the SO method is trapped by the computational costs, mainly applicable for low-dimensional management problems, where the number of design parameters is mostly less than ten (Javadi et al., 2015; Ketabchi & Ataie-Ashtiani, 2015; Yin et al., 2020; Coulon et al., 2022). Due to these excellent performances, the SSO method has increasingly become more popular in coastal groundwater management. To date, diverse mathematical functions have served as the surrogates in coastal groundwater management, popularly used ones including the GP model (Rajabi & Ketabchi, 2017; Lal & Datta, 2021), radial basis functions (Christelis & Mantoglou, 2016) and support vector machine regression model (Yin et al., 2022).

The typical ways to create surrogate models are either offline or online training. Offline-trained surrogate models are devoted to ensuring that estimates of surrogate models are characterized with global accuracy over the entire input space. They complete the development based on simulation data before the optimisation procedure, totally substituting the expensive SWI simulators to link with the optimisation approach in the subsequent optimisation stage. Online-trained surrogate models aim to quickly identify locally optimal solutions with low computational costs (Papadopoulou et al., 2010). Online training surrogate models is an iterative process, where surrogate models built by initial training samples immediately link with the optimisation approach to search for the optimal solutions and then the obtained potentially optimal points are added into the training data set for updating the surrogate models, repeating the previous step until there are no further changes in the optimal solutions. Figure 2 shows the flow charts for using these two types of surrogate models in the SSO framework.

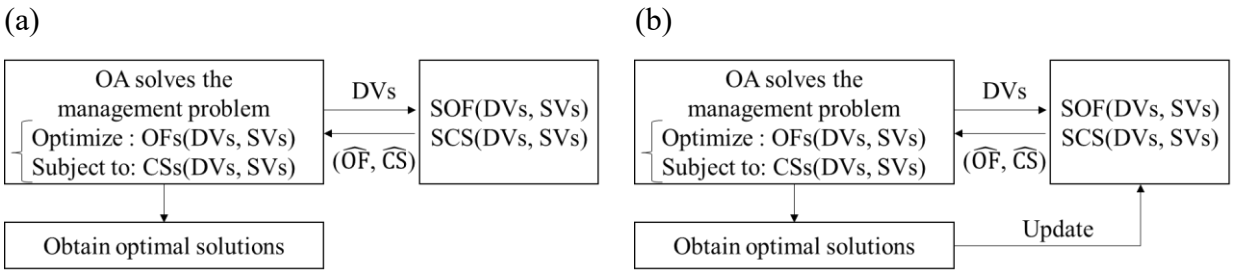

Figure 2. Flow charts for implementing the SSO framework with different types of surrogate models, (a) offline-trained surrogate models and (b) online-trained surrogate models. SOF and SCS are respectively the surrogates of OFs and CSs. $\widehat{OF}$ and $\widehat{CS}$ respectively denote the predicted values of OFs and CSs given by SOF and SCS.

Traditionally, offline training surrogate models depend on fitting a set of training samples at one time, and to ensure the global accuracy of surrogate model estimates, these training points cover the entire input space either uniformly or randomly (Fan et al., 2020; Han et al., 2021). However, since groundwater management objectives and SWI constraints are nonlinear, this traditional training approach can prove inefficient due to the potential oversampling of low-gradient areas and under-sampling of high-gradient areas. Therefore, to acquire reliable model estimates, surrogate models built by traditional offline training tend to consume more training samples than necessary, causing a certain proportion of the computational costs to be wasted. In the studies of Rajabi and Ketabchi (2017), Ranjbar and Mahjouri (2020) and Al-Maktoumi et al. (2021), offline-trained surrogate models consumed training samples that are hundreds of times the number of decision variables, indicating that there is a need to design an efficient algorithm for offline training surrogate models in coastal groundwater management.

The conventional approach for building an online-trained surrogate model involves updating it at each iteration by incorporating newly identified optimal pumping patterns into the training set (Christelis and Mantoglou, 2016; Song et al., 2018; Yu et al., 2021), enabling the derived optimal pumping schemes to gradually converge towards the actual ones. To prevent surrogate estimates from being trapped in local optima, Christelis et al. (2018) combined the information on objective value and minimum distance from the closest training point at each candidate to determine the next sampling point in a single-objective management problem. However, in the case of multi-objective management problems, the potential optimal pumping patterns obtained at each iteration are a set of points rather than a single solution in single-objective problems, which highlight a trade-off between conflict management objectives. This set of non-dominated solutions in a multi-objective optimisation problem is termed the Pareto front. In this case, applying the traditional way to build an online-trained surrogate model needs to sample multiple points at each iteration and ultimately consumes a larger number of training samples than expected. Yu et al. (2021) applied the online-trained SSO method to solve a three-objective pumping optimisation problem in a coastal region in Australia. Their online-trained surrogates converged after two updates, but each update required 1,000 training samples, finally consuming a total of 3,540 training samples for addressing this eight-decision-variable management problem. This highlights the necessity for proposing an efficient algorithm to develop online-trained surrogate models for addressing multi-dimensional coastal groundwater management problems.

It is worth noting that both offline and online-trained surrogate models bring about substantial improvements in computing efficiency due to their construction based on finite

training data from full-scale models, but that in turn inevitably introduces uncertainty into the surrogate model predictions (Sreekanth & Datta, 2011; Yin et al., 2022). The widely accepted way to deal with this challenge is to adopt the ensemble of surrogate models. In the ensemble approach, final predictions in SWI extent under the pumping are obtained by integrating estimates of multiple surrogate models, and the estimates of these surrogate models can be harnessed through weighted averaging (Roy & Datta, 2019; Han et al., 2020). The surrogate models involved in the ensemble approach can be either the diverse types of surrogate functions (Christelis et al., 2019; Yin et al., 2022) or a single surrogate function built multiple times using different realizations of training data (Sreekanth & Datta, 2011). Undoubtedly, building an ensemble of surrogate models, whether by training a single surrogate model using multiple groups of training samples or incorporating different types of surrogate models, inevitably increases the computational load.

Overall, applying surrogate models in coastal groundwater management must face three challenges at present, including 1) how to efficiently build surrogate models by offline training, 2) how to efficiently select new training points at each iteration when developing online-trained surrogate models to deal with multi-objective management problems, 3) how to efficiently quantify the uncertainties in derived optimal pumping solutions. To the best knowledge of the author, these challenges attract less attention and have not yet been resolved in coastal groundwater management. Motivated by these challenges, this paper endeavours to investigate efficient approaches for offline and online training of surrogate models in multi-objective coastal pumping optimisation problems as well as for deriving the optimal Pareto-front considering the prediction uncertainty. To reach the target, this study proposes three novel algorithms, which select training points based on the iterative search, for offline training surrogate models, while for online training, there are four algorithms developed for determining sampling points based on the probabilistic Pareto-front. The probabilistic Pareto-front accounts for the prediction uncertainty, where each non-dominated solution is characterized by a probability of Pareto-optimality. In this work, the GP modelling technique is adopted to predict management objectives and constraint values given pumping patterns, and a full enumeration approach is employed to determine the optimal pumping solutions according to surrogate predictions. Compared with other surrogate modelling techniques, GP models can simultaneously offer expected values and standard deviations of the unknown points, being able to quantify the uncertainty of the estimates. Therefore, a probabilistic Pareto-front can be obtained through repeated stochastic (Monte Carlo) running of GP models, which are computationally viable and efficient because of the inexpensiveness of the GP models.

This study focuses on a simplified two-dimensional coastal aquifer based on hydrogeological conditions observed in the island aquifer of San Salvador Island, Bahamas, and formulates a one-well bi-objective pumping optimisation problem. The optimisation problem aims at minimizing the groundwater supply operation cost associated with the groundwater abstraction and desalination treatment and maximizing the amount of qualified groundwater delivered to the communities, subject to constraints on SWI control, as quantified by the water table drawdown over the well system (Δs) and the salt mass increase in the aquifer (ΔSM). As a result, four GP models are required to be developed, respectively predicting objective and constraint values of each pumping pattern, and then an optimal Pareto-front can be achieved through the full enumeration evaluation method. The performance of GP models built by different training algorithms, at last, is tested to identify the efficient approaches for offline and online training GP models in coastal groundwater management.

This paper is organized as follows. The next section presents the simulation model for SWI, the management problem formulation (i.e., objective functions and their constraints), GP model development, and offline and online-trained GP model-based optimisation system. Results and their discussion are provided in the following section. The last section presents the conclusions drawn from the investigation.

2 Methodology

The goal of this study is to investigate the efficient approaches for applying offline and online-trained surrogate models in coastal groundwater management, using the San Salvador Island aquifer as a case study. San Salvador Island is located within the Bahamian Archipelago (Figure 3), about 600 km east-southeast of Miami, and sits on a small, isolated carbonate platform (Ho et al., 2014; McGee et al., 2010). The island is about 20 km long north-to-south and has an average width west-to-east of approximately 8 km (Martin & Moore, 2008). The topography is dominated by consolidated carbonate dune ridges, with elevations between 10 and 20 meters above sea level (Davis & Johnson, 1989). Characterized by a subtropical climate, San Salvador Island has an annual temperature ranging between 22 and 28 °C (McGee et al., 2010) and annual precipitation and potential evaporation of 1000-1250 mm/yr and 1250-1375 mm/yr, respectively (Moore, 2009).

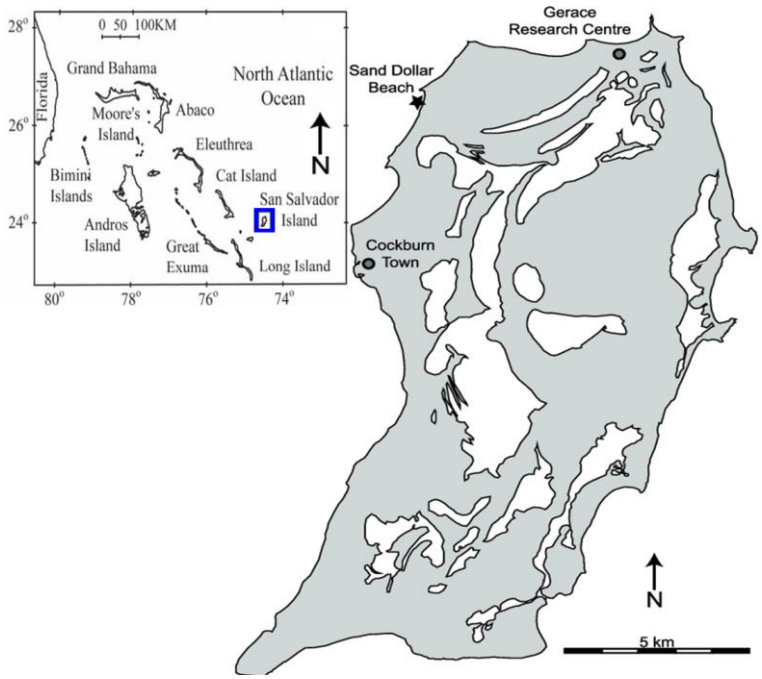

Figure 3. Location map of San Salvador Island (Moore, 2009). The dark grey and the light grey areas represent land and surface water, respectively.

2.1 Numerical simulation of SWI in the San Salvador Island aquifer

This work applies the SEAWAT model to simulate the SWI process in the island aquifer. SEAWAT couples the groundwater flow model MODFLOW and the solute transport model MT3DMS to solve the variable-density flow equations using a finite-difference numerical approach (Langevin et al., 2008; Kourakos & Mantoglou, 2013; Yao et al., 2019). Since the SEAWAT groundwater model can account for water density variations that depend on salt concentration, it is well-suited for simulating flow in aquifers characterized by freshwater-seawater interactions.

In the investigation of the island groundwater abstraction management, a simplified two-dimensional "cross-section" model is adopted. The island cross-section model is constructed as a rectangular domain, with a length of 8,000 m, a height of 480 m, and a width of 1 m. The aquifer domain is discretized into a finite-difference regular grid with cells of size 8 m × 8 m × 1 m. Two additional grid columns are used to represent the boundary conditions at the leftmost and rightmost ends of the domain, so that the finite-difference grid is made up of 1,002 columns and 60 rows, for a total of 60,120 cells. The pumping system is represented by a point sink located at a depth D, a distance WL from the shoreline, and a pumping rate Q, which represents the volume of groundwater extracted per unit time and per unit aquifer width.

Figure 4 shows a conceptualization of the aquifer domain along with the numerical model grid and its boundary conditions. A no-flow boundary is prescribed at the model bottom. The model top is a specified flux boundary, reflecting the aquifer recharge from precipitation, which

is assumed to be 0.2 m per year (Gulley et al., 2016). At the left and right boundaries, a constant head of 0.0 m is prescribed over the water column, which represents the sea level (at the datum). At the same boundaries, a constant concentration of 35.0 g/L is imposed, which represents the salt content in seawater.

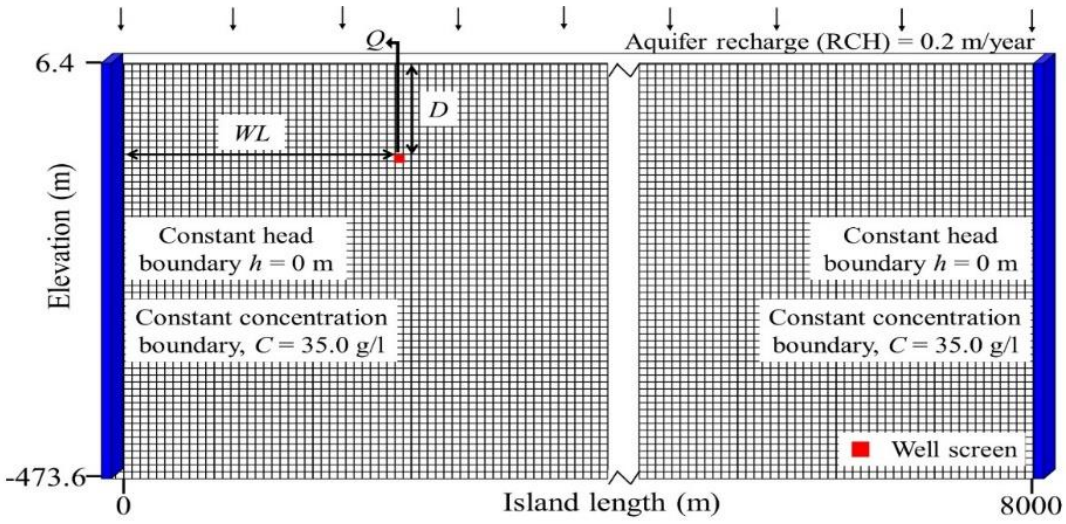

Figure 4. Island aquifer SEAWAT cross-sectional model grid along with the associated boundary conditions. The pumping system is simulated as a single cell located at depth *D* from the ground surface and distance *WL* from the shoreline.

To model SWI effects from groundwater abstraction at a steady state, the flow and solute transport are simulated as transient state processes with a sufficiently large period of constant groundwater pumping. A "baseline" scenario is first developed to simulate the island freshwater lens under steady-state conditions of natural groundwater recharge from precipitation only. This serves as the initial condition to model the aquifer freshwater distribution under various scenarios of groundwater pumping. For the simulations involving groundwater pumping, SEAWAT is run until a steady state is reached, which is typically between 2 and 30 years depending on the simulated pumping scheme. Correspondingly, the required CPU time for each simulation varies from a minimum of about 15 minutes to a maximum of over 1 hour. Table 1 provides a list of the relevant parameters adopted in the simulation model introduced above. These parameters are drawn from published works (Gulley et al., 2016; Holding & Allen, 2015) that have used San Salvador Island or nearby island aquifers as test cases.

Table 1. *Model Parameters Used for SWI Simulation in the San Salvador Island Aquifer*

Model Component	Parameters	Units	Values
Groundwater Flow	Aquifer recharge (*RCH*)	m/year	0.2
	Effective porosity	\	0.15
	Specific elastic storage	m^{-1}	1.0×10^{-5}
	Specific yield	\	0.15
	Horizontal hydraulic conductivity (HK)	m/day	50.0
	HK transversal anisotropy ratio	\	1.0
	HK vertical anisotropy ratio	\	1.0
Solute Transport	Longitudinal dispersivity	m	1.0
	Transversal dispersivity	m	0.1
	Vertical dispersivity	m	0.01
	Molecular diffusion coefficient	m^2/s	1.0×10^{-9}
	Aquifer recharge concentration	g/l	0
Density dependence	Freshwater density	kg/m^3	1000
	Seawater density	kg/m^3	1025
	Density/concentration slope[a]	\	0.7143

[a] The water density ρ_w [kg/m^3] varies linearly with the salt concentration C [kg/m^3] through the equation $\rho_w = 1000 + 0.7143 \cdot C$.

2.2 Groundwater management formulation

Managing fragile freshwater resources in the island aquifers is to identify cost-optimal pumping strategies, which balance the financial cost of groundwater supply and the volume of qualified groundwater supplied to the water network while mitigating SWI resulting from aquifer pumping. In this work, these tradeoffs are investigated through the formulation of a one-well bi-objective optimisation framework, which aims at minimizing the groundwater supply operation cost associated with pumping and desalination and maximizing the amount of qualified groundwater delivered to local communities, subject to Δs and ΔSM.

Each pumping pattern is characterized by three DVs, the depth D [L] at which pumping occurs, the distance WL [L] of the pumping system from the shoreline, and the intensity of constant pumping Q [L^2T^{-1}]. The management cost f_{OC} accounts for two main components: the pumping operation cost f_p, and the treatment operation cost f_t, per unit aquifer width and unit time [$\$L^{-1}T^{-1}$]. The former is the cost of energy utilization for lifting groundwater to the ground surface, whereas the latter is the cost of desalination by reverse osmosis, which is needed when the salt concentration in water exceeds 1.0 g/L, in accordance with World Health Organization guidelines for drinking water (Yao et al., 2019). The ultimate amount of water from the pumping delivered to the local communities Q_p [L^2T^{-1}] represents the amount of water after

the desalination when extracted groundwater concentration is larger than 1.0 g/L. Otherwise, Q_{p} is identical to the pumping intensity Q.

The cost objective function is formulated as:

$$f_{\mathrm{OC}} = f_p(Q, h, C) + f_t(Q, C) \tag{1}$$

where h [L] and C [ML^{-3}] are state variables, which represent the hydraulic head at the well screen and the salt concentration in the extracted water, respectively. Both h and C are functions of the DVs (D, WL, Q). f_p is expressed as (Mayer et al., 2002):

$$f_p(Q, h, C) = \rho_w(C) \cdot \mathrm{g} \cdot \left(z_{\mathrm{gs}} - h\right) \cdot Q \cdot c_{\mathrm{e}} \tag{2}$$

where ρ_w is the water density, which depends on the salt concentration C (Table 1), g denotes gravitational acceleration [LT^{-2}], and z_{gs} represents the ground surface elevation [L], set equal to 15.0 m. The coefficient c_{e} represents the unit energy cost [\$M^{-1}L^{-2}T^{2}], assumed equal to 0.1848 \$/kWh. The treatment cost, f_t, is estimated as (Avlonitis et al., 2012):

$$f_t(Q, C) = \rho_w(C) \cdot SEC(C) \cdot Q \cdot c_{\mathrm{e}} \tag{3}$$

where SEC [L^{2}T^{-2}] is the specific (per unit mass) energy consumption for water desalination (Stillwell & Webber, 2016), which depends on the salt concentration C. A detailed description of SEC is presented in the Supporting Information - Appendix A.

The objective function of the amount of groundwater delivered to the supply network is formulated as:

$$Q_{\mathrm{p}} = r(C, C_b, C_d) \cdot Q \tag{4}$$

where C_b and C_d are respectively the resulting brine concentration and target concentration in the permeate, assumed to be 1.0 g/L. r is the recovery ratio and it is equal to 1 when C is less than 1.0 g/L, depending on C, C_b and C_d. The relationship between C, C_b, C_d and r is elucidated in the Supporting Information - Appendix A.

The formulation of the island groundwater management problem is completed by two groups of constraints. The first group sets the range of variability of the DVs (D, WL, Q). The pumping depth D is subject to the inequality:

$$D_{\min} \leq D \leq D_{\max} \tag{4}$$

where $D_{\min}$ and $D_{\max}$ are the absolute depths below the groundwater surface, equal to 12.6 m and 484.6 m, respectively.

Since the model grid (Figure 4) is symmetric with respect to the island's central axis, the distance WL cannot exceed half of the island length L =8000 m. WL is thus constrained as:

$$WL_{\min} \leq WL \leq WL_{\max} \tag{5}$$

with $WL_{\min}$ equal to $0.05 \cdot L$ and $WL_{\max}$ equal to $0.5 \cdot L$. The pumping rate Q depends on the groundwater demand, which may be estimated based on the population density and the per capita water consumption and needs to be constrained in relation to the aquifer recharge rate RCH. Here, Q is assumed to be subject to:

$$Q_{\min} \leq Q \leq Q_{\max} \tag{6}$$

with $Q_{\min}$ equal to $0.05 \cdot RCH \cdot L$ and $Q_{\max}$ equal to $0.2 \cdot RCH \cdot L$. These values have been selected to cover a range of variability for Q large enough to study its effects on SWI and groundwater supply cost.

A second group of constraints is considered to minimize the extent of the SWI, thus addressing the environmental sustainability of groundwater abstraction. SWI is quantified by two indicators: the hydraulic head drawdown scaled to the water table elevation over the pumping system, and the increase in aquifer salt mass.

The drawdown at the pumping well is subject to the following constraint:

$$\Delta s \leq \Delta s_{\max} \tag{7}$$

where Δs is calculated as the percentage of water table drawdown at the well location with respect to the original water table level, and $\Delta s_{\max}$ is the maximum allowed value for Δs, which is calculated as:

$$\Delta s = \frac{H_0(WL) - H(D,WL,Q)}{H_0(WL)} \cdot 100 \leq \Delta s_{\max} \quad [\%] \tag{8}$$

where $H_0(WL)$ is the water table level over the pumping system prior to pumping (baseline scenario), and $H(D, WL, Q)$ is the corresponding steady-state water table level during pumping, which depends on the DV set. In this study, $\Delta s_{\max}$ is set as 0.15.

The aquifer salt mass increase is subject to the inequality:

$$\Delta SM \leq \Delta SM_{\max} \tag{9}$$

where ΔSM is the percentage of salt mass increase in the aquifer, given by:

$$\Delta SM = \frac{SM(D,WL,Q) - SM_0}{SM_0} \cdot 100 \leq \Delta SM_{\max} \quad [\%] \tag{10}$$

where SM_0 is the total salt mass in the aquifer prior to pumping and SM is the total salt mass at steady state during pumping. $\Delta SM_{\max}$ is the maximum allowed value for ΔSM. SM values are calculated by integrating the salt concentration multiplied by the pore volume over all model grid cells. In this study, $\Delta SM_{\max}$ is set as 0.025.

2.3 GP model development

GP models are non-parametric models, allowing for the modelling of complex relationships without imposing specific functional forms on the data, indicating the GP model

is advantageous in treating the nonlinear process with high efficiency (Redouane et al., 2019). As a type of Bayesian surrogate, the GP model provides the posterior predictive distributions for all points across the input space rather than the potentially best-fit values (Kopsiaftis et al., 2019), quantifying the epistemic uncertainties incurred by the finite training data. In addition, GP models can handle multi-dimensional problems and incorporate prior knowledge about the underlying system. Inspired by those advantages, the GP modelling technique is chosen to substitute the variable-density SEAWAT model in this study.

A GP is a collection of random variables, any finite number of which have a joint Gaussian distribution (Rasmussen & Williams, 2006). Such a GP is treated as a distribution over a space of continuous functions, fully specified by a mean function $m(\boldsymbol{x})$ and a covariance function $k(\boldsymbol{x}, \boldsymbol{x}')$. A sample from Gaussian processes is a function with its values at any location being distributed according to a Gaussian distribution (Cui et al., 2021). Let $f(\boldsymbol{x})$ represents an output variable of interest,

$$f(\boldsymbol{x}) \sim gp(m(\boldsymbol{x}), k(\boldsymbol{x}, \boldsymbol{x}')) \tag{11}$$

where $\boldsymbol{x} \in R^d$ is a d-dimensional input vector. $m(\boldsymbol{x})$, the expected value of the latent function at the point, and $k(\boldsymbol{x}, \boldsymbol{x}')$, also known as the kernel function, are the prior beliefs about the latent function.

In a Bayesian framework, the prior beliefs can be updated to a posterior distribution over the latent function that represents the output variables of interest by the observed training samples. The obtained posterior distribution offer predictions across the defined input space. Therefore, to apply a GP model, in general, there are mainly five steps, including 1) define a set of input points; 2) run the original simulation model by the specified input points, creating the input-output training dataset; 3) select appropriate mean and covariance functions; 4) update prior beliefs through training on the input-output dataset; 5) generate predictions for any unobserved point over the input space.

Let $\boldsymbol{X}_N = [\boldsymbol{x}_1, \boldsymbol{x}_2, \dots, \boldsymbol{x}_N]^{\mathrm{T}}$ and $\boldsymbol{Y}_N = [\boldsymbol{y}_1, \boldsymbol{y}_2, \dots, \boldsymbol{y}_N]^{\mathrm{T}}$ represent the set of training input and output data. The training set is denoted as the pair $\mathcal{D} = \{\boldsymbol{X}_N, \boldsymbol{Y}_N\}$. The prediction y_* for the new input vector $\boldsymbol{x}_*$ and $\boldsymbol{Y}_N$ have a joint Gaussian distribution, given by:

$$\begin{bmatrix} \boldsymbol{Y}_N \\ y_* \end{bmatrix} \sim \mathcal{N}\left(\begin{bmatrix} \boldsymbol{\mu}_N \\ \mu_* \end{bmatrix}, \begin{bmatrix} \boldsymbol{K} + \sigma_n^2 \boldsymbol{I} & \boldsymbol{k}(\boldsymbol{x}_*) \\ \boldsymbol{k}^{\mathrm{T}}(\boldsymbol{x}_*) & \kappa(\boldsymbol{x}_*) + \sigma_n^2 \end{bmatrix} \right) \tag{12}$$

where $\boldsymbol{\mu}_N = [m(\boldsymbol{x}_1), \dots, m(\boldsymbol{x}_N)]^{\mathrm{T}}$, $\mu_* = m(\boldsymbol{x}_*)$. $\boldsymbol{K}$ is a $N \times N$ matrix, where the (i, j)-th $(i, j = 1,2, \dots, N)$ entry of $\boldsymbol{K}$ is given by $k(\boldsymbol{x}_i, \boldsymbol{x}_j)$. σ_n^2 is the variance of random noise, and $\boldsymbol{I}$ is a $N \times N$ unit matrix. $\boldsymbol{k}(\boldsymbol{x}_*) = [k(\boldsymbol{x}_1, \boldsymbol{x}_*), k(\boldsymbol{x}_2, \boldsymbol{x}_*), \dots, k(\boldsymbol{x}_N, \boldsymbol{x}_*)]^{\mathrm{T}}$ is the $N \times 1$ vector of

covariances between the $\boldsymbol{X}_N$ and $\boldsymbol{x}_*$, while $\kappa(\boldsymbol{x}_*) = k(\boldsymbol{x}_*, \boldsymbol{x}_*)$ is the autocovariance of the input data at the prediction point. The posterior distribution of y_* conditioned on $\boldsymbol{X}_N$ and $\boldsymbol{Y}_N$ is given by (Rasmussen & Williams, 2006):

$$f(\boldsymbol{x}_*)|\mathcal{D} \sim gp(m_{\mathcal{D}}(\boldsymbol{x}_*), k_{\mathcal{D}}(\boldsymbol{x}_*, \boldsymbol{x}_*{}')) \tag{13}$$

where

$$m_{\mathcal{D}}(\boldsymbol{x}_*) = \mu_* + \boldsymbol{k}^{\mathrm{T}}(\boldsymbol{x}_*)[\boldsymbol{K} + \sigma_n^2\boldsymbol{I}]^{-1}\boldsymbol{Y}_N \tag{14}$$

$$k_{\mathcal{D}}(\boldsymbol{x}_*, \boldsymbol{x}_*{}') = \kappa(\boldsymbol{x}_*) - \boldsymbol{k}^{\mathrm{T}}(\boldsymbol{x}_*)[\boldsymbol{K} + \sigma_n^2\boldsymbol{I}]^{-1}\boldsymbol{k}(\boldsymbol{x}_*) \tag{15}$$

The term $\boldsymbol{k}^{\mathrm{T}}(\boldsymbol{x}_*)[\boldsymbol{K} + \sigma_n^2\boldsymbol{I}]^{-1}$ in Equation 14 can be interpreted as a set of smoothing coefficients determining the relative importance of each training point to y_*. Equation 15 demonstrates when the unexplored input point is far away from the training points, the correlation between this point and training points is small, lowering $\boldsymbol{k}^{\mathrm{T}}(\boldsymbol{x}_*)[\boldsymbol{K} + \sigma_n^2\boldsymbol{I}]^{-1}\boldsymbol{k}(\boldsymbol{x}_*)$ and thus increasing predicted variance at this point. Once the mean function and kernel function are determined, predictions at any unknown point over the input space can be given by the GP model. The mean function usually is set as a constant (Kim 2016; Siade et al., 2020), this study assumes it is equal to the average of training data. The kernel function in this work employs the commonly used squared exponential covariance function, (Kim 2016; Zhang et al., 2016; Cui et al., 2021). More details about GP models can be found in Rasmussen & Williams (2006).

In this work, four GP models need to be built for substituting SEAWAT simulations during the optimisation, respectively predicting values of f_{OC}, Q_{P}, Δs and ΔSM given DVs, correspondingly denoted as $\mathrm{GP}_{\mathrm{OC}}$, $\mathrm{GP}_{Q_{\mathrm{p}}}$, $\mathrm{GP}_{\Delta s}$ and $\mathrm{GP}_{\Delta SM}$. To let the predictions align with the realistic, there are some requirements for these GP model predictions, including 1) predicted f_{OC} larger than 0; 2) predicted Q_{p} larger than 0 and no more than total pumping rate Q; 3) predicted Δs larger than 0; 4) predicted ΔSM larger than -1 according to Equation 10, where SM is not equal to or fewer than 0. Regarding the limit on predicted Q_{p}, it can be treated that Q_{p}/Q, namely recovery ratio r, should be within the range of (0,1], indicating that 1-r should be within [0,1) and obtaining $\frac{1}{1-r}$ within (1, +∞). Overall, it requires positive predictions of f_{OC}, $\frac{r}{1-r}$, Δs and ΔSM+1 given by GP models. This study, to meet those requirements, first adopts log transformation technique, developing GP models to predict log-transformed f_{OC}, $\frac{r}{1-r}$, Δs and ΔSM+1 given DVs. Then, applying the reverse of the log transformation to get positive predictions of f_{OC}, $\frac{r}{1-r}$, Δs and ΔSM+1. Table 2 presents a summary of how to build $\mathrm{GP}_{\mathrm{OC}}$, $\mathrm{GP}_{Q_{\mathrm{p}}}$, $\mathrm{GP}_{\Delta s}$ and $\mathrm{GP}_{\Delta SM}$ to produce predictions aligning with the realistic.

Table 2. *Summary of GP Model Development in This Study*

GP model	Requirements for GP model estimate	Training of GP models		Values of objectives and constraints given DVs	
		Input	Output	Expected value	Confidence interval
GP_{OC}	$f_{OC} > 0$	DVs	$\log_{10} f_{OC}$	$10^{\mu_{OC}}$	$(10^{\mu_{OC}-\sigma_{OC}}, 10^{\mu_{OC}+\sigma_{OC}})$
GP_{Q_P}	$0 < Q_P \leq Q$ $(0 < r = \frac{Q_P}{Q} \leq 1)$	DVs	$\log_{10} \frac{r}{1-r}$	$\frac{Q}{1+10^{-\mu_P}}$	$(\frac{Q}{1+10^{-\mu_P+\sigma_P}}, \frac{Q}{1+10^{-\mu_P-\sigma_P}})$
$GP_{\Delta s}$	$\Delta s > 0$	DVs	$\log_{10} \Delta s$	$10^{\mu_{\Delta s}}$	$(10^{\mu_{\Delta s}-\sigma_{\Delta s}}, 10^{\mu_{\Delta s}+\sigma_{\Delta s}})$
$GP_{\Delta SM}$	$\Delta SM > -1$	DVs	$\log_{10}(1 + \Delta SM)$	$10^{\mu_{\Delta SM}}$-1	$(10^{\mu_{\Delta SM}-\sigma_{\Delta SM}}$-1, $10^{\mu_{\Delta SM}+\sigma_{\Delta SM}}$-1)

In Table 2, μ_{OC}, μ_P, $\mu_{\Delta s}$ and $\mu_{\Delta SM}$ are respectively the expected values of $\log_{10} f_{OC}$, $\log_{10} \frac{r}{1-r}$, $\log_{10} \Delta s$ and $\log_{10}(1 + \Delta SM)$ under the pumping, while σ_{OC}, σ_P, $\sigma_{\Delta s}$ and $\sigma_{\Delta SM}$ are the corresponding standard deviations of predictions respectively, all of which are provided by the GP models. To eliminate the effects of decision variable units on the GP model predictions, a scaling process is applied to all DVs, letting them fall within the range of 0 to 1.

2.4 GP model-based simulation-optimisation system

2.4.1 Offline-trained GP model-based simulation-optimisation system

Desired offline-trained GP models are not only to produce reliable global estimates but also to be developed highly efficiently, making the best of each training sample and thus consuming less computing time. Within the expectation, predictions given by the offline-trained GP models are characterized by smaller confidence intervals, and most training samples are drawn from the high-gradient regions, only a few being distributed across low-gradient regions. To achieve that target, this work introduces the iterative process into the offline-trained GP model development and proposes three strategies for identifying the new sampling points at each iteration, labelled from **F1** to **F3** and shown below.

F1: identify the input point that has the maximum distance from the closest training point as the next sampling point, expressed below,

$$\max\{dc_i\} \ (i = 1,2 \ldots, N_U) \tag{16}$$

where dc_i is the distance from the input point i to the closest training point and equal to $\min\{dc_{ij}\}$ $(i = 1,2 \ldots, N_U;\ j = 1,2, \ldots, N_T)$, dc_{ij} denotes the distance from the i-th input point to the j-th training point; N_U and N_T are respectively the number of unobserved input points and training points. If there are multiple points with the same maximum dc, the one with maximum estimated standard deviation will be chosen as the next sampling point.

F2: identify the input point that has the maximum gradient as the next sampling point, expressed below,

$$\max\{\|\nabla G(\boldsymbol{x}_i)\|_2\}\ (i = 1,2 \dots, N_{\mathrm{U}}) \tag{17}$$

where $\|\nabla G(\boldsymbol{x}_i)\|_2$ represents the absolute gradient at the input vector $\boldsymbol{x}_i$ $(i = 1,2 \dots, N_{\mathrm{U}})$. If there are multiple points with the same maximum ∇G, the one with the maximum estimated standard deviation will be chosen as the next sampling point.

F3: identify the input point that has the maximum score $R1$ as the next sampling point, which combines the information of dc and ∇G, expressed below,

$$\max\{R1_i\}\ (i = 1,2 \dots, N_{\mathrm{U}}) \tag{18}$$

where $R1_i$ is the score at the input point *i* and is calculated by the following equation,

$$R1_i = wa_1\overline{dc}_i + wa_2\overline{\nabla G}_i \tag{19}$$

where wa_1 and wa_2 are the weights representing the importance of dc and ∇G, respectively, satisfying $wa_1 + wa_2$=1. In this study, both wa_1 and wa_2 are equal to 0.5. $\overline{dc}_i$ and $\overline{\nabla G}_i$ are respectively the scaled values of dc and ∇G at the input point *i* for eliminating the effects of their units, varying between 0 and 1, equations for calculating them shown below,

$$\overline{dc}_i = \frac{dc_i - \min\{dc_k\}}{\max\{dc_k\} - \min\{dc_k\}}\ (i,k = 1,2 \dots, N_{\mathrm{U}}) \tag{20}$$

$$\overline{\nabla G}_i = \frac{\|\nabla G(\boldsymbol{x}_i)\|_2 - \min\{\|\nabla G(\boldsymbol{x}_k)\|_2\}}{\max\{\|\nabla G(\boldsymbol{x}_k)\|_2\} - \min\{\|\nabla G(\boldsymbol{x}_k)\|_2\}}\ (i,k = 1,2 \dots, N_{\mathrm{U}}) \tag{21}$$

To prevent the issue of local trapping during the model development, occurring when new sampling points are placed too close to training points, this study introduces two strategies for assessing whether, in the subsequent iterations, it is necessary to consider the input spaces where a new training point is added. In the *d*-dimensional input space, when a new training point is added, the search space that includes this point can be discretized into up to 2^d sub-spaces by using the new point as one of the corners of a hypercube. The two strategies are respectively based on the domain size of the newly discretized subspace (*DSSP*), and average changes in model estimates over the newly divided subspace between before and after adding this new training sample (*ACSP*). If either the *DSSP* or *ACSP* of a newly discretized subspace is quite small, it is believed that there is no need to pay attention to this input space in the subsequent, eliminating it from the search space. In this study, threshold values of *DSSP* and *ACSP* are set to 0.001 and 0.05 respectively.

The performance of strategies **F1**, **F2**, and **F3** is compared to the conventional offline training approach, where GP models are trained using a relatively large batch of samples at

once. Typically, these training samples are uniformly drawn from and distributed across the entire input space using the LHS method, which is labelled **F4** in this study.

Figure 5 presents the flowchart for offline training GP models by proposed strategies. Figure 5 shows that offline training comes to a halt under any one of three conditions: 1) when the current search space is empty, 2) when the value of $\sigma_{\text{avg}}/\max|y_{\text{est}}|$ falls below the specified tolerance level, and 3) when the number of SWI simulations exceeds the maximum allowed. The indicator $\sigma_{\text{avg}}/\max|y_{\text{est}}|$ quantifies the relative average standard deviation, where σ_{avg} denotes the average standard deviation of GP model estimates and $\max|y_{\text{est}}|$ is the maximum absolute GP model estimate. In this study, the maximum allowed size of SWI simulations during the training is defined as seventy-five, twenty-five times the size of the DVs, and tolerance level for $\sigma_{\text{avg}}/\max|y_{\text{est}}|$ is defined as 0.03.

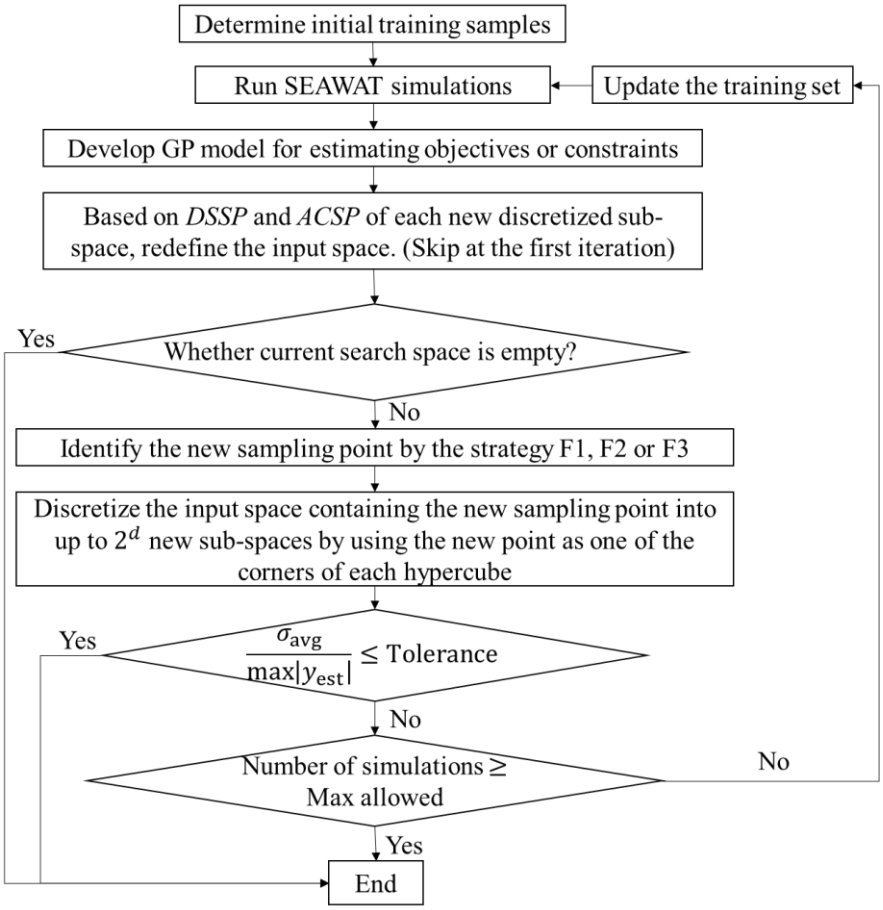

Figure 5. Flow chart for offline training GP models by proposed strategies **F1**, **F2** or **F3**.

2.4.2 Online-trained GP model-based simulation-optimisation system

In the online training framework, developed GP models are used for identifying optimal pumping patterns at each iteration, and then determining new sampling points based on the optimal solutions updates the training set and thus GP models, repeating the previous step until

obtaining stable optimal solutions. For multi-objective management problems, optimal solutions, maintaining trade-offs between conflicting objectives, are a series of schemes rather than a single individual. These optimal solutions are known as the non-dominated points over the management objective space, constituting a Pareto front, each of which corresponds to a set of DVs (i.e., a certain pumping pattern in this work). As a result, the central challenge in online training of GP models lies in the highly effective selection of sampling points at each iteration from the obtained optimal solutions. To tackle this challenge, four strategies are proposed for enhancing the efficiency of obtaining stable optimal solutions by the online-trained GP models, labelled from **N1** to **N4** and shown in the following. All these four strategies take the prediction uncertainty into account, namely considering the pumping patterns with associated probabilities to be optimal schemes.

N1: rank the input points that are potentially Pareto optimal schemes by their probabilistic distances from the closest training points from the largest to the smallest, and then choose top N_{nt} points as the new sampling points, expressed below,

$$\text{Rank } \{PPO_i \cdot \overline{dc_i}\} \quad (i = 1,2 \dots, N_{\text{P}}) \tag{22}$$

where PPO_i denotes the probability of the *i*-th Pareto optimal candidate schemes and N_{P} is the number of potentially optimal pumping schemes. More details about PPO_i can be found in the next section.

The strategies **N2**, **N3**, and **N4** share the same philosophy, distributing the sampled Pareto optimal points as extensively as possible across the objective space. The first step of these three strategies is to scale each dimension of the Pareto optimal objective space to a range between 0 and 1, eliminating the effects of different objective units, and then the scaled space is divided into N_D uniformly equal sub-square regions. The difference among N2, N3, and N4 is to determine the new sampling points in each sub-region, and details about them are shown below.

N2: determining the new sampling point in each sub-region by the following equation,

$$\max\left\{PPO_i \cdot \overline{dc_i} | (i = 1,2 \dots, NP_v) \in SR_v\right\} (v = 1,2, \dots, N_D) \tag{23}$$

where NP_v denotes the number of potentially Pareto optimal solutions in the v-th discretized sub-region while SR_v represents the v-th discretized sub-region.

N3: determining the new sampling point in each sub-region by the following equation,

$$\max\left\{PPO_i \cdot \overline{dIO_i} | (i = 1,2 \dots, NP_v) \in SR_v\right\} (v = 1,2, \dots, N_D) \tag{24}$$

where dIO_i is the distance from the *i*-th Pareto optimal solution to the ideal objective point (*IO*). At *IO*, f_{OC} and Q_{p} reach their respective optimal values, the location of which in the

scaled coordinate system is (0, 1). $\overline{dIO}_i$ is the scaled value of dIO_i, calculated by the following equation,

$$\overline{dIO}_i = \frac{\max\{dIO_k\} - dIO_i}{\max\{dIO_k\} - \min\{dIO_k\}} \ (i, k = 1,2 \dots, NP_v) \tag{25}$$

N4: determining the new sampling point in each sub-region by the following equation,

$$\max\left\{PPO_i \cdot \overline{dC}_i | (i = 1,2 \dots, NP_v) \in SR_v\right\} \ (v = 1,2, \dots, N_D) \tag{26}$$

where dC_i $((i = 1,2 \dots, NP_v) \in SR_v)$ represents the distance from the i-th Pareto optimal solution to the centre of the v-th discretized sub-region in the objective space, and $\overline{dC}_i$ is the scaled value of dC_i, calculated by,

$$\overline{dC}_i = \frac{\max\{dC_k\} - dC_i}{\max\{dC_k\} - \min\{dC_k\}} \ (i, k = 1,2 \dots, NP_v) \tag{27}$$

In this work, the value of N_{nt} in strategy **N1** is set to three, while the value of N_D for strategies **N2**, **N3** and **N4** is set to four, ensuring the size of sampled points at each iteration under different training strategies is approximately same. Figure 6 presents the flowchart for solving the multi-objective coastal groundwater management problem using online-trained GP models.

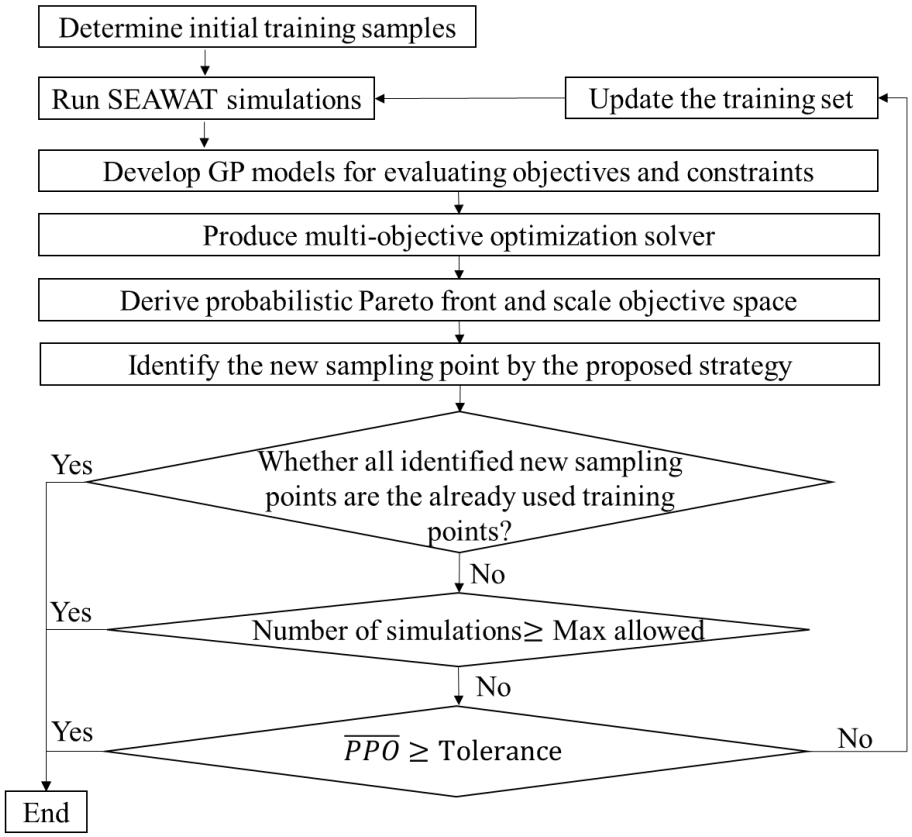

Figure 6. Flow chart for solving multi-objective coastal groundwater management problem using online-trained GP models.

Figure 6 shows that offline training comes to a halt under any one of three conditions: 1) when the newly identified sampling points are the already known training points, 2) when the number of SWI simulations consumed exceeds the maximum allowed, and 3) average probability of optimal Pareto solutions ($\overline{PPO}$) reaches the specified tolerance level. In this study, the maximum allowed size of SWI simulations during the training is the same as that defined in the offline training framework.

2.5 Performance evaluation metrics

To assess the performance of GP models built by different training strategies, this study depends on the statistics of GP model estimates, developing three performance evaluation metrics to evaluate whether developed GP models offer reliable estimates or not, including the correlation coefficients (CC) between GP model predictions, $\overline{PPO}$ and percentage of optimal solutions achieving specified probability threshold ($Per_{\text{prob\_threshold}}$).

(1) CC

Based on the developed GP models, CC between f_{OC} and Q_{p} and that between Δs and ΔSM over the search space can be determined, respectively denoted as $CC_{\text{OC\_}Q_{\text{p}}}$ and $CC_{\Delta s\_\Delta SM}$. In view of Equations 1-4 where both f_{OC} and Q_{p} are functions of Q, to some extent, there should be a positive correlation between predicted f_{OC} and Q_{p}. In addition, Δs and ΔSM exhibit a strong and consistent relationship in reflecting the SWI extent. Large values of Δs or ΔSM indicate a more severe level of SWI, conversely, it suggests a milder degree of SWI when the values of Δs or ΔSM are small. That implies the predicted values of Δs and ΔSM should be strongly positively correlated, resulting in a high $CC_{\Delta s\_\Delta SM}$. As a result, if $CC_{\text{OC\_}Q_{\text{p}}}$ can show at least a mild correlation between f_{OC} and Q_{p} while $CC_{\Delta s\_\Delta SM}$ can demonstrate Δs and ΔSM have a strong positive correlation, the GP models built by the proposed strategy can produce trustable results. Otherwise, the results given by the GP models are believed to be unreliable.

(2) $\overline{PPO}$

Predictions at the unobserved points generated by GP models fluctuate around the expected values with certain standard deviations, reflecting the epistemic uncertainties in the GP model estimates. Therefore, predicted f_{OC}, Q_{p}, Δs and ΔSM at the unknown points in this work are uncertain, causing the derived Pareto-optimal solutions may change at a different stochastic run and each pumping scheme is characterized by a probability of Pareto-optimality (PPO). $\overline{PPO}$ can be employed to evaluate whether the results given by GP models are stable and reliable or not, expression for calculating $\overline{PPO}$ presented below:

$$\overline{PPO} = \frac{1}{N_{\mathrm{P}}}\sum_{i=1}^{N_{\mathrm{P}}} PPO_i \tag{28}$$

where N_{P} denotes the number of potential Pareto-optimal solutions, and PPO_i is the probability of the *i*-th pumping candidate as a Pareto-optimal solution. Computing PPO_i relies on the repeated stochastic simulations (Monte Carlo) runs, which is computationally viable because of the inexpensiveness of the GP models, calculated by

$$PPO_i = \frac{\mathcal{N}_i}{\mathcal{N}} \tag{29}$$

where $\mathcal{N}$ denotes the total number of Monte Carlo runs, set as 1,000 in this work, while $\mathcal{N}_i$ is the times of input *i* serving as a Pareto-optimal solution. A detailed description of how to calculate predicted values of f_{OC}, Q_{p}, Δs and ΔSM for each Monte Carlo run is presented in the Supporting Information – Appendix B.

(3) $Per_{\mathrm{prob\_threshold}}$

$$Per_{\mathrm{prob\_threshold}} = \frac{N_{\mathrm{Pt}}}{N_{\mathrm{P}}} \times 100\% \tag{30}$$

where N_{Pt} is the number of derived optimal pumping schemes reaching the specified probability level.

3 Results and Discussion

3.1 Performance investigations of offline training GP models

GP models trained for predicting f_{OC}, Q_{p}, Δs and ΔSM using strategies **F1**, **F2** or **F3**, all commence with eight initial training samples. These initial samples are drawn by the Latin Hypercube sampling (LHS) method, dividing each decision variable dimension into two intervals and then sampling the centre point of each cube. The results indicate that for convergence, strategies **F1**, **F2** and **F3** require a total of 52, 46, and 64 SWI simulations, respectively. To compare the performance of GP models constructed by strategies **F1**, **F2** and **F3** under equal computational costs, even achieving convergence, GP models continue to be trained in the cases of using strategies **F1** and **F2** until they reach the same computational costs as that of strategy **F3**. Meantime, to assess the differences in GP model performance among using the strategies **F1**, **F2**, **F3** and the traditional offline training approach **F4**, this study employs **F4** to develop GP models under two distinct computational cost conditions, respectively involving 64 and 125 SWI simulations. These 64 and 125 training samples are drawn by the LHS method. Table 3 presents *CC* between $\log_{10} f_{\mathrm{OC}}$ and $\log_{10}\frac{r}{1-r}$ ($CC_{l\_\mathrm{OC}\_r}$), *CC* between $\log_{10}\Delta s$ and $\log_{10}(\Delta SM + 1)$ ($CC_{l\_\Delta s\_\Delta SM}$), $CC_{\mathrm{OC}\_Q_{\mathrm{p}}}$ and $CC_{\Delta s\_\Delta SM}$ derived from the training data, as well as the $CC_{\mathrm{OC}\_Q_{\mathrm{p}}}$ and $CC_{\Delta s\_\Delta SM}$ from the GP model predictions over the

input space in the various cases of offline training tests, while Figures 7-8 show $\overline{PPO}$ and $Per_{\text{prob\_threshold}}$ for all offline training tests, respectively.

Table 3. *For Various Offline Training Tests, the Values of the $CC_{l\_OC\_r}$, $CC_{l\_\Delta s\_\Delta SM}$, $CC_{OC\_Q_p}$ and $CC_{\Delta s\_\Delta SM}$ Derived from the Training Data, as well as the $CC_{OC\_Q_p}$ and $CC_{\Delta s\_\Delta SM}$ Obtained from the GP Model Predictions Over the Entire Defined Input Space.*

Strategy of offline training		**F1**		**F2**		**F3**	**F4**	
Number of training samples		52	64	46	64	64	64	125
Training data	$CC_{l\_\text{OC}\_r}$	-0.75	-0.74	-0.69	-0.73	-0.72	-0.85	-0.84
	$CC_{l\_\Delta s\_\Delta SM}$	0.60	0.62	0.63	0.62	0.68	0.71	0.63
	$CC_{\text{OC}\_Q_\text{p}}$	0.63	0.60	0.71	0.76	0.55	0.59	0.60
	$CC_{\Delta s\_\Delta SM}$	0.88	0.88	0.95	0.95	0.90	0.96	0.95
GP model estimates	$CC_{\text{OC}\_Q_\text{p}}$	0.49	0.57	0.01	0.08	0.47	0.37	0.46
	$CC_{\Delta s\_\Delta SM}$	0.47	0.56	0.02	-0.02	0.74	0.52	0.57

Observing Table 3, $CC_{l\_\text{OC}\_r}$ and $CC_{l\_\Delta s\_\Delta SM}$ in the training data range from -0.85 to -0.69 and from 0.60 to 0.71, respectively, indicating that there is a moderate-strong negative correlation between $\log_{10} f_{\text{OC}}$ and $\log_{10}\frac{r}{1-r}$ and a moderate positive correlation between $\log_{10}\Delta s$ and $\log_{10}(1+\Delta SM)$ in the training data. Values of $CC_{l\_\text{OC}\_r}$ and $CC_{l\_\Delta s\_\Delta SM}$ derived from the training data are used to generate z_{OC}, z_{p}, $z_{\Delta s}$ and $z_{\Delta SM}$ in the Equations B1-B4, producing stochastic estimates of f_{OC}, Q_{p}, Δs and ΔSM. The values of $CC_{\text{OC}\_Q_\text{p}}$ and $CC_{\Delta s\_\Delta SM}$ in the training data vary within the ranges of 0.55 to 0.76 and 0.88 to 0.96, respectively, demonstrating that there is a moderate positive correlation between f_{OC} and Q_{p} while a strong positive correlation between Δs and ΔSM in the training data. That is consistent with the prior conjecture about the relationship between f_{OC} and Q_{p} and the relationship between Δs and ΔSM throughout the input space.

Table 3 shows in the case of using strategy **F1**, the values of $CC_{\text{OC}\_Q_\text{p}}$ and $CC_{\Delta s\_\Delta SM}$ in the GP model predictions are respectively 0.49 and 0.47 when employing 52 training samples and are respectively 0.57 and 0.56 if the training samples increase to 64. This observation suggests over the input space there are moderate positive correlations between estimated f_{OC} and Q_{p}, and between estimated Δs and ΔSM, and their correlations tend to strengthen with the size of training data increasing. Similarly, GP models developed through strategy **F4** exhibit the capability to generate moderately correlated f_{OC} and Q_{p}, as well as moderately correlated Δs and ΔSM, and both sets of correlations intensify as the size of training samples expands from 64 to 125. Clearly, over the entire input space, predictions from the GP models developed by strategy **F1** or **F4** fail to show a strong positive correlation between Δs and ΔSM, suggesting

that estimates in Δs or/and ΔSM highly contain some errors. When employing strategy **F2**, both the values of $CC_{\mathrm{OC}\_Q_\mathrm{p}}$ and $CC_{\Delta s\_\Delta SM}$ under the conditions of consuming either 46 or 64 SWI simulations are nearly zero, demonstrating that predicted f_{OC} and Q_p are uncorrelated and the same for predicted Δs and ΔSM. It suggests that the GP models built by strategy **F2** are prone to offer unreliable estimates of f_{OC}, Q_p, Δs and ΔSM across the input space. However, a moderate positive correlation between f_{OC} and Q_p and an approximately strong positive correlation between Δs and ΔSM in the GP model predictions exist in the case of offline training using strategy **F3** with 64 training samples. Specifically, the values of $CC_{\mathrm{OC}\_Q_\mathrm{p}}$ and $CC_{\Delta s\_\Delta SM}$ in the GP model predictions are 0.47 and 0.74, respectively.

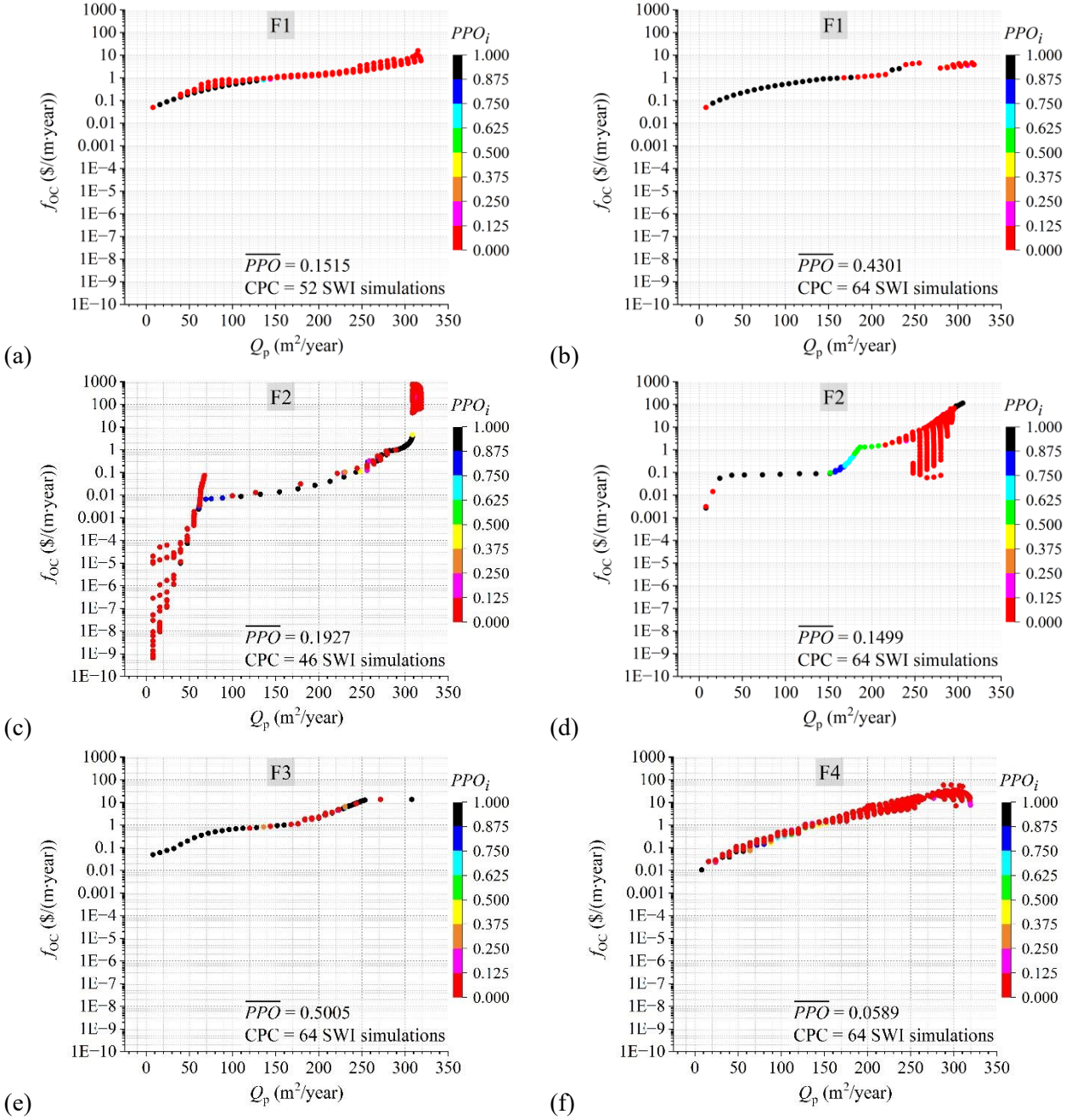

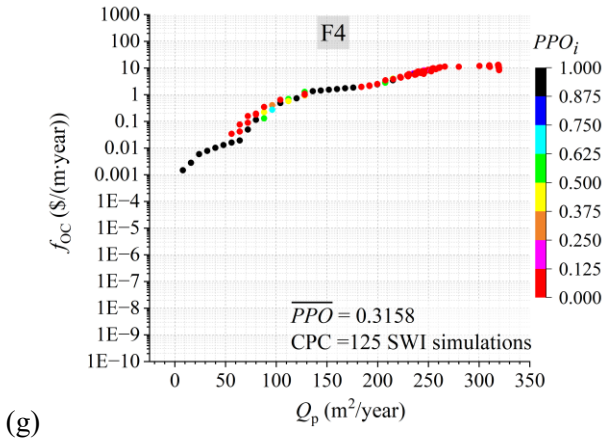

(g)

Figure 7. $\overline{PPO}$ under the various conditions of offline training GP models: a) strategy F1, use 52 SWI simulations; b) strategy F1, use 64 SWI simulations; c) strategy F2, use 46 SWI simulations; d) strategy F2, use 64 SWI simulations; e) strategy F3, use 64 SWI simulations; f) strategy F4, use 64 SWI simulations; g) strategy F4, use 125 SWI simulations.

Figures 7a-c-e depict the probabilistic optimal Pareto fronts derived from the converged offline training GP models using strategies **F1**, **F2**, and **F3**, respectively. In these three figures, Pareto optimal solutions in the region characterized by larger values of f_{OC} and Q_{p} are usually with lower probabilities (i.e., higher uncertainties) compared with those located in the region characterized by the lower values of f_{OC} and Q_{p}. This phenomenon arises due to the utilization of the log-transformation technique during GP model development, where the forecasted values f_{OC}, Q_{p}, Δs or ΔSM are determined calculated using a base of ten raised to the power of the GP model estimates. Therefore, for the points with larger GP model estimates, although standard deviations are small, there are higher uncertainties. This explanation is also adaptable to the similar phenomenon occurring in Figures 7b-d-f-g.

Comparing Figures 7a-c-e, the offline-trained GP models based on strategy **F1** require a total of 52 SWI simulations to converge and produce the lowest $\overline{PPO}$, equal to 0.1515. Offline training GP models built by strategy **F2** consume the least computational expense, with only 46 SWI simulations, and the corresponding $\overline{PPO}$ is identical to 0.1927, slightly larger than that in Figure 7a. It is significantly noticeable that the probabilistic optimal Pareto front in Figure 7c has a larger range in the dimension of f_{OC} than those in Figures 7a and 7e. This is because strategy F2 determines new sampling points during GP model development only based on the gradients rather than covering as much entire search space as possible, leading to most training data gathering the higher gradient regions. That results in the situation where GP model estimates exhibit a tendency for higher gradients across all unknown points, causing a significant range in f_{OC} as depicted in Figure 7c. Offline training of GP models using strategy **F3** demands the most extensive training dataset for achieving convergence, involving 64 SWI simulations, but these GP models produce the highest value of $\overline{PPO}$, which is up to 0.5005. Overall, the outcomes illustrated in Figures 7a-c-e highlight that employing either strategy **F1**

or **F2** for GP model training, sampling new points by covering as much entire search space as possible or by taking the points with the highest gradients, can achieve the convergence with lower computational costs, but yields an optimal Pareto front with a lower $\overline{PPO}$. In contrast, GP models established through strategy **F3**, which combines information about the input point distribution over the search space and model estimate gradients, incur greater computational expense, but produce more reliable optimal Pareto front compared to the ones generated by GP models trained using strategies **F1** and **F2**.

Figures 7b-d-e-f respectively illustrate the probabilistic optimal Pareto front obtained from the GP models built by strategies **F1**, **F2**, **F3**, and **F4**, all with equivalent computational costs. With the number of training samples increasing from 52 to 64, GP models trained using strategy **F1** offer a more dependable optimal Pareto front, $\overline{PPO}$ remarkably increasing from 0.1515 to 0.4301. In contrast, Figure 7d shows that with the size of training samples growing from 46 to 64, although GP models built by strategy **F2** offer more reliable Pareto optimal solutions at the region characterized by lower values of f_{OC} and Q_{p} compared to what is observed in Figure 7c, they generate less reliable optimal Pareto front over whole search space, $\overline{PPO}$ reducing from 0.1927 to 0.1499. As Figure 7e indicates that $\overline{PPO}$ in the case of applying strategy **F3** and consuming 64 SWI simulations is up to 0.5005, this observation leaves no room to dispute that under the same computational budget, strategy **F3** outperforms strategies **F1** and **F2** in training GP models to yield more trustworthy optimal pumping schemes. Moreover, comparing the performance of offline training GP models built by the proposed strategies **F1**, **F2** and **F3** with that of the GP models created through 64 SWI simulations and employing the traditional offline training strategy **F4**, it is obvious that the latter produces the least reliable optimal Pareto front, where $\overline{PPO}$ is only equal to 0.0589.

Figure 7g demonstrates that as the volume of training data almost doubles, rising from 64 to 125 SWI simulations, $\overline{PPO}$ of the probabilistic optimal Pareto front obtained from the GP models, which are built through the traditional strategy **F4**, experiences an approximately sixfold increase from 0.0589 to 0.3158 However, this value remains lower than 0.4301 obtained from the GP models trained by strategy **F1** and 0.5005 derived from the GP models trained by strategy **F3**, both of which involve 64 SWI simulations. It can be inferred that to attain an equivalent level of reliability in the resulting optimal Pareto front, training GP models via strategy **F1** or **F3** can save at least 50% computational costs compared to using the traditional offline training strategy **F4**.

Overall, according to Figure 7, it can conclude that:

1) Applying strategies **F1** and **F2** for offline training GP models can result in quicker convergence compared to employing strategy **F3**.

2) After convergence, increasing the size of training data can improve the overall robustness of the optimal Pareto front given by the GP models built by strategy **F1**.

3) After convergence, increasing the size of training data to build GP models by strategy **F2** fails to enhance $\overline{PPO}$ and even decrease $\overline{PPO}$, implying that using strategy **F2** develops GP models possibly generates unstable optimal Pareto front.

4) GP models trained via strategy **F3** consume more computational costs to converge than those using strategy **F1** or **F2**, but they provide a more reliable optimal Pareto front than GP models built by strategies **F1** and **F2**. Even if the size of training data for building GP models by strategies **F1** and **F2** is increased to be equal to that for developing GP models using strategy **F3**, applying strategy **F3** remains superior in training GP models to generate reliable optimal solutions.

5) To achieve an acceptable level of probabilistic optimal Pareto front, employing the traditional strategy **F4** for building GP models necessitates a larger number of training samples (Figure 7g). Otherwise, the resulting probabilistic optimal Pareto front exhibits notably high uncertainties, $\overline{PPO}$ close to 0 (Figure 7f).

6) To reach a moderate reliable level of the derived optimal Pareto front, such as $\overline{PPO}$ over 0.3, applying strategies **F1** and **F3** to train GP models can cause over 50% reduction in computational costs compared to the implementation of traditional strategy **F4**.

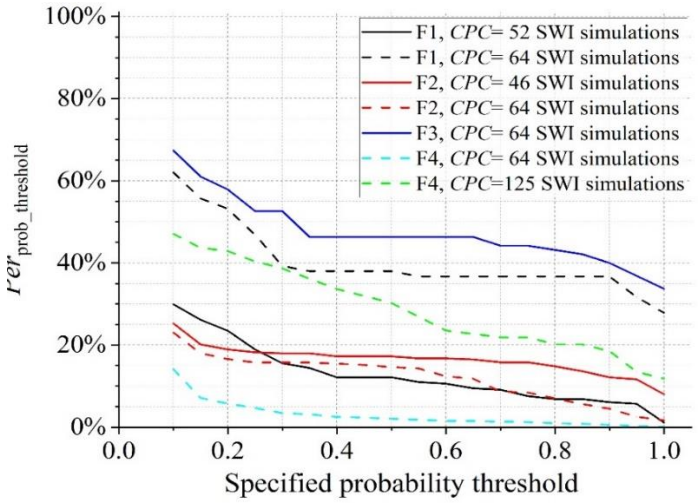

Figure 8. $Per_{\text{prob\_threshold}}$ varying with the specified probability threshold under various offline training tests.

Figure 8 shows that all curves in general, exhibit a monotonically decreasing behaviour, values of $Per_{\text{prob\_threshold}}$ dropping with the specified probability threshold enhancing. These curves can be roughly divided into two groups. Across the range of specified probability

thresholds, one group is situated in the region with a relatively high value of $Per_{\text{prob\_threshold}}$, while the other is overall positioned in the low $Per_{\text{prob\_threshold}}$ region. The former comprises three instances: training GP models using strategy **F3** with 64 SWI simulations, training GP models using strategy **F1** with 64 SWI simulations, and training GP models using strategy **F4** with 125 SWI simulations. Clearly, the blue solid curve representing GP models built with strategy **F3** and 64 SWI simulations is always higher than the black dashed curve representing GP models built with strategy **F1** and 64 SWI simulations, while the black dashed curve is always higher than that green dashed curve representing GP models built with strategy **F4** and 125 SWI simulations. That corresponds to the order of $\overline{PPO}$ under these three cases (Figures 7b-e-g), demonstrating that given any probability threshold, the value of $Per_{\text{prob\_threshold}}$ under the condition with a higher $\overline{PPO}$ is greater than that under the condition with a lower $\overline{PPO}$.

In the remaining four cases, the values of $Per_{0.1}$ fall within the range of roughly 15% to 30%, in other words, the percentages of Pareto-optimal solutions characterized by high uncertainties in these cases, probabilities of being Pareto-optimal solutions fewer than 0.1, range from 70% to nearly 85%, indicating that derived Pareto-optimal solutions, on the whole, are with low probabilities. According to Figure 7, values of $\overline{PPO}$ for these four cases are also quite low, ranging between 0.0589 and 0.1927. Prior to gaining access to the information illustrated in Figure 8, the occurrence of lower $\overline{PPO}$ in certain cases (e.g., Figures 7a-c-d-f) can be attributed to two distinct situations. The first situation is that all derived potentially optimal solutions are with lower probabilities, consequently leading to an overall lower $\overline{PPO}$. The second situation is that despite the moderate or high percentage of high-probable optimal solutions, there exists a certain proportion of optimal solutions with exceedingly low probabilities, serving as outliers and contributing to an overall lower $\overline{PPO}$. Therefore, Figure 8 eliminates the potential that the case with a low $\overline{PPO}$ is due to a certain proportion of very-low-probable optimal solutions, highlighting that a low $\overline{PPO}$ arises from overall low probabilities of derived optimal solutions.

In summary, according to the analysis of Table 3 and Figures 7-8, offline training GP models employing strategy **F1** or **F3** and consuming 64 SWI simulations are expected to guarantee prediction accuracy across the entire input space and generate a more reliable optimal Pareto front, compared with other offline training tests. Applying strategy **F1** for training GP models facilitates rapid convergence, but the reliability of the resulting optimal Pareto front is inferior to that using strategy **F3**, remaining true even when the computational budget is

increased to match that used for training GP models with strategy **F3**. Therefore, strategy **F3** is believed to be the best algorithm for offline training GP models among all proposed strategies in this paper.

3.2 Performance investigations of online training GP models

GP models trained for identifying the optimal pumping schemes using strategies **N1**, **N2**, **N3** or **N4**, all start with the same eight initial training samples that are employed in the offline training framework. Online training GP models using strategies **N1**, **N2**, **N3**, and **N4** adhere to the sequence outlined in the flowchart depicted in Figure 4. Values of $\overline{PPO}$ changing with the size of training data under different online training tests are presented in Figure 9, showing the tendency of convergence.

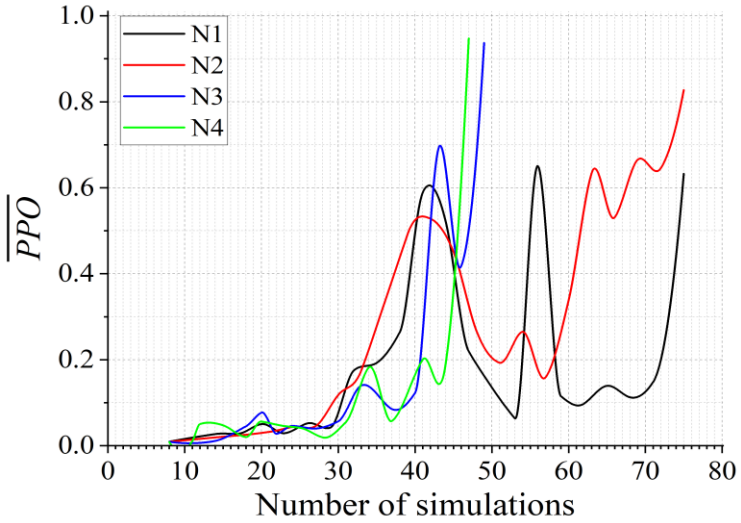

Figure 9. $\overline{PPO}$ changing with the size of training data under various online training tests.

Figure 9 demonstrates that online training GP models via strategy **N1** fail to converge within the maximum allowed computational budget, while those built by strategies **N2**, **N3** and **N4** achieve the convergence at the costs of 75, 47, and 45 SWI simulations. In the case of using strategy **N1**, the values of $\overline{PPO}$ obtained from online training GP models display a pronounced fluctuation ranging from around 0.1 to approximately 0.65 without showing a trend toward convergence. This observation implies that elevating the computational budget does not promptly facilitate the convergence of online-trained GP models using strategy **N1**, suggesting that the GP models trained through this strategy offer an unstable optimal Pareto front. When employing strategy **N2**, the value of $\overline{PPO}$ exhibits a general upward trend with the increase in training data size, despite the presence of fluctuations, and reaches 0.8274 at the cost of 75 SWI simulations. Strategy **N2** shares similarities with strategy **N1**, both searching for new sampling points in each iteration by ranking the probabilistic distance from the unknown point to the closest training point, but the former is based on the discretization of the scaled objective

space. The performance of strategies **N1** and **N2** preliminarily indicates that discretizing objective space for sampling new points helps online training GP models to converge. Likewise, both online training strategies **N3** and **N4** depend on objective space discretization. Under the conditions of employing strategies **N3** and **N4**, the values of $\overline{PPO}$ exhibit an overall increasing trend along with fluctuations as the number of training samples increases, respectively reaching 0.9367 with a cost of 47 SWI simulations and 0.9474 with a cost of 45 SWI simulations. That again highlights the effectiveness of discretizing objective space for identifying new sampling points in enhancing training efficiency, and it also demonstrates strategies **N3** and **N4** are not only more efficient but also lead to a more reliable optimal Pareto front compared to strategy **N2**.

Moreover, Figure 9 reveals that when the number of training samples ranges from 8 to approximately 30, the values of $\overline{PPO}$ under all online training tests exhibit fluctuations and remain low, below 0.1. Subsequently, beyond 30 training samples, the values of $\overline{PPO}$ in all cases begin to rise, almost greater than 0.1. This observation suggests that there exists a minimum threshold for the number of training samples in online-trained GP models to avoid high uncertainties in the resulting optimal Pareto front, which is nearly ten times the number of decision variables.

The accuracy and reliability of derived optimal Pareto front from the GP models developed by strategies N1, N2, N3 and N4 are further validated by CC, $\overline{PPO}$ and $Per_{\text{prob\_threshold}}$. Table 4 presents the values of $CC_{l\_\text{OC}\_r}$, $CC_{l\_\Delta s\_\Delta SM}$, $CC_{\text{OC}\_Q_\text{p}}$ and $CC_{\Delta s\_\Delta SM}$ derived from the training data, as well as the $CC_{\text{OC}\_Q_\text{p}}$ and $CC_{\Delta s\_\Delta SM}$ obtained from the GP model predictions over the probabilistic optimal Pareto front in the various cases of online training tests, while Figures 10-11 show $\overline{PPO}$ and $Per_{\text{prob\_threshold}}$ for all online training tests, respectively.

Table 4. *For Various Online Training Tests, the Values of $CC_{l\_OC\_r}$, $CC_{l\_\Delta s\_\Delta SM}$, $CC_{OC\_Q_p}$ and $CC_{\Delta s\_\Delta SM}$ Derived from the Training Data, as well as the $CC_{OC\_Q_p}$ and $CC_{\Delta s\_\Delta SM}$ Obtained from the GP Model Predictions over the Probabilistic Optimal Pareto front.*

Strategy of online training		**N1**	**N2**	**N3**	**N4**
Number of training samples		75	75	47	45
Training data	$CC_{l\_\text{OC}\_r}$	-0.91	-0.90	-0.88	-0.95
	$CC_{l\_\Delta s\_\Delta SM}$	0.57	0.63	0.61	0.67
	$CC_{\text{OC}\_Q_\text{p}}$	0.57	0.61	0.47	0.44
	$CC_{\Delta s\_\Delta SM}$	0.80	0.90	0.79	0.85
GP model predictions	$CC_{\text{OC}\_Q_\text{p}}$	0.63	0.88	0.84	0.90
	$CC_{\Delta s\_\Delta SM}$	0.55	0.73	0.86	0.89

Observing Table 4, $CC_{l\_\mathrm{OC}\_r}$ and $CC_{l\_\Delta s\_\Delta SM}$ in the training data range from -0.88 to -0.95 and from 0.57 to 0.67, respectively, indicating that there is a strong negative correlation between $\log_{10} f_{\mathrm{OC}}$ and $\log_{10}\frac{r}{1-r}$ and a moderate positive correlation between $\log_{10}\Delta s$ and $\log_{10}(1+\Delta SM)$ in the training data. Values of $CC_{l\_\mathrm{OC}\_r}$ and $CC_{l\_\Delta s\_\Delta SM}$ derived from the training data are used to generate z_{OC}, z_{p}, $z_{\Delta s}$ and $z_{\Delta SM}$ in the Equations 33-36, producing stochastic estimates of f_{OC}, Q_{p}, Δs and ΔSM. For various online training tests, the values of $CC_{\mathrm{OC}\_Q_{\mathrm{p}}}$ and $CC_{\Delta s\_\Delta SM}$ in the training data fall within the ranges of 0.44 to 0.61 and 0.79 to 0.90, respectively, demonstrating that there is a moderate positive correlation between f_{OC} and Q_{p} while a strong positive correlation between Δs and ΔSM in the training data. Those almost align with the presumptions about the correlation between f_{OC} and Q_{p} and the correlation between Δs and ΔSM across the input space.

Considering the purpose of online training GP models, aiming to quickly determine locally optimal solutions with low computational costs, Table 4 offers the values of $CC_{\mathrm{OC}\_Q_{\mathrm{p}}}$ and $CC_{\Delta s\_\Delta SM}$ obtained from the GP model predictions across the probabilistic optimal Pareto front. As seen from Table 4, the values of $CC_{\mathrm{OC}\_Q_{\mathrm{p}}}$ derived from the GP model predictions vary from 0.63 to 0.90, signifying a moderate to a strong positive correlation between the predicted f_{OC} and Q_{p} within the attained Pareto-optimal solutions. That is different from what is observed in the offline training tests, but it can be understood. As the Pareto front comprises non-dominant points usually characterized by low f_{OC} and high Q_{p}, it suggests that f_{OC} in most cases does not include the component of f_{t} according to Equations 1-4, which often leads to a higher f_{OC}. Consequently, both f_{OC} and Q_{p} are almost the functions of Q, resulting in a strong positive correlation between them. In view of that, predicted values of f_{OC} and Q_{p} within the attained Pareto-optimal solutions under the conditions of employing strategies **N2**, **N3** and **N4**, where forecasted f_{OC} and Q_{p} are strongly positively correlated, are more trustworthy than those using strategy **N1**. Likewise, the values of $CC_{\Delta s\_\Delta SM}$ are expected to reflect a strong correlation between predicted Δs and ΔSM in the derived Pareto-optimal solutions. Table 4 shows that the values of $CC_{\Delta s\_\Delta SM}$ in the obtained Pareto-optimal solutions in the cases of using strategy **N1**, **N2**, **N3** and **N4** are 0.55, 0.73, 0.86 and 0.89, respectively, highlighting that utilizing strategies **N2**, **N3** and **N4** can generate dependable estimates of Δs and ΔSM in proximity to the potential Pareto-optimal solutions. Overall, according to the values of $CC_{\mathrm{OC}\_Q_{\mathrm{p}}}$ and $CC_{\Delta s\_\Delta SM}$ within

predicted Pareto-optimal solutions, using strategies **N2**, **N3** and **N4** are believed to generate more dependable Pareto-optimal pumping schemes.

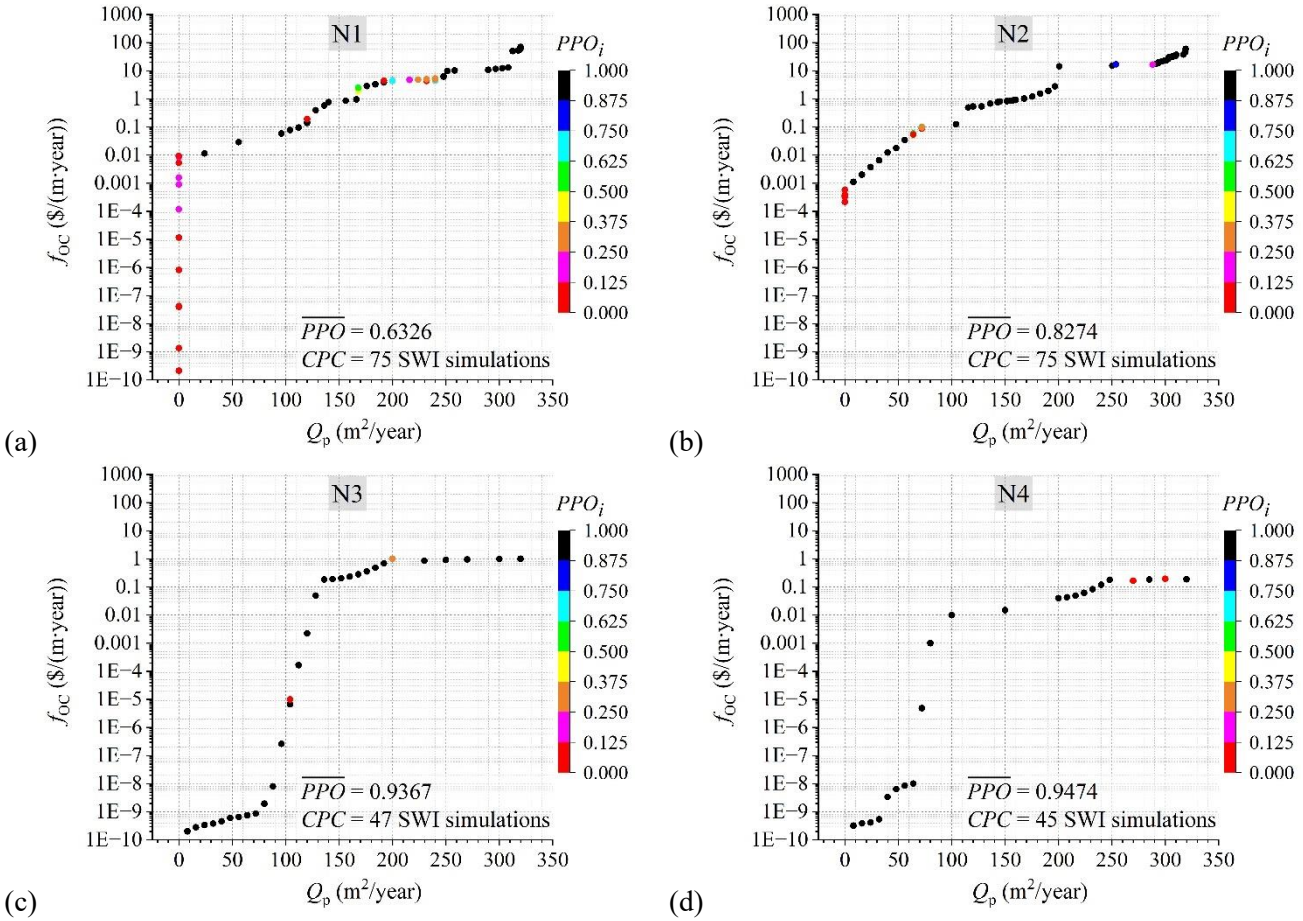

Figure 10. $\overline{PPO}$ under various conditions of online training GP models: a) strategy N1, use 75 SWI simulations; b) strategy N2, use 75 SWI simulations; c) strategy N3, use 47 SWI simulations; d) strategy N4, use 45 SWI simulations.

Figures 10a-d show the resulting optimal Pareto front under various cases of online training GP models. Figures 10a-b depict that there are some Pareto-optimal pumping schemes with low probability when Q_p is identical to 0. This disobeys common knowledge, in which zero Q_p should correspond to zero financial cost, suggesting that the beginning point of the obtained optimal Pareto front should have both low values of f_{OC} and Q_p, like those in Figures 10c-d. It indicates that GP models trained by strategy **N1** with 75 SWI simulations or strategy **N2** with 75 SWI simulations possibly generate an undependable optimal Pareto front. On the other hand, Figures 10a-d illustrate that for various online training tests, the value range of Q_p in the optimal Pareto front remains relatively consistent, but that of f_{OC} exhibits a noticeable difference, especially maximum values of f_{OC}. In Figures 10a-d, maximum values of f_{OC} in the obtained Pareto front are respectively 70.48, 59.70, 1.01 and 0.20 $/(m·year), GP models

trained by strategy N3 with 47 SWI simulations or strategy N4 with 45 SWI simulations are able to produce more cost-effective optimal Pareto front.

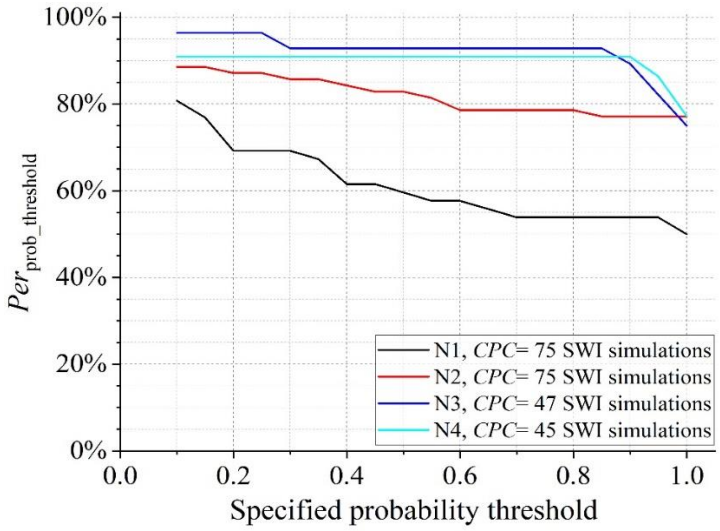

Figure 11. $Per_{\text{prob\_threshold}}$ varying with the specified probability threshold under various online training tests.

In Figure 11, values of $Per_{\text{prob\_threshold}}$ under all online training tests generally exhibit a monotonically decreasing behaviour with the specified probability threshold enhancing. Under the conditions of employing strategies **N1**, **N2**, **N3** and **N4**, values of $Per_{0.1}$ are respectively around 81%, 89%, 96% and 91%, while values of $Per_{1.0}$ reach 50%, 77%, 75% and 77% respectively. This highlights the fact that online training GP models can cause the proportion of very-low-probable optimal pumping schemes (i.e., probability fewer than 0.1) within the derived Pareto front is low, fewer than 20%, and the proportion of deterministic optimal pumping schemes in the resulting Pareto front is high when applying strategy **N2**, **N3** or **N4**, up to around 75%. It is noted that the values of $Per_{\text{prob\_threshold}}$ under the condition of using strategy **N2** gradually drop with the increase in the probability threshold, while those under the conditions of taking strategies **N3** and **N4** nearly remain unchanged before the probability threshold reaching 0.9, revealing that derived Pareto-optimal pumping schemes using strategies **N3** and **N4** are more reliable and stable than those based on strategy **N2**. Moreover, Figure 11 explains the reason for low $\overline{PPO}$ when using strategy **N1** is because derived Pareto optimal solutions generally possess lower probabilities on the whole compared to those in the cases of using the other three strategies. Herein, this explanation eliminates the possibility that an overall lower $\overline{PPO}$ is due to a certain proportion of exceedingly low-probable optimal solutions despite the moderate or high percentage of high-probable optimal solutions.

In summary, according to the analysis of Table 4 and Figures 10-11, online training GP models employing strategy **N2**, **N3** or **N4** are expected to guarantee prediction accuracy of the

derived Pareto-optimal solutions and generate a more reliable optimal Pareto front, compared with online training GP models by strategy **N1**. That highlights the importance of discretizing the objective space when identifying new sampling points, ensuring that these new points are distributed across a wider expanse of the objective space rather than being concentrated in specific regions. However, compared with strategies **N3** and **N4**, applying strategy **N2** for online training GP models facilitates slow convergence, and the reliability of the resulting optimal Pareto front is inferior to those under the conditions of using strategy **N3** and **N4**. Therefore, it is inferred that strategies **N3** and **N4** stand out as the top two algorithms for effectively online training GP models in tackling the formulated bi-objective groundwater management problem. Especially, strategy **N4** exhibits a slight edge over strategy **N3** in terms of both the computing efficiency and reliability of the resulting optimal Pareto front.

3.3 Performance comparison of offline and online training GP models

In section 3.1, this study tests seven offline training scenarios, where each scenario involves a combination of adopted strategy and consumed training samples as follows: 1) **F1** with 52 SWI simulations, 2) **F1** with 64 SWI simulations, 3) **F2** with 46 SWI simulations, 4) **F2** with 64 SWI simulations, 5) **F3** with 64 SWI simulations, 6) **F4** with 64 SWI simulations, and 7) **F4** with 125 SWI simulations. The values of $\overline{PPO}$ correspond to these seven offline training tests are 0.1515, 0.4301, 0.1927, 0.1499, 0.5005, 0.0589 and 0.3158. The values of $Per_{0.1}$ correspond to these seven offline training tests are roughly 30%, 62%, 25%, 23%, 67%, 14% and 47%, while the values of $Per_{1.0}$ in the cases of these seven offline training tests are approximately 1%, 28%, 8%, 2%, 34%, 0 and 12%.

In section 3.2, four online training scenarios are tested, where each scenario involves a combination of adopted strategy and consumed training samples as follows: 1) **N1** with 75 SWI simulations, 2) **N2** with 75 SWI simulations, 3) **N3** with 47 SWI simulations, 4) **N4** with 45 SWI simulations. The values of $\overline{PPO}$ correspond to these four online training tests are 0.6326, 0.8274, 0.9367 and 0.9474. The values of $Per_{0.1}$ correspond to these seven offline training tests are 81%, 89%, 96% and 91%, while the values of $Per_{1.0}$ in the cases of these seven offline training tests are 50%, 77%, 75% and 77%.

When comparing the performance of offline training tests to online training tests, it is apparent that the values of $\overline{PPO}$, as well as the values of $Per_{0.1}$ and $Per_{1.0}$ associated with resulting Pareto-optimal pumping schemes in the cases of adopting offline training GP models, are notably lower than those derived from online training GP models. This highlights that given the coastal groundwater management problem, online training GP models are more

advantageous than offline training GP models in offering dependable Pareto-optimal pumping schemes. The values of $CC_{\mathrm{OC\_}Q_\mathrm{p}}$ and $CC_{\Delta s\_\Delta SM}$ in the resulting optimal Pareto front (Table 4) also validate the prediction accuracy of Pareto-optimal pumping schemes given by online training GP models. Moreover, as analysed in sections 3.1 and 3.2, to efficiently generate reliable Pareto-optimal pumping schemes by GP models, the best approach for offline training is employing strategy **F3** and correspondingly consuming 64 SWI simulations, while for online training, the most appropriate choices are adopting strategies **N3** and **N4**, which respectively require 47 and 45 SWI simulations. This reveals that online-trained GP models are more computationally efficient than offline-trained GP models in deriving optimal Pareto front. Probabilistic optimal Pareto fronts in the cases of using strategy **F3** and 64 SWI simulations, strategy **N3** and 47 SWI simulations, and strategy **N4** and 45 SWI simulations are presented in Figure 12. Figure 12 shows that optimal Pareto fronts given by online-trained GP models are lower than that obtained from offline training GP models, demonstrating that online-trained GP models are more capable of generating cost-effective Pareto-optimal pumping schemes. This can be understood because potentially Pareto-optimal solutions serve as new sampling points at each iteration, promoting the resulting optimal Pareto front to gradually approach the actual with the update.

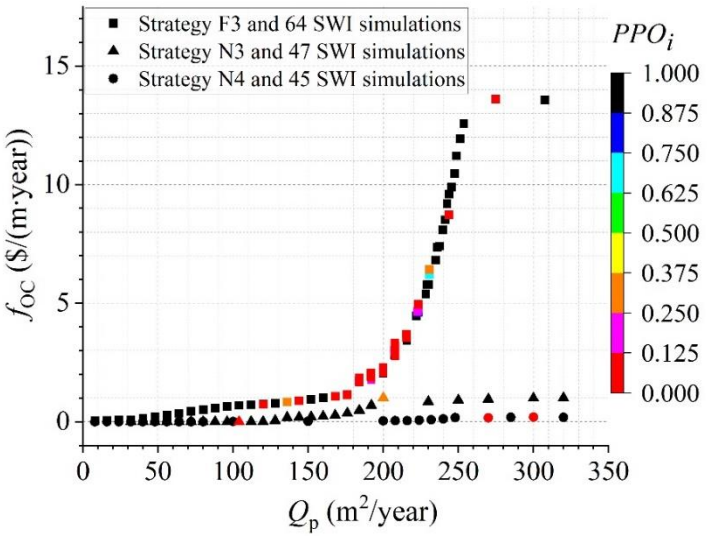

Figure 12. Probabilistic optimal Pareto fronts in the cases of using strategy **F3** and 64 SWI simulations, strategy **N3** and 47 SWI simulations, strategy **N4** and 45 SWI simulations.

Even though offline-trained GP models yield less dependable Pareto-optimal solutions, the benefits of utilizing these models to identify optimal pumping schemes in coastal groundwater management should not be ignored. First, according to the values of $CC_{\mathrm{OC\_}Q_\mathrm{p}}$ and $CC_{\Delta s\_\Delta SM}$ in the GP model predictions over the entire defined input space (Table 3), offline training GP models by strategies **F1**, **F3** and **F4** are believed to be able to produce dependable

predictions over the entire input space. Beneficial from this characteristic, apart from its use in identifying optimal pumping strategies, GP models created through offline training have the potential to tackle other issues that demand multiple pumping outputs throughout the input space, such as investigating the impacts of pumping patterns on f_{OC}, Q_{p}, Δs or ΔSM.

Second, GP models created by offline training complete the development before the optimisation stage, and thus they are independent of the changes in SWI constraint conditions. In other words, offline-trained GP models can still be in use to identify optimal Pareto front when the threshold values of $\Delta s_{\max}$ (Equation 7) or/and $\Delta SM_{\max}$ (Equation 9) change, while online-trained GP models must be re-trained. Figure 13 presents potential Pareto-optimal pumping schemes derived from offline-trained GP models built using strategy **F3** and 64 training samples, under three distinct SWI constraint conditions. Figure 13 reveals that offline-trained GP models correctly capture the impact of SWI constraint condition changes in the resulting optimal Pareto fronts, loosening limitations on SWI control can lowering financial costs while maintaining the desired amount of qualified groundwater. This highlights the applicability of offline-trained GP models for conducting sensitivity analysis of optimal pumping strategies to SWI constraint conditions.

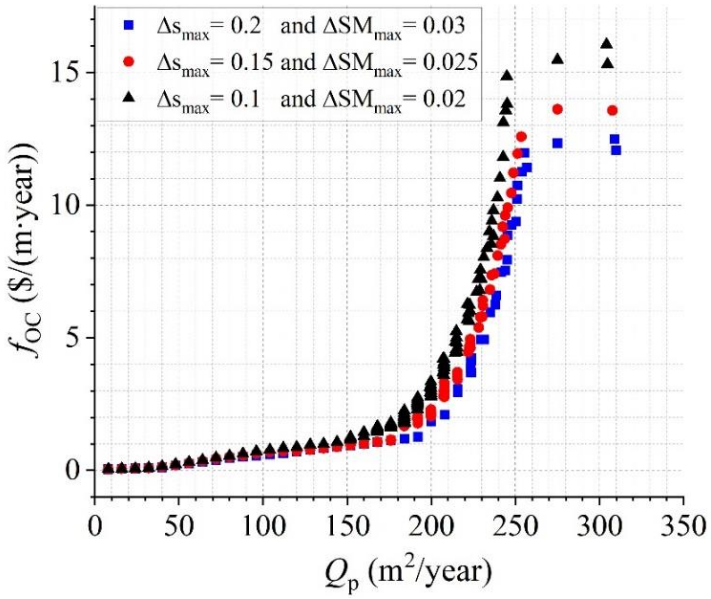

Figure 13. Potentially Pareto-optimal pumping schemes derived from offline-trained GP models built using strategy **F3** and 64 training samples, under three distinct SWI constraint conditions.

4 Conclusions

To investigate the efficient approaches for offline and online training of GP models in coastal groundwater management, this paper first formulates a one-well bi-objective pumping optimisation problem in a simplified two-dimensional island aquifer model based on

hydrogeological conditions observed in San Salvador Island, Bahamas. Then it proposes three novel strategies for offline training GP models and four strategies for online training GP models, all of which are based on the iterative search algorithm to select training points.

The results demonstrated that compared with traditional offline training, introducing the iterative procedure can improve the computing efficiency and reliability of the resulting Pareto front. The strategy, integrating information about the gradient of estimate values and the distance to the closest training point to determine training points at each iteration, is proved as the most appropriate and efficient offline training approach, outperforming strategies considering them separately in terms of global prediction accuracy and reliability of derived Pareto front. Furthermore, when aiming to attain a Pareto front with moderate reliability, applying this strategy can achieve a reduction of over 50% in computational expenses compared to the traditional offline training approach.

Regarding online training strategies, the results indicated that discretizing the objective space into equal sub-regions based on the obtained Pareto front and then selecting sampling points within these sub-regions can facilitate the convergence of GP models with low computational costs, thereby enhancing computational efficiency. Findings demonstrated that among the proposed online training strategies for building GP models, the efficient ones for identifying new sampling points at each iteration rely on information about either the distance between Pareto-optimal solutions and the ideal point within the objective space, or the distance between Pareto-optimal solutions and their sub-region centre within the objective space. The latter slightly outperforms the former.

In view of the performance of applying efficient offline and online approaches for training GP models in solving bi-objective groundwater management problem, it can be concluded that given limitations on SWI control, employing online-trained GP models can produce more reliable, cost-effective Pareto front with higher computing efficiency compared to adopting offline-trained GP models. However, offline-trained GP models can provide considerably trustworthy predictions over the entire input space and are independent of changes in SWI constraint conditions. It suggests that offline-trained GP models have a wider range of applications than the online-trained GP models, such as investigating the effects of pumping patterns on groundwater water supply cost, and SWI extent or conducting sensitivity analysis of Pareto front to SWI constraint conditions. Overall, this paper identifies some efficient approaches for offline and online training GP models in coastal groundwater management, and the findings regarding the performance of these trained GP models in generating Pareto-optimal

pumping strategies align with the prevailing understanding of the characteristics associated with offline and online training surrogate models.

APPENDIX A. Energy consumption for water desalination by reverse-osmosis.

As reverse osmosis (RO) is the most popular technique for desalinating brackish water and seawater in coastal groundwater management (Abd-Elhamid & Javadi, 2011; Hussain et al., 2019) it is the method considered in this work to treat groundwater whose salt concentration exceeds accepted potability standards. The specific (per unit mass) energy consumption for desalination SEC [L^2T^{-2}] by RO is estimated as (Stillwell & Webber, 2016):

$$SEC(C) = \frac{R \cdot T_s}{M_w} \cdot \left\{ \frac{x_{sF} - x_{sP}}{x_{sB} - x_{sF}} \cdot \left[x_{sB} \cdot \ln\left(\frac{x_{sB}}{x_{sF}}\right) + x_{wB} \cdot \ln\left(\frac{x_{wB}}{x_{wF}}\right) \right] + \left[x_{sP} \cdot \ln\left(\frac{x_{sP}}{x_{sF}}\right) + x_{wP} \cdot \ln\left(\frac{x_{wP}}{x_{wF}}\right) \right] \right\} \quad \text{(A1)}$$

where R is the universal gas constant, T_s is the saturation absolute temperature [K], and M_w is the water molecular weight [e.g., M/mole]. The symbols x represents mole fractions [/], with the subscripts "s" and "w" referring to salt and water, respectively. The subscript F indicates the "feed", that is, the water abstracted that undergoes desalination; the subscript P stands for "permeate", that is, the water distributed to users after desalination; and the subscript B denotes "brine", that is, the by-product high salinity water produced by RO, which is typically disposed.

The salt mole fraction of the feed, x_{sF}, can be calculated from the feed water concentration C as (Avlonitis et al., 2012):

$$x_{sF} = \frac{C/M_s}{C/M_s + [\rho_w(C) - C]/M_w} \quad \text{(A2)}$$

where M_s is the salt molecular weight [M/mole]. The water mole fraction of the feed x_{wF} is:

$$x_{wF} = 1 - x_{sF} \quad \text{(A3)}$$

The mole fractions of the permeate, x_{sP} and x_{wP}, are obtained using Equations A2-A3 with C equal to the target concentration C_d in the permeate, assumed to be 1.0 g/l. Likewise, the mole fractions for the brine, x_{sB} and x_{wB}, are calculated using Equations A2-A3, with C equal to the brine concentration C_b, whose value varies depending on the adopted desalination system. If this is designed to provide a fixed recovery ratio r between the flow rate Q_d sent to water users and the feed flow rate Q ($r = Q_d/Q$), then the brine mole fractions can be derived by combining the mass balance equations of water and salt for the treatment plant (Avlonitis et al., 2012):

$$x_{sB} = \frac{x_{sF} - r x_{sP}}{1 - r} \quad \text{(A4)}$$

$$x_{wB} = \frac{1 - x_{sF} - r x_{wP}}{1 - r} \quad \text{(A5)}$$

The resulting brine concentration can then be calculated as:

$$C_b = \frac{1}{1-r} \cdot C - \frac{r}{1-r} \cdot C_d \quad \text{(A6)}$$

Equation A6 shows that C_b may result in excessively large for high recovery ratios (e.g., r > 0.8) and large feed concentrations C, which ultimately leads to cost-ineffective energy consumption (Squire, 2000). On the other hand, if the feed concentrations C is slightly above the target C_d, large quantities of brine with relatively low concentration are discarded, which may result in cost-ineffective as well.

If the desalination system is designed to achieve a fixed brine concentration C_b, Equations A2-A3 with C=C_b are still valid, but the recovery ratio r results in a function of the feed concentrations C, which is obtained from Equation A6 as:

$$r = \frac{C_b - C}{C_b - C_d} \quad \text{(A7)}$$

In this work, we adopt the latter approach, and select a fixed brine concentration value C_b of 150.0 g/l (Ahunbay, 2019; Azerrad et al., 2019). For C_d = 1 g/l, and C ranging from 1 to 35 g/l, r values vary between 0.77 and 1 (Equation A7).

APPENDIX B. Predicting management objective and constraint values for each Monte Carlo run.

For each Monte Carlo run, expressions for calculating predicted values of f_{OC}, Q_{p}, Δs and ΔSM under the i-th pumping candidate, are given by:

$$\tilde{f}_{\mathrm{OC},i} = 10^{(\mu_{\mathrm{OC},i} + z_{\mathrm{OC}} \cdot \sigma_{\mathrm{OC},i})} \quad \text{(B1)}$$

$$\tilde{Q}_{\mathrm{p},i} = Q/(1 + 10^{-\mu_{\mathrm{p},i} + z_{\mathrm{p}} \cdot \sigma_{\mathrm{p},i}}) \quad \text{(B2)}$$

$$\Delta\tilde{s}_i = 10^{(\mu_{\Delta s_i} + z_{\Delta s} \cdot \sigma_{\Delta s_i})} \quad \text{(B3)}$$

$$\Delta\widetilde{SM}_i = 10^{(\mu_{\Delta SM_i} + z_{\Delta SM} \cdot \sigma_{\Delta SM_i})} - 1 \quad \text{(B4)}$$

$\mu_{\mathrm{OC},i}$, $\mu_{\mathrm{p},i}$, $\mu_{\Delta s_i}$ and $\mu_{\Delta SM_i}$ are respectively the expected values of f_{OC}, Q_{p}, Δs and ΔSM under the pumping scheme i, while $\sigma_{\mathrm{OC},i}$, $\sigma_{\mathrm{p},i}$, $\sigma_{\Delta s_i}$ and $\sigma_{\Delta SM_i}$ are respectively the standard deviations of predicted f_{OC}, Q_{p}, Δs and ΔSM at this input vector, all of which are provided by the GP models. z_{OC}, z_{p}, $z_{\Delta s}$ and $z_{\Delta SM}$ are the random variables following the standard normal distribution, interpreted as a measure of uncertainty, quantifying the deviation of the estimate from the expected value. As both f_{OC} and Q_{p} are functions of pumping intensities, while Δs, and ΔSM are used to quantify the SWI extent, it is believed that f_{OC} and Q_{p}, Δs and ΔSM have certain correlations, indicating the values of z_{OC}, z_{p}, $z_{\Delta s}$ and $z_{\Delta SM}$ cannot be determined independently at each run and should consider the corresponding correlations. Generating

values of z_{OC}, z_{p}, $z_{\Delta s}$ and $z_{\Delta SM}$ with considering the correlation can refer to the following general equations.

Given the correlation coefficient between two random variables, *X* and *Y*, data on them can be obtained by the following equations.

$$X = Z_1 \tag{B5}$$

$$Y = \vartheta Z_1 + \sqrt{1-\vartheta^2} Z_2 \tag{B6}$$

where Z_1 and Z_2 are two independent random variables, both of which follow the normal standard distribution. ϑ is the correlation coefficient between *X* and *Y*, and $\vartheta \in [-1,1]$.

Values of z_{OC}, z_{P}, $z_{\Delta s}$ and $z_{\Delta SM}$ in Equations B1-B4 can be determined by the above equations, and correlation coefficients between them are calculated by the training data.

Acknowledgements

The authors have no relevant financial or non-financial interests to declare that are relevant to the content of this article. This work was partially supported by the EPSRC grant no. EP/T018542/1, and the NSF under grant agreement CBET-EPSRC 2022278. The authors also would like to thank the editor and anonymous reviewers for their kind feedback and insightful comments, which helped improve the clarity of this paper.

References

Kishi, Y., & Fukuo, Y. (1977). Studies on salinization of groundwater, I: Theoretical consideration on the three-dimensional movement of the salt water interface caused by the pumpage of confined groundwater in fan-shaped alluvium. *Journal of Hydrology*, *35*(1), 1-29. https://doi.org/10.1016/0022-1694(77)90074-9

Davis, R. L. & Johnson, C. R. (1989). Karst Hydrology of San Salvador. In Mylroie, J.E. (Ed.), Proceedings of the Fourth Symposium on the Geology of the Bahamas. Bahamian Field Station, San Salvador Island, Bahamas, pp. 118–135.

Squire, D. (2000). Reverse osmosis concentrate disposal in the UK. *Desalination*, *132*(1), 47-54. https://doi.org/10.1016/S0011-9164(00)00134-X

Mayer, A. S., Kelley, C. T., & Miller, C. T. (2002). Optimal design for problems involving flow and transport phenomena in saturated subsurface systems. *Advances in Water Resources*, *25*(8), 1233–1256. https://doi.org/10.1016/S0309-1708(02)00054-4

Mantoglou, A. (2003). Pumping management of coastal aquifers using analytical models of saltwater intrusion. *W*ater *R*esources *R*esearch, *39*(12), 1335. https://doi.org/10.1029/2002WR001891

Rasmussen, C. E., & Williams, C. K. I., (2006). Gaussian Processes for Machine Learning. MIT Press.

Martin, J. B., & Moore, P. J. (2008). Sr concentrations and isotope ratios as tracers of groundwater circulation in carbonate platforms: Examples from San Salvador Island and Long Island, Bahamas. *Chemical Geology*, *249*(1), 52-65. https://doi.org/10.1016/j.chemgeo.2007.11.009

Langevin, C. D., Thorne, D. T., Jr., Dausman, A. M., Sukop, M. C., & Guo, W. (2008). *SEAWAT version 4: A computer program for simulation of multi-species solute and heat transport* (Rep. 2328-7055). Geological Survey (US).

Moore, P. J. (2009). Controls on the generation of secondary porosity ineogenetic karst: examples from San Salvador Island, Bahamas and north-central Florida, USA, (Doctoral dissertation). Gainesville, FL: University of Florida.

McGee, D. K., Wynn, J. G., Onac, B. P., Harries, P. J., & Rothfus, E. A. (2010). Tracing groundwater geochemistry using $\delta^{13}C$ on San Salvador Island (southeastern Bahamas): implications for carbonate island hydrogeology and dissolution. *Carbonates Evaporites*, *25*(2), 91–105. https://doi.org/10.1007/s13146-010-0013-6

Papadopoulou, M. P., Nikolos, I. K., & Karatzas, G. P. (2010). Computational benefits using artificial intelligent methodologies for the solution of an environmental design problem: saltwater intrusion. *W*ater *S*cience & *T*echnology, 62(7), 1479–1490. https://doi.org/10.2166/wst.2010.442

Abd-Elhamid, H. F., & Javadi, A. A. (2011). A cost-effective method to control seawater intrusion in coastal aquifers. *Water Resources Management*, *25*, 2755–2780. https://doi.org/10.1007/s11269-011-9837-7

Kourakos, G., & Mantoglou, A. (2011). Simulation and multi-Objective management of coastal aquifers in semi-arid regions. *W*ater *R*esources *M*anagement, *25*, 1063–1074. https://doi.org/10.1007/s11269-010-9677-x

Sreekanth, J., & Datta, B. (2011). Coupled simulation-optimisation model for coastal aquifer management using genetic programming-based ensemble surrogate models and multiple-realization optimisation. *Water Resources Research*, *47*(4), W04516. https://doi.org/10.1029/2010WR009683

Avlonitis, S. A., Avlonitis, D. A., & Panagiotidis, Th. (2012). Experimental study of the specific energy consumption for brackish water desalination by reverse osmosis. *International Journal of Energy Research*, *36*, 36-45. https://doi.org/10.1002/er.1780

Kourakos, G., & Mantoglou, A. (2013). Development of a multi-objective optimisation algorithm using surrogate models for coastal aquifer management. *Journal of Hydrology*, *479*, 13-23. https://doi.org/10.1016/j.jhydrol.2012.10.050

Ho, H. C., Mylroie, J. E., Infante, L. R., & Rodgers, J. C. (2014). Fuzzy-based spatial modeling approach to predict island karst distribution: a conceptual model. *Environmental Earth Sciences*, *71*(3), 1369–1377. https://doi.org/10.1007/s12665-013-2543-4

Holding, S., & Allen, D. M. (2015). From days to decades: numerical modelling of freshwater lens response to climate change stressors on small low-lying islands. *Hydrology and Earth System Sciences*, *19*(2), 933–949. https://doi.org/10.5194/hess-19-933-2015

Javadi, A., Hussain, M., Sherif, M., & Farmani, R. (2015). Multi-objective optimisation of different management scenarios to control seawater intrusion in coastal aquifers. *W*ater *R*esources *M*anagement, *29*, 1843–1857. https://doi.org/10.1007/s11269-015-0914-1

Ketabchi, H., & Ataie-Ashtiani B. (2015). Evolutionary algorithms for the optimal management of coastal groundwater: A comparative study toward future challenges. *J*ournal of *H*ydrology, *520*, 193-213. https://doi.org/10.1016/j.jhydrol.2014.11.043

Christelis, V., & Mantoglou, A. (2016). Pumping optimisation of coastal aquifers assisted by adaptive metamodelling methods and radial basis functions. *Water Resources Management*, *30*, 5845–5859. https://doi.org/10.1007/s11269-016-1337-3

Gulley, J. D., Mayer, A. S., Martin, J. B., & Bedekar, V. (2016). Sea level rise and inundation of island interiors: Assessingimpacts of lake formation and evaporationon water resources in arid climates. *Geophysical Research Letters*, *43*(18), 9712-9719. https://doi.org/10.1002/2016GL070667

Kim, Y. J., (2016). Comparative study of surrogate models for uncertainty quantification of building energy model: Gaussian Process Emulator vs. Polynomial Chaos Expansion. *Energy and Buildings*, *133*, 46-58. https://doi.org/10.1016/j.enbuild.2016.09.032

Stillwell, A. S., & Webber, M. E. (2016). Predicting the specific energy consumption of reverse osmosis desalination. *Water*, *8*(12), 601. https://doi.org/10.3390/w8120601

Zhang, J., Li, W., Zeng, L., & Wu, L. (2016). An adaptive Gaussian process-based method for efficient Bayesian experimental design in groundwater contaminant source identification problems. *Water Resources Research*, *52*(8), 5971-5984. https://doi.org/10.1002/2016WR018598

Rajabi, M. M., & Ketabchi, H. (2017). Uncertainty-based simulation-optimisation using Gaussian process emulation: Application to coastal groundwater management. *J*ournal of *H*ydrology, *555*, 518-534. https://doi.org/10.1016/j.jhydrol.2017.10.041

Christelis, V., Regis, R. G., & Mantoglou, A. (2018). Surrogate-based pumping optimisation of coastal aquifers under limited computational budgets. *J*ournal *of H*ydroinformatics, *20*(1), 164–176. https://doi.org/10.2166/hydro.2017.063

Song, J., Yang, Y., Wu, J., Wu, J., Sun, X., & Lin, J. (2018). Adaptive surrogate model based multiobjective optimisation for coastal aquifer management. *J*ournal of *H*ydrology, *561*, 98-111. https://doi.org/10.1016/j.jhydrol.2018.03.063

Ahunbay, M. G. (2019). Achieving high water recovery at low pressure in reverse osmosis processes for seawater desalination. *Desalination*, *465*, 58–68. https://doi.org/10.1016/j.desal.2019.04.023

Azerrad, S. P., Isaacs, M., & Dosoretz, C. G. (2019). Integrated treatment of reverse osmosis brines coupling electrocoagulation with advanced oxidation processes. *Chemical Engineering Journal*, *356*, 771–780. https://doi.org/10.1016/j.cej.2018.09.068

Christelis, V., Kopsiaftis, G., & Mantoglou, A. (2019). Performance comparison of multiple and single surrogate models for pumping optimisation of coastal aquifers. *H*ydrological *S*ciences *J*ournal, *64*(3), 336–349. https://doi.org/10.1080/02626667.2019.1584400

Hussain, M. S., Abd-Elhamid, H. F., Javadi, A. A., & Sherif, M. M. (2019). Management of seawater intrusion in coastal aquifers: a review. *Water*, *11*(12), 2467. https://doi.org/10.3390/w11122467

Kopsiaftis, G., Protopapadakis, E., Voulodimos, A., Doulamis, N., & Mantoglou, A. (2019). Gaussian process regression tuned by Bayesian optimisation for seawater intrusion prediction. *Computational Intelligence and Neuroscience*, *2019*, 2859429. https://doi.org/10.1155/2019/2859429

Redouane, K., Zeraibi, N., & Amar, M. N. (2019). Adaptive surrogate modeling with evolutionary algorithm for well placement optimisation in fractured reservoirs. *Applied Soft Computing Journal*, *80*, 177-191. https://doi.org/10.1016/j.asoc.2019.03.022

Roy, D. K., & Datta, B. (2019). Adaptive management of coastal aquifers using entropy-set pair analysis–based three-dimensional sequential monitoring network design. *Journal of Hydrologic Engineering*, *24*(3), 04018072. https://doi.org/10.1061/(ASCE)HE.1943-5584.000176

Yao, Y., Andrews, C., Zheng, Y., He, X., Babovic, V., & Zheng, C. (2019). Development of fresh groundwater lens in coastal reclaimed islands. *Journal of Hydrology*, *573*, 365–375. https://doi.org/10.1016/j.jhydrol.2019.03.062

Fan, Y., Lu, W., Miao, T., Li, J., & Lin, J. (2020). Multiobjective optimisation of the groundwater exploitation layout in coastal areas based on multiple surrogate models', *E*nvironmental *S*cience *and P*ollution *R*esearch, *27*, 19561–19576. https://doi.org/10.1007/s11356-020-08367-2

Han, Z., Lu, W., Fan, Y., Lin, J., & Yuan, Q. (2020). A surrogate-based simulation–optimisation approach for coastal aquifer management. *W*ater *S*upply, *20*(8), 3404–3418. https://doi.org/10.2166/ws.2020.259

Jasechko, S., Perrone, D., Seybold, H., Fan, Y., & Kirchner, J. W. (2020). Groundwater level observations in 250,000 coastal US wells reveal scope of potential seawater intrusion. *Nature Communications*, *11*, 3229. https://doi.org/10.1038/s41467-020-17038-2

Ranjbar, A., & Mahjouri, N. (2020). Multi-objective freshwater management in coastal aquifers under uncertainty in hydraulic parameters. *N*atural *R*esources *R*esearch, *29*(4), 2347–2368. https://doi.org/10.1007/s11053-019-09585-3

Siade, A. J., Cui, T., Karelse, R. N., & Hampton, C. (2020). Reduced-dimensional Gaussian process machine learning for groundwater allocation planning using swarm theory. *Water Resources Research*, *56*(3), e2019WR026061. https://doi.org/10.1029/2019WR026061

Yin, J., Pham, H. V., & Tsai, F. T. C. (2020). Multiobjective spatial pumping optimisation for groundwater management in a multiaquifer system. *J*ournal of *W*ater *R*esources *P*lanning *and M*anagement, *146*(4), 04020013. https://doi.org/10.1061/(ASCE)WR.1943-5452.0001180

Agoubi, B. (2021) A review: saltwater intrusion in North Africa's coastal areas-current state and future challenges. *Environmental Science and Pollution Research*, *8*(14), 17029-17043. https://doi.org/10.1007/s11356-021-12741-z

Al-Maktoumi, A., Rajabi, M. M., Zekri, S., & Triki, C. (2021). A probabilistic multiperiod simulation–optimisation approach for dynamic coastal aquifer management. *W*ater *R*esources *M*anagement, *35*, 3447–3462. https://doi.org/10.1007/s11269-021-02828-0

Cui, T., Pagendam, D., & Gilfedder, M. (2021). Gaussian process machine learning and Kriging for groundwater salinity interpolation. *Environmental Modelling & Software*, *144*, 105170. https://doi.org/10.1016/j.envsoft.2021.105170

Han, Z., Lu, W., Fan, Y., Xu, J., & Lin, J. (2021). Surrogate-based stochastic multiobjective optimisation for coastal aquifer management under parameter uncertainty. *W*ater *R*esources *M*anagement, *35*, 1479–1497. https://doi.org/10.1007/s11269-021-02796-5

Lal, A., & Datta, B. (2021). Optimal pumping strategies for the management of coastal groundwater resources: application of Gaussian Process Regression metamodel-based simulation-optimisation methodology. *ISH J*ournal of *H*ydraulic *E*ngineering, *27*(sup1), 136-145. https://doi.org/10.1080/09715010.2019.1599304

Yu, X., Sreekanth, J., Cui, T., Pickett, T., & Xin, P. (2021). Adaptative DNN emulator-enabled multi-objective optimisation to manage aquifer−sea flux interactions in a regional coastal aquifer. *A*gricultural *W*ater *M*anagement, 245, 106571. https://doi.org/10.1016/j.agwat.2020.106571

Coulon, C., Lemieux, J. M., Pryet, A., Bayer, P., Young, N. L., & Molson, J. (2022). Pumping optimisation under uncertainty in an island freshwater lens using a sharp-interface seawater intrusion model. *W*ater *R*esources *R*esearch, *58*, e2021WR031793. https://doi.org/10.1029/2021WR031793

Dey, S., & Prakash, O. (2022). Coupled sharp-interface and density-dependent model for simultaneous optimisation of production well locations and pumping in coastal aquifer. *W*ater *R*esources *M*anagement, *36*, 2327–2341. https://doi.org/10.1007/s11269-022-03145-w

Wang, Z., Yang, Y., Wu, J., Sun, X., Lin, J., & Wu, J. (2022). Multi-objective optimisation of the coastal groundwater abstraction for striking the balance among conflicts of resource-environment-economy in Longkou City, China. *W*ater *R*esearch, *211*, 118045. https://doi.org/10.1016/j.watres.2022.118045

Yin, J., Tsai, F. T. C., & Lu, C. (2022). Bi-objective extraction-injection optimisation modeling for saltwater intrusion control considering surrogate model uncertainty. *W*ater *R*esources *M*anagement, *36*, 6017–6042. https://doi.org/10.1007/s11269-022-03340-9

Chapter 4

Applying an efficient surrogate-based multi-objective optimisation framework for sustainable island groundwater management

Publications included in this chapter:

Yu, W., Baù, D., Mayer, A.S. and Geranmehr, M. Applying an efficient surrogate-based multi-objective optimisation framework for sustainable island groundwater management (intended for publication).

Applying an efficient surrogate-based multi-objective optimisation framework for sustainable island groundwater management

Weijiang Yu[1*], Domenico Baù[1], Alex S. Mayer[2], Mohammadali Geranmehr[1]

[1]Department of Civil and Structural Engineering, University of Sheffield, Sheffield, UK.
[2]Department of Civil Engineering, University of Texas at El Paso, USA.
*Corresponding author: Weijiang Yu (wyu18@sheffield.ac.uk)

Abstract

Computational burden, resulting from intensive executions of simulators during optimisation, often hinders the application of the simulation-optimisation (SO) method for deriving optimal pumping schemes in coastal groundwater management and impedes conducting sensitivity analysis of optimal pumping strategies to management constraints. For quickly identifying optimal pumping strategies under various constraints, this study develops an efficient framework, where adopting a lower-resolution simulator generates data to build surrogate models with a novel offline training algorithm and then applying the full enumeration method to determine optimal solutions according to the surrogate predictions. Traditional offline training approach involves developing surrogates before optimisation, often using training datasets that cover the input space either uniformly or randomly, which can prove inefficient due to potential oversampling of low-gradient areas and under-sampling of high-gradient areas. This study proposes an iterative search algorithm that efficiently selects training points by first scoring each unknown point based on its distance to the closest training point and the gradient of the surrogate estimate and then choosing the input candidate with the maximum score as the next sampling point. The proposed surrogate-based optimisation framework is applied to solve a two-objective groundwater management problem formulated on a three-dimensional island aquifer, using hydrogeological conditions observed on San Salvador Island (Bahamas). Gaussian Process (GP) techniques are employed to construct model surrogates, predicting management objectives and constraint values, alongside quantifying associated uncertainties. By conducting repeated Monte Carlo simulations using these GP models, it becomes possible to ascertain the probability of Pareto-optimality for each pumping scheme. Derived optimal pumping schemes are characterized by the Pareto-optimal probabilities and validated by the higher-resolution simulator. Results indicate that the proposed surrogate-based multi-objective optimisation framework can efficiently provide trustable optimal pumping schemes and be used to analyse the sensitivity of optimal groundwater supply cost to the constraints.

Key words: seawater intrusion; groundwater management; Gaussian Process models; offline training; optimal pumping schemes; sensitivity analysis.

1 Introduction

Seawater intrusion (SWI), a global environmental issue, is a phenomenon of subsurface freshwater-seawater interface migrating landward and the subsequent salinization of coastal aquifers. It is widely acknowledged that SWI is driven by excessive groundwater extraction and climate change, which result in the recession in the hydraulic gradient between seaward-discharging freshwater and landward-moving seawater (Kishi & Fukuo, 1977). The adverse effects of SWI are serious, contaminating coastal aquifer ecosystems and endangering access to subsurface freshwater for coastal communities (Jasechko et al., 2020; Agoubi, 2021). Particularly, SWI poses a serious threat to island subsurface freshwater resources, which are in the shape of a freshwater lens floating above seawater due to the density difference (Morgan & Werner, 2014; Vandenbohede et al., 2014). For the small-area or very-low-elevation islands, the greatest thickness of the freshwater lens is usually only a few meters (Gingerich et al., 2017), and thus the freshwater body within the lens is vulnerable to being polluted by SWI. To meet local water demand and subsurface environment protection simultaneously, coastal groundwater pumping optimisation has increasingly become a widely accepted strategy for sustainable groundwater use. Deriving optimal pumping schemes for keeping a balance between conflicting objectives usually depends on the SO method.

Figure 1 shows the flow chart for generally implementing the SO framework to solve optimisation problems. In the SO system, OA is responsible for solving the optimisation problem, exploring the input space to identify multiple potentially optimal DVs, and these searched DVs are used as inputs for the SM to generate corresponding SVs. These DVs and SVs form pairs of data that feed the OA. Subsequently, guided by feedback from the simulation results, the OA decides how to adjust the DVs toward better solutions. Upon convergence, the OA returns a set of DVs, considered the optimal solutions to the management problem.

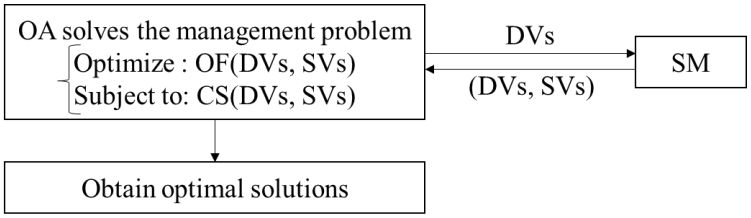

Figure 1. Flow chart for generally implementing the SO framework to solve optimisation problems. OF and CS are respectively the objectives and constraints, functions of DVs and SVs. DVs and SVs represent decision variables and state variables, respectively. OA denotes the optimisation algorithm, while SM represents the simulation model.

In coastal groundwater management, popular variable-density groundwater simulation models include SEAWAT (Kourakos & Mantoglou, 2013), HydroGeoSphere (Christelis et al., 2019) and SUTRA (Ketabchi & Ataie-Ashtiani, 2015a, b). Compared with the full enumeration method, the SO method largely reduces the required number of SWI simulations during the optimisation, saving computational costs remarkably. Over the past decades, the SO method has been successfully applied in multi-objective coastal aquifer management problems (Kourakos & Mantoglou, 2011; Javadi et al., 2015; Wang et al., 2022).

The fact is that the computational advantage of the SO method usually weakens or disappears in practical applications, attributed to the characteristic of the SO method, requiring repeated calls of SWI simulators. When the times of calling simulation model are numerous or/and each call is time-consuming, employing that to determine optimal pumping schemes certainly turns into computationally intractable. To mitigate the computational burden arising from time-consuming SWI simulations, some strategies are adopted, such as employing the analytical solution approach to simulate SWI (Ketabchi & Ataie-Ashtiani, 2015a; Jamal et al., 2022), SWI simulation model developed based on the sharp-interface assumption (Coulon et al., 2022; Dey & Prakash, 2020), developing SWI simulation models with the coarse resolution (Ketabchi & Ataie-Ashtiani, 2015b; Yang et al., 2021), or conducting the parallel computing strategy that uses multiple processors or computers working in parallel to simulate aquifer response under the pumping (Mostafaei-Avandari & Ketabchi, 2020; Yin et al., 2020).

However, computational challenges persist when applying the SO method to solve groundwater pumping optimisation problems formulated in the three-dimensional (3D) coastal aquifers, despite those mitigation measures taken. Both Kourakos & Mantoglou (2015) and Zekri et al. (2015) adopted the SO method, where SWI simulators are built using the sharp-interface assumption, to solve coastal groundwater management problems formulated in the 3D aquifer. In these two studies, 3D simulators respectively composed of 576,925 and 475,404 grids and management problems respectively with 41 and 48 DVs, the computing time required for identifying optimal pumping schemes are respectively 548 hours and 28 days. In the study of Song et al. (2018), although they used the coarse resolution to discretize a 3D coastal aquifer model, each grid with an area of 0.04 km^2, solving a two-objective pumping optimisation problem with 18 DVs costed them 332 hours when they employed the SO method. To solve a coastal groundwater management problem with 64 DVs, Mostafaei-Avandari & Ketabchi (2020) adopted the parallel computing strategy along with a lower-resolution 3D SWI simulation model, a large-scale study area with around 700 km^2 discretized by 48,400 meshes, to implement the SO method, and they spent nearly 461 hours deriving optimal solutions.

Likewise, Yin et al. (2020) applied the SO method to solve a three-objective pumping optimisation problem with 6 to 10 DVs by employing the parallel computing strategy and creating the 3D SWI simulator based on the sharp-interface assumption. They, at last, spent around 60 hours obtaining optimal pumping schemes, as the SWI simulator comprises 808,078 grids, leading to each call of simulation consuming considerable time. Overall, 3D aquifer models usually comprise hundreds of thousands of grids, causing much time consumed in running SWI simulations and hindering the applications of the SO method. When the groundwater management problems formulated on the 3D aquifer are with dozens of DVs, applying the SO method to derive optimal pumping schemes is further time-consuming and may just be theoretically viable (Han et al., 2021; Yin et al., 2022).

Currently, a popular strategy to mitigate the computational time required for implementing the SO method in coastal groundwater management is to replace computationally expensive SWI simulators with data-driven surrogate models. Surrogate models are built by training data generated from the original simulators, and then provide statistically approximated relationships between input and output variables. Upon completing surrogate model development, they can substitute the SWI simulators to link with OA, immediately offering values of required state variables or objective and constraint estimates when the pumping pattern is given, thereby saving computational costs. This type of surrogate model finishing training before the optimisation is usually known as the offline-trained surrogate model (Papadopoulou et al., 2010). Figure 2 presents a flow chart for generally implementing the surrogate-based simulation-optimisation (SSO) framework to solve optimisation problems, where surrogate models are responsible for predicting management objectives and constraint values. In some cases, assisted by the surrogate modelling technique, savings in runtime can be nearly up to 100% by the SSO method compared to employing the SO method (Al-Maktoumi et al., 2021; Fan et al., 2020; Rajabi & Ketabchi, 2017; Ranjbar & Mahjouri, 2020; Yin et al., 2022), exhibiting a noticeable improvement in computing efficiency. Their capabilities in providing accurate and reliable SWI extent estimates given the pumping pattern and in deriving trustable optimal pumping solutions are validated in many publications (Fan et al., 2020; Yin et al., 2022).

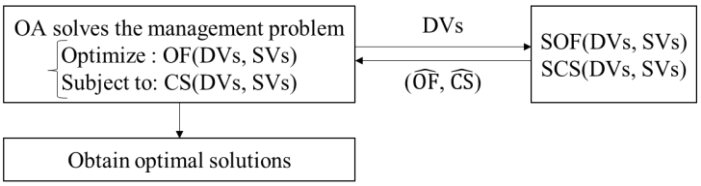

Figure 2. Flow chart for generally applying the SSO framework to solve optimisation problems.

Traditionally, offline training surrogate models depend on fitting a set of training samples at one time, and to ensure the global accuracy of surrogate model estimates, these training points cover the entire input space either uniformly or randomly (Fan et al., 2020; Han et al., 2021). However, since groundwater management objectives and SWI constraints are nonlinear, this traditional training approach can prove inefficient due to the potential oversampling of low-gradient areas and under-sampling of high-gradient areas. Therefore, to acquire reliable model estimates, surrogate models built by traditional offline training tend to consume more training samples than necessary, causing a certain proportion of the computational costs to be wasted. In the studies of Rajabi & Ketabchi (2017), Ranjbar & Mahjouri (2020) and Al-Maktoumi et al. (2021), offline-trained surrogate models consumed training samples that are hundreds of times the number of decision variables, indicating that there is a need to design an efficient algorithm for offline training surrogate models in coastal groundwater management.

Another challenge of employing surrogate models is the uncertainties in results, as surrogate model development only depends on finite training data from full-scale models (Sreekanth & Datta, 2011; Yin et al., 2022). The widely accepted way to deal with this challenge is to adopt the ensemble of surrogate models. In the ensemble approach, final predictions in SWI extent under the pumping are obtained by integrating estimates of multiple surrogate models, such as through weighted averaging (Roy & Datta, 2019; Han et al., 2020). The surrogate models involved in the ensemble approach can be either the diverse types of surrogate functions (Christelis et al., 2019; Yin et al., 2022) or a single surrogate function built multiple times using different realizations of training data (Sreekanth & Datta, 2011). Undoubtedly, building an ensemble of surrogate models, whether by training a single surrogate model using multiple groups of training samples or incorporating different types of surrogate models, inevitably increases the computational load.

Given the numerous cells involved within 3D aquifer models, using the SO method for solving pumping optimisation formulated on 3D coastal aquifers often requires huge computational costs, despite efforts to reduce SWI simulation runtime. Applying the SSO framework is a feasible option, where SWI simulators are replaced by the offline-trained surrogate models, but there exist unignorable challenges, including inefficient sampling of traditional offline-trained surrogate models and uncertainties in surrogate predictions. In view of that, this study develops an efficient SSO framework for groundwater management formulated on the 3D island aquifers. This framework adopts lower-resolution variable-density SWI simulations to generate training data and introduces a novel iterative search algorithm for building offline-trained surrogates, selecting the input candidate with the highest scores at each

iteration as a new sampling point. The score of every unknown point is calculated based on its distance to the closest training point and the gradient of the surrogate estimate. In this work, the GP modelling technique is adopted to construct surrogate models, predicting management objectives and constraint values given pumping patterns, and the full enumeration method is applied to identify optimal pumping schemes according to GP model predictions.

Compared with other surrogate modelling techniques, GP models can return both expected values and standard deviations at the unknown points, being able to quantify the uncertainties in the estimates. The set of non-dominated solutions in a multi-objective optimisation problem is usually termed the Pareto front. A probabilistic Pareto front can be obtained through repeated stochastic (Monte Carlo) running of GP models, which are computationally viable and efficient because of the inexpensiveness of the GP models. The average probability of Pareto-optimality is used to determine the optimal training sample size, after which further increases in the training data size do not noticeably enhance the average probability of Pareto-optimality. The robustness of optimal solutions obtained through the proposed SSO framework is assessed using a high-resolution groundwater simulator. After validation, the proposed SSO method is employed to analyse the effects of constraint conditions on optimal pumping schemes.

This study focuses on a simplified 3D island aquifer created by hydrogeological conditions observed in San Salvador Island (Bahamas) and formulates a two-objective pumping optimisation problem. The optimisation problem aims at minimizing the groundwater supply operation cost associated with the pumping and desalination treatment and maximizing the amount of qualified groundwater delivered to the communities, subject to constraints on SWI control, as quantified by the water table drawdown over the well system (Δs) and the salt mass increase in the aquifer (ΔSM).

This paper is organized as follows. The next section presents the simulation model for SWI, the management problem formulation, GP model development, proposed offline-trained GP model-based optimisation system. Results and their discussion are provided in the following section. The last section summarizes the conclusions drawn from the investigation.

2 Methodology

The goal of this study is to investigate the optimal pumping schemes of a two-objective island groundwater management through the proposed efficient SSO framework, using the San Salvador Island aquifer as a case study. San Salvador Island is located within the Bahamian Archipelago (Figure 3), about 600 km east-southeast of Miami, and sits on a small, isolated carbonate platform (Ho et al., 2014; McGee et al., 2010). The island is about 20 km long north-

to-south and has an average width west-to-east of approximately 8 km (Martin & Moore, 2008). The topography is dominated by consolidated carbonate dune ridges, with elevations between 10 and 20 meters above sea level (Davis & Johnson, 1989). Characterized by a subtropical climate, San Salvador Island has an annual temperature ranging between 22 and 28 ℃ (McGee et al., 2010) and annual precipitation and potential evaporation of 1000-1250 mm/yr and 1250-1375 mm/yr, respectively (Moore, 2009).

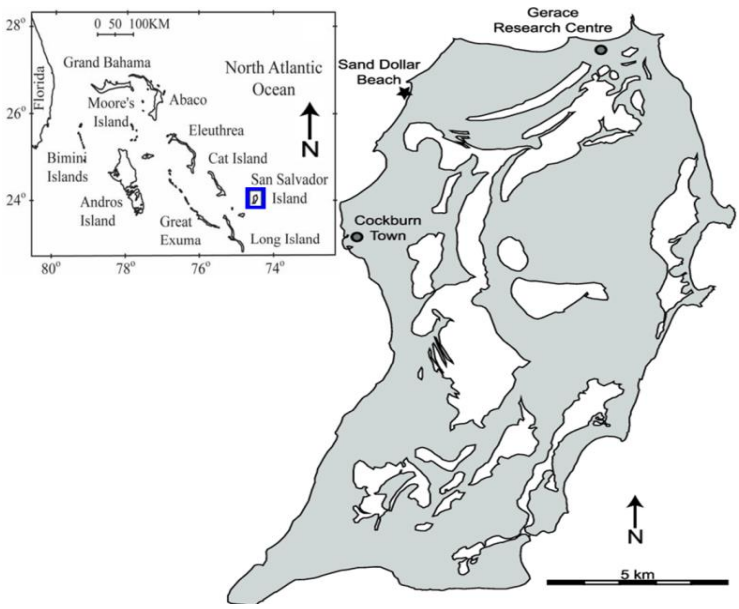

Figure 3. Location map of San Salvador Island (Moore, 2009). The dark grey and the light grey areas represent land and surface water, respectively.

2.1 Numerical simulation of SWI in the San Salvador Island aquifer

This work applies the SEAWAT model to simulate the SWI process in the island aquifer. SEAWAT couples the groundwater flow model MODFLOW and the solute transport model MT3DMS to solve the variable-density flow equations using a finite-difference numerical approach (Langevin et al., 2008; Kourakos & Mantoglou, 2013; Yao et al., 2019). Since the SEAWAT groundwater model can account for water density variations that depend on salt concentration, it is well-suited for simulating flow in aquifers characterized by freshwater-seawater interactions.

In the investigation of the island groundwater abstraction management, a simplified 3D model is adopted. Figure 4 shows a conceptualization of the aquifer domain. This island model is constructed as a regular cuboid, with a length of 20,000 m (*X*-axis), a width of 8,000 m (*Y*-axis), and a height of 480 m (*Z*-axis), as shown in Figure 4a. The elevation of the model top is 7.5 m while that of the model bottom is -472.5 m. Since island subsurface freshwater resources are stored in the upper aquifer and exhibit in the shape of the lens, in the dimension of Z, the upper aquifer is discretized with finer resolution than the lower aquifer to ensure simulation

efficiency and accuracy. Herein, the thickness of the top twelve layers and bottom three layers are 15 m and 100 m, respectively. A coarse resolution (200 m × 200 m) in the horizontal is selected to create the variable-density groundwater simulation model. A detailed description of the choice of grid resolution in the horizontal is presented in the Supporting Information - Appendix A.

(a) (b)

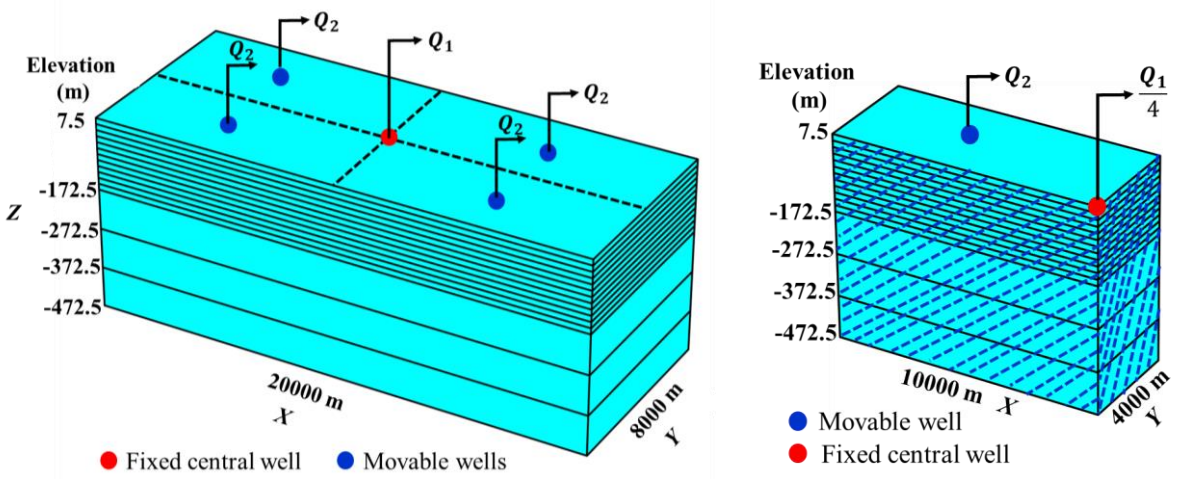

Figure 4. (a) A conceptualization of the whole island aquifer domain. (b) One-quarter of the SEAWAT model domain. Shadow areas with blue represent a no-flow boundary.

A no-flow boundary is prescribed at the model bottom. The model top is a specified flux boundary, reflecting the aquifer recharge from precipitation, which is assumed to be 0.2 m per year (Gulley et al., 2016). At the surrounding boundaries, a constant head of 0.0 m is prescribed over the water column, which represents the sea level (at the datum). At the same boundaries, a constant concentration of 35.0 g/L is imposed, which represents the salt content in seawater.

To model SWI effects from groundwater abstraction at a steady state, the flow and solute transport are simulated as transient state processes with a sufficiently large period of constant groundwater pumping. A "baseline" scenario is first developed to simulate the island freshwater lens under steady-state conditions of natural groundwater recharge from precipitation only. This serves as the initial condition to model the aquifer freshwater distribution under various scenarios of groundwater pumping. The pumping system consists of five wells, where one well is located at the island centre with pumping rate Q_1 while the remaining four wells are symmetrically positioned relative to this central well and with the same pumping rate Q_2(Figure 4a). Each pumping well is represented a point sink located within the aquifer. To enhance computational efficiency, pumping simulations are conducted within one-quarter of the SEAWAT model domain, capitalizing on the symmetry of both well distribution and the model domain (Figure 4b). For the simulations involving groundwater

pumping, SEAWAT is run until a steady state is reached, depending on the simulated pumping scheme. Correspondingly, the required CPU time for each simulation is around several minutes. Table 1 provides a list of the relevant parameters adopted in the simulation model introduced above. These parameters are drawn from published works (Gulley et al., 2016; Holding & Allen, 2015) that have used San Salvador Island or nearby island aquifers as test cases.

Table 1. *Model Parameters Used for SWI Simulation in the San Salvador Island Aquifer*

Model Component	Parameters	Units	Values
Groundwater Flow	Aquifer recharge (*RCH*)	m/year	0.2
	Effective porosity	\	0.15
	Specific elastic storage	m^{-1}	1.0×10^{-5}
	Specific yield	\	0.15
	Horizontal hydraulic conductivity (HK)	m/day	50.0
	HK transversal anisotropy ratio	\	1.0
	HK vertical anisotropy ratio	\	1.0
Solute Transport	Longitudinal dispersivity	m	1.0
	Transversal dispersivity	m	0.1
	Vertical dispersivity	m	0.01
	Molecular diffusion coefficient	m^2/s	1.0×10^{-9}
	Aquifer recharge concentration	g/l	0
Density dependence	Freshwater density	kg/m^3	1000
	Seawater density	kg/m^3	1025
	Density/concentration slope[a]	\	0.7143

[a] The water density ρ_w [kg/m^3] varies linearly with the salt concentration C [kg/m^3] through the equation $\rho_w = 1000 + 0.7143 \cdot C$.

2.2 Formulation of groundwater management problem

Managing fragile freshwater resources in the island aquifers is to identify cost-optimal pumping strategies, keeping a balance between the financial cost of groundwater supply and the volume of qualified groundwater supplied to the water network while mitigating SWI resulting from aquifer pumping. In this work, those tradeoffs are investigated through the formulation of a two-objective optimisation framework, which aims at minimizing the groundwater supply operation cost associated with pumping and desalination and maximizing the amount of qualified groundwater delivered to local communities, subject to Δs and ΔSM.

As shown in Figure 4b, there are two types of wells placed in the study region to abstract groundwater. One well is located at the island centre and the other well is uncertain in location.

For the central well, it is characterized by two DVs, using D_1 and $Q_1/4$. For the second well, defined by four DVs, including X_2, Y_2, D_2 and Q_2. D_1 [L] and $Q_1/4$ [L^3T^{-1}] are the depth at which pumping occurs and the pumping intensity for the well located at the island centre, respectively. X_2 [L] and Y_2 [L] are respectively the distances of the unfixed wells from the vertical and horizontal shorelines, while D_2 [L] and Q_2 [L^3T^{-1}] are the depth at which pumping occurs and the pumping intensity for this well system, respectively. In total, there are six decision variables, denoted as (D_1, $Q_1/4$, X_2, Y_2, D_2, Q_2).

The first management objective is to lower the operation cost resulting from pumping activities as much as possible, defined as:

$$\text{Minimize} \qquad f_{\mathrm{OC}} = f_p + f_t \tag{1}$$

where f_{OC} [$T^{-1}] is the management cost of the pumping scheme. In this study, f_{OC} accounts for two main parts: the pumping operation cost f_{p} [$T^{-1}], and the treatment operation cost f_{t} [$T^{-1}]. The former is the cost of energy utilization for lifting groundwater to the ground surface, whereas the latter is the cost of desalination by reverse osmosis, which is needed when the salt concentration in water exceeds 1.0 g/L, in accordance with World Health Organization guidelines for drinking water (Yao et al., 2019). f_p is calculate by the following equation,

$$f_{\mathrm{p}} = 4 \times \left(f_{\mathrm{p},1}(Q_1/4\,, h_1, C_1) + f_{\mathrm{p},2}(Q_2, h_2, C_2) \right) \tag{2}$$

where total pump cost f_{p} [$T^{-1}] is four times the sum of the pump cost at the central well $f_{\mathrm{p},1}$ [$T^{-1}] and the pump cost at the movable well $f_{\mathrm{p},2}$ [$T^{-1}]. Pump cost is a function of Q, h and C. Q [$L^3T^{-1}] is the pumping rate at the well, while h [L] and C [$ML^{-3}] are state variables at the well, which represent the hydraulic head at the well screen and the salt concentration in the extracted water, respectively. Both h and C are functions of the DVs. Pump cost $f_{\mathrm{pc}}(Q, h, C)$ is expressed as (Mayer et al., 2002):

$$f_{\mathrm{pc}}(Q, h, C) = \rho_w(C) \cdot \mathrm{g} \cdot \left(z_{\mathrm{gs}} - h \right) \cdot Q \cdot c_{\mathrm{e}} \tag{3}$$

where ρ_w is the water density, which depends on the salt concentration C (Table 1), g denotes gravitational acceleration [$LT^{-2}], and z_{gs} represents the ground surface elevation [L], set equal to 15.0 m. The coefficient c_{e} represents the unit energy cost [$\$M^{-1}L^{-2}T^2$], assumed equal to 0.1848 \$/kWh. Calculating $f_{\mathrm{p},1}$ and $f_{\mathrm{p},2}$ refers to Equation 3. The treatment cost, f_t, is estimated as (Avlonitis et al., 2012):

$$f_{\mathrm{t}}(Q_{\mathrm{f}}, C_{\mathrm{f}}) = \rho_w(C_{\mathrm{f}}) \cdot SEC(C_{\mathrm{f}}) \cdot Q_{\mathrm{f}} \cdot c_{\mathrm{e}} \tag{4}$$

where Q_{f} [$L^3T^{-1}] represents the total volume of groundwater feed to the desalination system, equal to $(Q_1 + 4Q_2)$, and SEC [$L^2T^{-2}] is the specific (per unit mass) energy consumption for

water desalination (Stillwell & Webber, 2016), which depends on the salt concentration of feed water C_f. A detailed description of SEC is presented in the Supporting Information - Appendix B. C_f can be obtained by the following equation,

$$C_f = \frac{Q_1 \cdot C_1 + 4Q_2 \cdot C_2}{Q_1 + 4Q_2} \quad (5)$$

The second management objective is to maximize the amount of qualified groundwater sent to the local communities, formulated as:

$$\text{Maximize} \qquad Q_p = r(C_f, C_b, C_d) \cdot Q_f \quad (6)$$

where Q_p represents the ultimate amount of water from the pumping system delivered to the water network [L^3T^{-1}]. It is the amount of water after the desalination when extracted groundwater concentration is larger than 1.0 g/L. Otherwise, Q_p is identical to the total pumping intensity ($Q_1 + 4Q_2$). r is the recovery ratio and it is equal to 1 when C is less than 1.0 g/L, depending on C_f, $C_b$and C_d. C_b is the resulting brine concentration, and C_d is the target concentration in the permeate, assumed to be 1.0 g/L. The relationship between C_f, C_b, C_d and r is elucidated in the Supporting Information - Appendix B.

The formulation of the island groundwater management problem is completed by two groups of constraints. The first group sets the range of variability of the DVs (D_1, $Q_1/4$, X_2, Y_2, D_2, Q_2). The pumping depths D_1, D_2, pumping rates Q_1, Q_2, and the unfixed well location X_2, Y_2 are subject to the following inequalities:

$$D_{min} \le D_1, \ D_2 \le D_{max} \quad (7)$$

$$Q_{min} \le Q_1, \ Q_2 \le Q_{max} \quad (8)$$

$$X_{min} \le X_2 \le X_{max} \quad (9)$$

$$Y_{min} \le Y_2 \le Y_{max} \quad (10)$$

where D_{min} and D_{max} are the absolute depths below the groundwater surface, defined as 15 m and 120 m, respectively. Pumping rate limits on the well depend on the groundwater demand, which may be estimated based on the population density and the per capita water consumption. Herein, Q_{min} is set to 0 and Q_{max} is set to 350 m^3/day according to Crouch et al. (2021). As the well should be situated inside the modelling region (Figure 4b), X_{min} and X_{max} are identical to 0 and 10,000 m, while Y_{min} and Y_{max} are equal to 0 and 4,000 m. Herein, D_1, D_2, Q_1, Q_2, X_2 and Y_2 have 8, 8, 8, 8, 10 and 4 candidate values, respectively. Therefore, this management problem has a total of 163,840 candidate pumping patterns.

A second group of constraints is considered to minimize the extent of the SWI, thus addressing the environmental sustainability of groundwater abstraction. SWI is quantified by

two indicators: the hydraulic head drawdown scaled to the water table elevation over the pumping system, and the increase in aquifer salt mass.

The drawdown at the pumping well is subject to the following constraint:

$$\Delta s_i \leq \Delta s_{\max} \quad (i = 1, 2) \tag{11}$$

where Δs_i is the drawdown at the i-th pumping well, calculated as the percentage of water table drawdown at the well location with respect to the original water table level, and $\Delta s_{\max}$ is the maximum allowed value for Δs_i. The equation for calculating Δs_i given by:

$$\Delta s_i = \frac{H_{i,0} - H_i}{H_{i,0}} \leq \Delta s_{\max} \tag{12}$$

where $H_{i,0}$ is the water table level over the i-th pumping system prior to pumping (baseline scenario), and H_i is the corresponding steady-state water table level during pumping, which depends on the DVs set.

The aquifer salt mass increase is subject to the inequality:

$$\Delta SM \leq \Delta SM_{\max} \tag{13}$$

where ΔSM is the percentage of salt mass increase in the aquifer, given by:

$$\Delta SM = \frac{SM - SM_0}{SM_0} \leq \Delta SM_{\max} \tag{14}$$

where SM_0 is the total salt mass in the aquifer prior to pumping and SM is the total salt mass at steady state during pumping. $\Delta SM_{\max}$ is the maximum allowed value for ΔSM. SM values are calculated by integrating the salt concentration multiplied by the pore volume over all model grid cells.

2.3 GP model development

GP models are non-parametric models, allowing for the modelling of complex relationships without imposing specific functional forms on the data, indicating the GP model is advantageous in treating the nonlinear process with high efficiency (Redouane et al., 2019). As a type of Bayesian surrogate, the GP model provides the posterior predictive distributions for all points across the input space rather than the potentially best-fit values (Kopsiaftis et al., 2019), quantifying the epistemic uncertainties incurred by the finite training data. In addition, GP models can handle multi-dimensional problems and incorporate prior knowledge about the underlying system. Inspired by these advantages, the GP modelling technique is chosen to substitute the variable-density SEAWAT model in this study.

A GP is a collection of random variables, any finite number of which have a joint Gaussian distribution (Rasmussen & Williams, 2006). Such a GP is treated as a distribution over a space of continuous functions, fully specified by a mean function $m(\boldsymbol{x})$ and a covariance function

$k(\boldsymbol{x}, \boldsymbol{x}')$. A sample from Gaussian processes is a function with its values at any location being distributed according to a Gaussian distribution (Cui et al., 2021). Let $f(\boldsymbol{x})$ represents an output variable of interest,

$$f(\boldsymbol{x}) \sim gp(m(\boldsymbol{x}), k(\boldsymbol{x}, \boldsymbol{x}')) \tag{15}$$

where $\boldsymbol{x} \in R^d$ is a d-dimensional input vector. $m(\boldsymbol{x})$, the expected value of the latent function at the point, and $k(\boldsymbol{x}, \boldsymbol{x}')$, also known as the kernel function, are the prior beliefs about the latent function.

In a Bayesian framework, the prior beliefs can be updated to a posterior distribution over the latent function that represents the output variables of interest by the observed training samples. The obtained posterior distribution offer predictions across the defined input space. Therefore, to apply a GP model, in general, there are mainly five steps, including 1) define a set of input points; 2) run the original simulation model by the specified input points, creating the input-output training dataset; 3) select appropriate mean and covariance functions; 4) update prior beliefs through training on the input-output dataset; 5) generate predictions for any unobserved point over the input space.

Let $\boldsymbol{X}_N = [\boldsymbol{x}_1, \boldsymbol{x}_2, \dots, \boldsymbol{x}_N]^{\mathrm{T}}$ and $\boldsymbol{Y}_N = [\boldsymbol{y}_1, \boldsymbol{y}_2, \dots, \boldsymbol{y}_N]^{\mathrm{T}}$ represent the set of training input and output data. The training set is denoted as the pair $\mathcal{D} = \{\boldsymbol{X}_N, \boldsymbol{Y}_N\}$. The prediction y_* for the new input vector $\boldsymbol{x}_*$ and $\boldsymbol{Y}_N$ have a joint Gaussian distribution, given by:

$$\begin{bmatrix} \boldsymbol{Y}_N \\ y_* \end{bmatrix} \sim \mathcal{N}\left(\begin{bmatrix} \boldsymbol{\mu}_N \\ \mu_* \end{bmatrix}, \begin{bmatrix} \boldsymbol{K} + \sigma_n^2 \boldsymbol{I} & \boldsymbol{k}(\boldsymbol{x}_*) \\ \boldsymbol{k}^{\mathrm{T}}(\boldsymbol{x}_*) & \kappa(\boldsymbol{x}_*) + \sigma_n^2 \end{bmatrix} \right) \tag{16}$$

where $\boldsymbol{\mu}_N = [m(\boldsymbol{x}_1), \dots, m(\boldsymbol{x}_N)]^{\mathrm{T}}$, $\mu_* = m(\boldsymbol{x}_*)$. $\boldsymbol{K}$ is a $N \times N$ matrix, where the (i, j)-th $(i, j = 1,2, \dots, N)$ entry of $\boldsymbol{K}$ is given by $k(\boldsymbol{x}_i, \boldsymbol{x}_j)$. σ_n^2 is the variance of random noise, and $\boldsymbol{I}$ is a $N \times N$ unit matrix. $\boldsymbol{k}(\boldsymbol{x}_*) = [k(\boldsymbol{x}_1, \boldsymbol{x}_*), k(\boldsymbol{x}_2, \boldsymbol{x}_*), \dots, k(\boldsymbol{x}_N, \boldsymbol{x}_*)]^{\mathrm{T}}$ is the $N \times 1$ vector of covariances between the $\boldsymbol{X}_N$ and $\boldsymbol{x}_*$, while $\kappa(\boldsymbol{x}_*) = k(\boldsymbol{x}_*, \boldsymbol{x}_*)$ is the autocovariance of the input data at the prediction point. The posterior distribution of y_* conditioned on $\boldsymbol{X}_N$ and $\boldsymbol{Y}_N$ is given by (Rasmussen & Williams, 2006):

$$f(\boldsymbol{x}_*)|\mathcal{D} \sim gp(m_{\mathcal{D}}(\boldsymbol{x}_*), k_{\mathcal{D}}(\boldsymbol{x}_*, \boldsymbol{x}_*{}')) \tag{17}$$

where

$$m_{\mathcal{D}}(\boldsymbol{x}_*) = \mu_* + \boldsymbol{k}^{\mathrm{T}}(\boldsymbol{x}_*)[\boldsymbol{K} + \sigma_n^2 \boldsymbol{I}]^{-1} \boldsymbol{Y}_N \tag{18}$$

$$k_{\mathcal{D}}(\boldsymbol{x}_*, \boldsymbol{x}_*{}') = \kappa(\boldsymbol{x}_*) - \boldsymbol{k}^{\mathrm{T}}(\boldsymbol{x}_*)[\boldsymbol{K} + \sigma_n^2 \boldsymbol{I}]^{-1} \boldsymbol{k}(\boldsymbol{x}_*) \tag{19}$$

The term $\boldsymbol{k}^{\mathrm{T}}(\boldsymbol{x}_*)[\boldsymbol{K} + \sigma_n^2 \boldsymbol{I}]^{-1}$ in Equation 18 can be interpreted as a set of smoothing coefficients determining the relative importance of each training point to y_*. Equation 19 demonstrates when the unexplored input point is far away from the training points, the correlation between this point and training points is small, lowering $\boldsymbol{k}^{\mathrm{T}}(\boldsymbol{x}_*)[\boldsymbol{K} + \sigma_n^2 \boldsymbol{I}]^{-1} \boldsymbol{k}(\boldsymbol{x}_*)$

and thus increasing predicted variance at this point. Once the mean function and kernel function are determined, predictions at any unknown point over the input space can be given by the GP model. The mean function usually is set as a constant (Kim 2016; Siade et al., 2020), this study assumes it is equal to the average of training data. The kernel function in this work employs the commonly used squared exponential covariance function, (Kim 2016; Zhang et al., 2016; Cui et al., 2021). More details about GP models can be found in Rasmussen & Williams (2006).

In this work, five GP models need to be built for substituting SEAWAT simulations during the optimisation, respectively predicting values of f_{OC}, Q_{P}, Δs_1, Δs_2 and ΔSM given DVs, correspondingly denoted as $\mathrm{GP}_{\mathrm{OC}}$, $\mathrm{GP}_{Q_{\mathrm{p}}}$, $\mathrm{GP}_{\Delta s_1}$, $\mathrm{GP}_{\Delta s_2}$ and $\mathrm{GP}_{\Delta SM}$. To let the predictions align with the realistic, there are some requirements for these GP model predictions, including 1) predicted f_{OC} larger than 0; 2) predicted Q_{p} larger than 0 and no more than total pumping rate Q (equal to $Q_1 + 4Q_2$); 3) predicted Δs_1 and Δs_2 larger than 0; 4) predicted ΔSM larger than -1 according to Equation 14, where *SM* is not equal to or fewer than 0. Regarding the limit on predicted Q_{p}, it can be treated that Q_{p}/Q, namely recovery ratio *r*, should be within the range of (0,1], indicating that 1-*r* should be within [0,1) and obtaining $\frac{1}{1-r}$ within (1, +∞). Overall, it requires positive predictions of f_{OC}, $\frac{r}{1-r}$, Δs_1, Δs_2 and ΔSM+1 given by GP models. This study, to meet those requirements, first adopts log transformation technique, developing GP models to predict log-transformed f_{OC}, $\frac{r}{1-r}$, Δs_1, Δs_2 and ΔSM+1 given DVs. Then, applying the reverse of the log transformation to get positive predictions of f_{OC}, $\frac{r}{1-r}$, Δs_1, Δs_2 and ΔSM+1. Table 2 presents a summary of how to build $\mathrm{GP}_{\mathrm{OC}}$, $\mathrm{GP}_{Q_{\mathrm{p}}}$, $\mathrm{GP}_{\Delta s_1}$, $\mathrm{GP}_{\Delta s_2}$ and $\mathrm{GP}_{\Delta SM}$ to produce predictions aligning with the realistic.

Table 2. *Summary of GP Model Development in This Study*

GP model	Requirements for GP model estimate	Training of GP models		Values of objectives and constraints given DVs	
		Input	Output	Expected value	Confidence interval
$\mathrm{GP}_{\mathrm{OC}}$	$f_{\mathrm{OC}} > 0$	DVs	$\log_{10} f_{\mathrm{OC}}$	$10^{\mu_{\mathrm{OC}}}$	$(10^{\mu_{\mathrm{OC}}-\sigma_{\mathrm{OC}}}, 10^{\mu_{\mathrm{OC}}+\sigma_{\mathrm{OC}}})$
$\mathrm{GP}_{Q_{\mathrm{p}}}$	$0 < Q_{\mathrm{P}} \le Q$ $(0 < r = \frac{Q_{\mathrm{P}}}{Q} \le 1)$	DVs	$\log_{10} \frac{r}{1-r}$	$\frac{Q}{1+10^{-\mu_{\mathrm{p}}}}$	$(\frac{Q}{1+10^{-\mu_{\mathrm{p}}+\sigma_{\mathrm{p}}}}, \frac{Q}{1+10^{-\mu_{\mathrm{p}}-\sigma_{\mathrm{p}}}})$
$\mathrm{GP}_{\Delta s_1}$	$\Delta s_1 > 0$	DVs	$\log_{10} \Delta s_1$	$10^{\mu_{\Delta s_1}}$	$(10^{\mu_{\Delta s_1}-\sigma_{\Delta s_1}}, 10^{\mu_{\Delta s_1}+\sigma_{\Delta s_1}})$
$\mathrm{GP}_{\Delta s_2}$	$\Delta s_2 > 0$	DVs	$\log_{10} \Delta s_2$	$10^{\mu_{\Delta s_2}}$	$(10^{\mu_{\Delta s_2}-\sigma_{\Delta s_2}}, 10^{\mu_{\Delta s_2}+\sigma_{\Delta s_2}})$
$\mathrm{GP}_{\Delta SM}$	$\Delta SM > -1$	DVs	$\log_{10}(1 + \Delta SM)$	$10^{\mu_{\Delta SM}}$-1	$(10^{\mu_{\Delta SM}-\sigma_{\Delta SM}}$-1, $10^{\mu_{\Delta SM}+\sigma_{\Delta SM}}$-1)

In Table 2, μ_{OC}, μ_{p}, $\mu_{\Delta s_1}$, $\mu_{\Delta s_2}$ and $\mu_{\Delta SM}$ are respectively the expected values of $\log_{10} f_{\mathrm{OC}}$, $\log_{10}\frac{r}{1-r}$, $\log_{10}\Delta s_1$, $\log_{10}\Delta s_2$ and $\log_{10}(1+\Delta SM)$ under the pumping, while σ_{OC}, σ_{p}, $\sigma_{\Delta s_1}$, $\sigma_{\Delta s_2}$ and $\sigma_{\Delta SM}$ are the corresponding standard deviations of predictions respectively, all of which are provided by the GP models. To eliminate the effects of decision variable units on the GP model predictions, a scaling process is applied to all DVs, letting them fall within the range of 0 to 1.

2.4 Offline-trained GP model-based simulation-optimisation system

Desired offline-trained GP models are not only to produce reliable global estimates but also to be developed highly efficiently, making the best of each training sample and thus consuming less computing time. Specifically, within the expectation, predictions given by the offline-trained GP models are characterized by smaller confidence intervals, and most training samples are drawn from the high-gradient regions, only a few being distributed across low-gradient regions. To achieve that target, this work proposes a novel offline training algorithm by introducing the iterative process into the offline-trained GP model development. It identifies the input point that has the maximum score $R1$ as the new sampling point, which integrates the information of the distance to the closest training point in the input space (dc) and the gradient of estimate (∇G), expressed below,

$$\max\{R1_i\}\ (i = 1,2\ldots, N_{\mathrm{U}}) \tag{20}$$

where $R1_i$ is the score at the input point i and N_{U} is the number of unobserved input points. $R1_i$ is calculated by the following equation,

$$R1_i = wa_1\overline{dc}_i + wa_2\overline{\nabla G}_i \tag{21}$$

where wa_1 and wa_2 are the weights representing the importance of dc and ∇G, respectively, satisfying $wa_1 + wa_2$=1. In this study, both wa_1 and wa_2 are equal to 0.5. $\overline{dc}_i$ and $\overline{\nabla G}_i$ are respectively the scaled values of dc and ∇G at the input point i for eliminating the effects of their units, varying between 0 and 1, equations for calculating them shown below,

$$\overline{dc}_i = \frac{dc_i - \min\{dc_k\}}{\max\{dc_k\} - \min\{dc_k\}}\ (i,k = 1,2\ldots, N_{\mathrm{U}}) \tag{22}$$

$$\overline{\nabla G}_i = \frac{\|\nabla G(\boldsymbol{x}_i)\|_2 - \min\{\|\nabla G(\boldsymbol{x}_k)\|_2\}}{\max\{\|\nabla G(\boldsymbol{x}_k)\|_2\} - \max\{\|\nabla G(\boldsymbol{x}_k)\|_2\}}\ (i,k = 1,2\ldots, N_{\mathrm{U}}) \tag{23}$$

where dc_i is the distance from the input point i to the closest training point and equal to $\min\{dc_{ij}\}$ $(i = 1,2\ldots, N_{\mathrm{U}};\ j = 1,2,\ldots, N_{\mathrm{T}})$, dc_{ij} denotes the distance from the i-th input point to the j-th training point; N_{T} is the number of training points. $\|\nabla G(\boldsymbol{x}_i)\|_2$ represents the

absolute gradient at the input vector $\boldsymbol{x}_i$ $(i = 1,2 \ldots, N_{\mathrm{U}})$. Figure 5 presents the flow chart for offline training GP models by the proposed strategy.

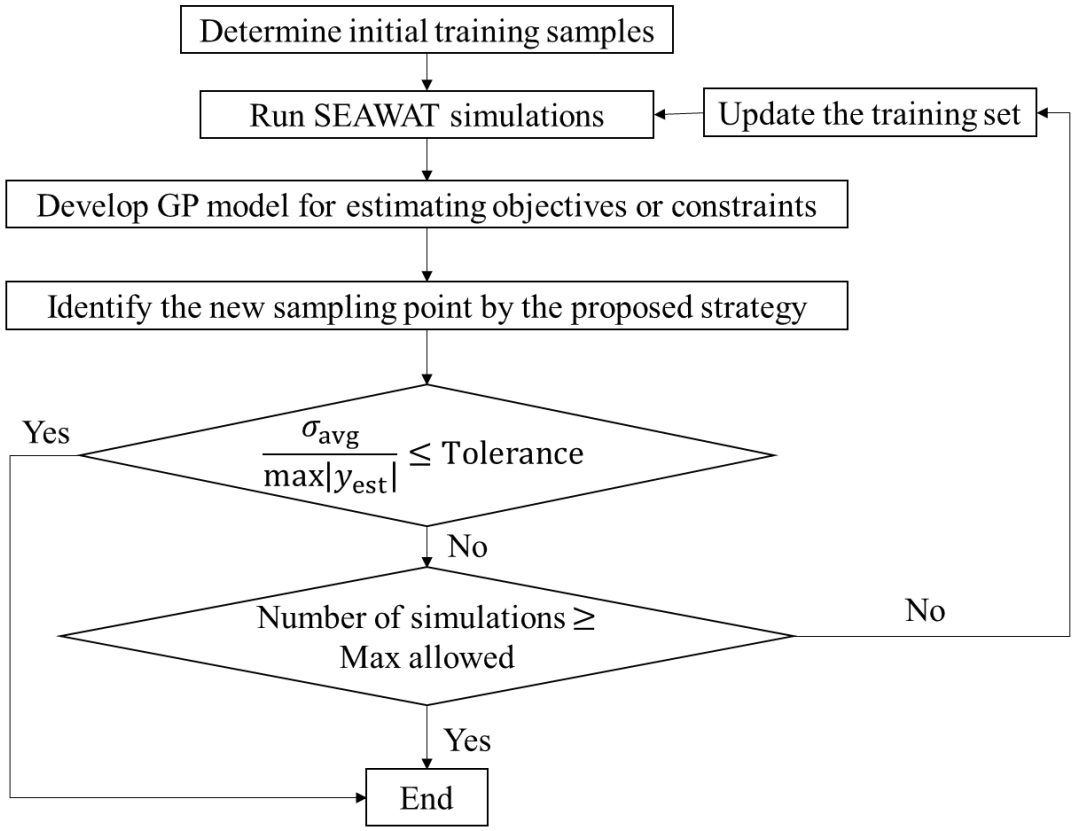

Figure 5. Flow chart for offline training GP models by the proposed strategy.

Figure 5 shows that offline training comes to a halt under any one of two conditions: 1) when the value of $\sigma_{\mathrm{avg}}/\max|y_{\mathrm{est}}|$ falls below the specified tolerance level, and 2) when the number of SWI simulations exceeds the maximum allowed. The indicator $\sigma_{\mathrm{avg}}/\max|y_{\mathrm{est}}|$ quantifies the relative average standard deviation, where σ_{avg} denotes the average standard deviation of GP model estimates and $\max|y_{\mathrm{est}}|$ is the maximum absolute GP model estimate. In this study, the tolerance level for $\sigma_{\mathrm{avg}}/\max|y_{\mathrm{est}}|$ is defined a small value, 0.005.

2.5 Performance evaluation metrics

Before applying the proposed SSO framework to investigate optimal pumping schemes under various constraint conditions, the necessary step is to evaluate its performance in producing optimal solutions, as GP model estimates are approximations of the underlying functions. Three statistical indices are used to evaluate the performance of the developed SSO framework in deriving optimal pumping schemes, including average probability of optimal Pareto solutions ($\overline{PPO}$), normalized root mean square error (*NRMSE*), Pearson's correlation coefficient (*CCE*).

(1) $\overline{PPO}$

Predictions at the unobserved points generated by GP models fluctuate around the expected values with certain standard deviations, reflecting the epistemic uncertainties in the GP model estimates. Therefore, predicted f_{OC}, Q_{p}, Δs_1, Δs_2 and ΔSM at the unknown points in this work are uncertain, causing the derived Pareto-optimal solutions may change at a different stochastic run and each pumping scheme is characterized by a probability of Pareto-optimality (PPO). $\overline{PPO}$ can be employed to evaluate whether the results given by GP models are stable and reliable or not, expression for calculating $\overline{PPO}$ presented below:

$$\overline{PPO} = \frac{1}{N_{\mathrm{P}}} \sum_{i=1}^{N_{\mathrm{P}}} PPO_i \tag{24}$$

where N_{P} denotes the number of potential Pareto-optimal solutions, and PPO_i is the probability of the *i*-th pumping candidate as a Pareto-optimal solution. Computing PPO_i relies on the repeated stochastic simulations (Monte Carlo) runs, which is computationally viable because of the inexpensiveness of the GP models, calculated by

$$PPO_i = \frac{\mathcal{N}_i}{\mathcal{N}} \tag{25}$$

where $\mathcal{N}$ denotes the total number of Monte Carlo runs, set as 1,000 in this work, while $\mathcal{N}_i$ is the times of input *i* serving as a Pareto-optimal solution. A detailed description of how to calculate predicted values of f_{OC}, Q_{p}, Δs_1, Δs_2 and ΔSM for each Monte Carlo run is presented in the Supporting Information – Appendix C. To avoid the effect of outliers (i.e., very-low-probable optimal patterns, occurring a few times in 1,000) on results, this work defines a probability threshold (*PT*). The Pareto-optimal possibilities of pumping patterns that do not reach the PT are kicked out and not in use for calculating $\overline{PPO}$.

(2) *NRMSE*

$$NRMSE = \sqrt{\frac{1}{N_{\mathrm{V}}} \sum_{i=1}^{N_{\mathrm{V}}} (y_i - y_i^*)^2} / (\max\{y_i\} - \min\{y_i\}) \tag{26}$$

(3) *CCE*

$$CCE = \frac{\sum_{i=1}^{N_{\mathrm{V}}} (y_i - \bar{y})(y_i^* - \overline{y^*})}{\sqrt{\sum_{i=1}^{N_{\mathrm{V}}} (y_i - \bar{y})^2 \sum_{i=1}^{N_{\mathrm{V}}} (y_i^* - \overline{y^*})^2}} \ (i = 1, \dots, N_{\mathrm{V}}) \tag{27}$$

In Equations 26-27, N_{V} denotes the number of Pareto-optimal solutions used to check the performance of the proposed SSO framework. y_i and y_i^* are respectively the *i*-th output values from the high-resolution SEAWAT model and GP models. $\bar{y}$ and $\overline{y^*}$ are the mean of exact values and GP model predictions, respectively. Let *NRMSE*(f_{OC}), *NRMSE*(Q_{P}), *NRMSE*(Δs_1), *NRMSE*(Δs_2) and *NRMSE*(ΔSM) represent NRMSE between GP model predictions and exact

values in f_{OC}, Q_{P}, Δs_1, Δs_2 and ΔSM, while $CCE(f_{\mathrm{OC}})$, $CCE(Q_{\mathrm{P}})$, $CCE(\Delta s_1)$, $CCE(\Delta s_2)$ and $CCE(\Delta SM)$ represent *CCE* between GP model predictions and exact values in f_{OC}, Q_{P}, Δs_1, Δs_2 and ΔSM.

Applying the Monte Carlo method generates a probabilistic Pareto-optimal front, which inherently encompasses numerous optimal pumping patterns with different-level probabilities. This study selects the top 20 optimal pumping schemes with the highest possibilities to calculate *NRMSE* and *CCE* in each case, namely N_{V} equal to 20 in this work. According to the analysis in Appendix A and considering the rations of model resolution, this study adopts the fine resolution 100 m ×100 m in the horizontal (i.e., $\Delta x \times \Delta y$ of Figure 4) to build SEAWAT model to run the optimal pumping schemes given by GP models. The expected outcome is to achieve higher $\overline{PPO}$, lower *NRMSE* and larger *CCE*, which would demonstrate the reliability and trustworthiness of the proposed SSO framework in providing optimal pumping schemes.

2.6 Morris method for global sensitivity analysis

To aid decision-makers in better understanding the relationship between defined constraint conditions and optimal pumping schemes, it is necessary to conduct a global sensitivity analysis. Herein, $\Delta s_{\max}$ and $\Delta SM_{\max}$ serve as two input variables, while Pareto-optimal f_{OC} and Q_{p} are treated as the output variables. The information obtained through the sensitivity analysis allows the groundwater managers to assess the impacts of changing SWI limitations on Pareto-optimal solutions, to identify the key constraint condition, and to evaluate the interplay between $\Delta s_{\max}$ and $\Delta SM_{\max}$ in deriving optimal pumping schemes. By applying the SSO framework, global sensitivity analysis is computationally viable.

The Morris method is employed in this work to implement a sensitivity analysis. This method is made up of an individually randomized 'one-step-at-a-time' experiment, where only one input variable gets perturbation and computes a corresponding output value in each run (Morris, 1991; Xu et al., 2018). For all input parameters, their ranges are evenly divided by p levels, and then global sensitivity analysis of these parameters depends on evaluating the differences in function values at these p points by altering one parameter at a time, which is called an elementary effect (*EE*) (Xu et al., 2018). Let $\mathcal{G}$ be a function with l independent input variables and let $\{x_1, x_2 \ldots, x_l\}$ be a group of values assigned to l input variables. If only the i-th input value x_i gets a change by Δ, EE_i can be expressed as below:

$$EE_i = \frac{\mathcal{G}(x_1,\ldots x_{i-1},x_i+\Delta,x_{i+1},x_l)-\mathcal{G}(x_1,\ldots x_{i-1},x_i,x_{i+1},x_l)}{\Delta} \tag{28}$$

The above definition is based on the one-at-a-time design, and to evaluate the global sensitivity of the function value to the i-th input, that needs to repeat p times using different

values of inputs. More details about how to calculate EE_i can be found in Morris (1991), King & Perera (2013) and Ge & Menendez (2017).

Two sensitivity measurement indicators are developed by the EE_i, including 1) the absolute mean μ_i^*evaluates the overall impact of the i-th input on the output; 2) the standard deviation σ_i^* assesses the nonlinear effect between input and output and/or the input variable interactions (Saltelli et al., 2004; Herman et al., 2013). μ_i^* and σ_i^* are given as below,

$$\mu_i^* = \frac{1}{p}\sum_{j=1}^{p}\left|EE_{i,j}\right| \tag{29}$$

$$\sigma_i^* = \sqrt{\frac{1}{p}\sum_{j=1}^{p}\left(EE_{i,j} - \mu_i\right)^2} \quad \left(\mu_i = \frac{1}{p}\sum_{j=1}^{p} EE_{i,j}\right) \tag{30}$$

where $EE_{i,j}$ represents the j-th EE of the i-th input parameter.

According to the values of μ_i^* and σ_i^*, the i-th input variable can be treated as: 1) a non-influential input when μ_i^* approaches zero; 2) an influential input with negligible interactions with other inputs if μ_i^* is high but σ_i^* is low; 3) an influential input with strong interactions with other inputs when both μ_i^* and σ_i^* are high (Morris, 1991; Campolongo et al., 2007).

3 Results and Discussion

3.1 Validation of the proposed SSO framework

Five GP models are required to substitute SEAWAT simulations to offer management objective and constraint values during the optimisation, and they are developed by the proposed offline training strategies (Figure 5). Initial samples for training these five GP models are the same and drawn by the Latin Hypercube sampling method (), size of which is equal to 64.

This section evaluates the performance of the proposed SSO framework in deriving Pareto-optimal pumping schemes with considering the GP model prediction uncertainty and identifies an appropriate sample size for training GP models. Figures 6a-c depict the performance of the proposed SSO framework varying with the maximum allowed training sample size in the case of $\Delta s_{\max}$ equal to 0.1 and $\Delta SM_{\max}$ equal to 0.001, respectively evaluated by the indicators: (a) $\overline{PPO}$; (b) *NRMSE*; (c) *CCE*.

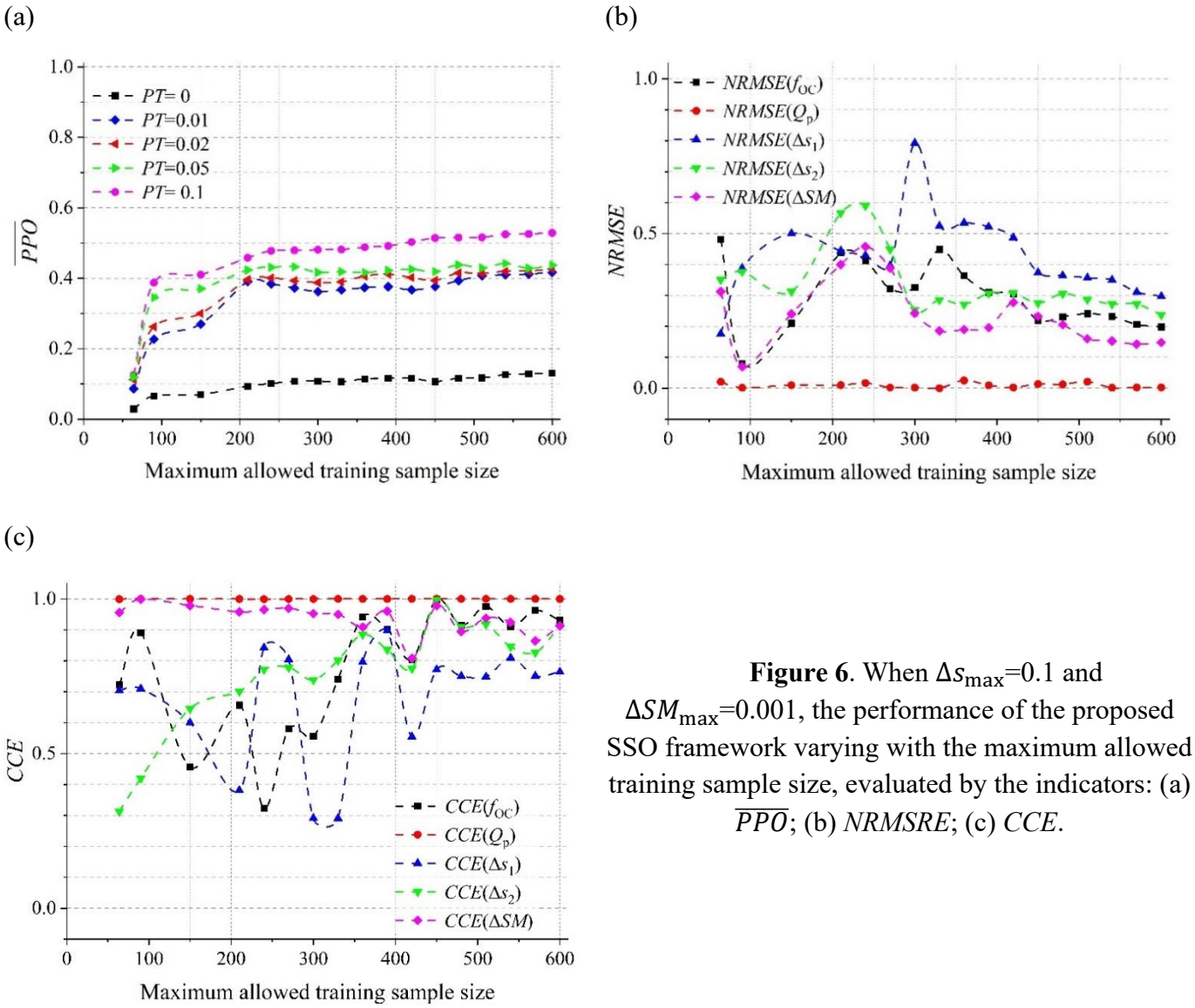

Figure 6. When $\Delta s_{\max}$=0.1 and $\Delta SM_{\max}$=0.001, the performance of the proposed SSO framework varying with the maximum allowed training sample size, evaluated by the indicators: (a) $\overline{PPO}$; (b) *NRMSRE*; (c) *CCE*.

Figure 6a illustrates that $\overline{PPO}$ values under different conditions of *PT* grow noticeably with the maximum allowed training samples increasing from 64 to around 210, and after that, $\overline{PPO}$ values exhibit a gradually subtle-growing tendency accompanied by minor fluctuations. That demonstrates that in terms of improving $\overline{PPO}$, the cost-effective training sample size is around 210. When GP models built by consuming 210 training points, $\overline{PPO}$ values in the cases of *PT* equal to 0.1 and 0.05 are between 0.4 and 0.5, highlighting the obtained Pareto-optimal pumping solutions are characterized by a certain degree of reliability. Moreover, $\overline{PPO}$ values in the case of *PT* equal to 0 are much lower than those under other case of *PT*, indicating that using the Monte Carlo method is prone to produce some extreme-low-probable Pareto-optimal solutions and calculating $\overline{PPO}$ without removing them underestimates the results' reliability.

Observing Figure 6b, when the maximum allowed computational budget is fewer than 450 training samples, curves showing *NRMSE* of f_{OC}, Δs_1, Δs_2 and ΔSM fluctuate without any

tendency to fall, but they show a gradually decreasing behaviour when the allowed sample size overpasses 450. That demonstrates the sample size fewer than 450 generates unstable predictions about management objective and constraint values, failing to produce trustable predictions with lower *NRMSE*.

Similarly, Figure 6c depicts that *CCE*(f_{OC}) and *CCE*(Δs_1) fluctuate significantly when the maximum allowed sample size is between 64 and 450. *CCE*(Δs_2) experiences a general growth with the allowed training sample size increasing, but it exhibits stable fluctuation between high *CCE* values of 0.8 and 1.0 until the maximum allowed training samples approximately reach 450. That is true for all curves, stably fluctuating in the range of high *CCE* values or nearly keeping unchanged at the high *CCE* values, when the allowed computational budget is larger than 450 samples. This again highlights that to ensure accurate predictions of f_{OC}, Q_{P}, Δs_1, Δs_2 and ΔSM, GP models trained by the proposed strategy (Figure 5) require at least 450 samples.

Through the observations in Figures 6a-c, it can conclude that the optimal computational budget for applying the proposed SSO framework to solve the formulated groundwater management problem is to consume 450 training samples.

3.2 Groundwater management under single SWI constraint condition

After validating the proposed SSO framework's performance in determining optimal pumping schemes and identifying the suitable training sample size, this section explores sustainable groundwater management under the single SWI constraint condition, assisted by the proposed SSO framework. To be specific, it investigates the effects of constraint threshold values (values of $\Delta s_{\max}$ and $\Delta SM_{\max}$) on optimal pumping solutions. According to the findings from the previous section, GP models trained by consuming 450 samples are employed to produce Pareto front of the management problem limited by only one SWI constraint condition, Equation 11 or 13. Figures 7a-b present the Pareto front derived under different conditions of $\Delta s_{\max}$ and $\Delta SM_{\max}$, respectively.

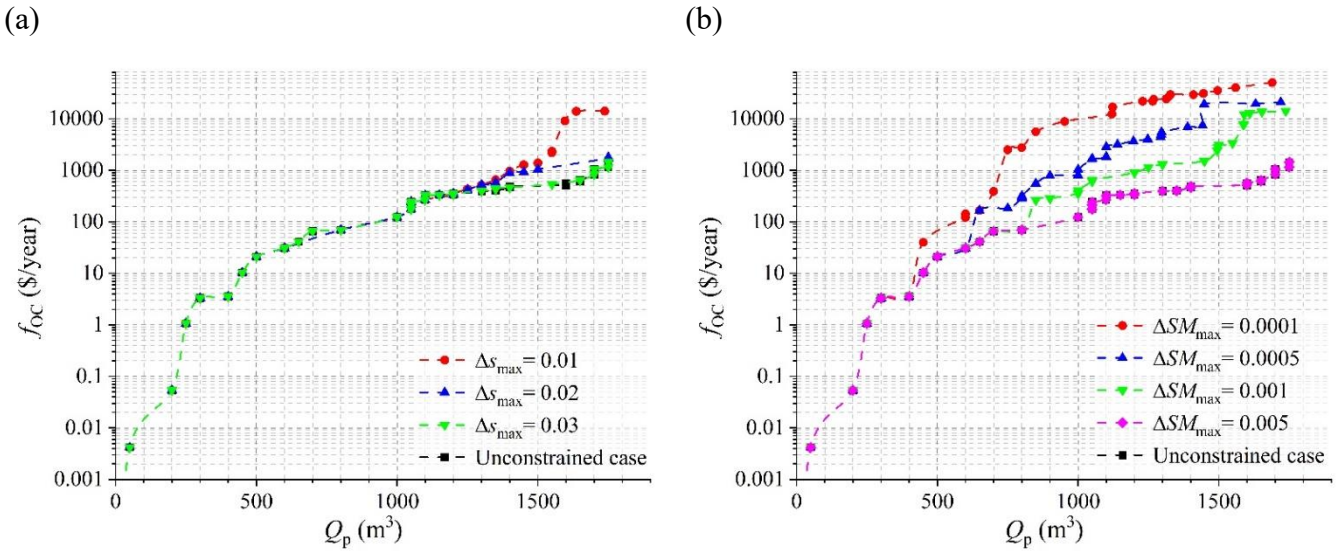

Figure 7. GP models generating Pareto fronts of the groundwater management problem in the different cases of constraint bounds, (a) for $\Delta s_{\max}$; (b) for $\Delta SM_{\max}$. f_{OC} profiles in subpanel (a) and (b) falling below 0.001 $/year indicate that no is required when Q_{P} is zero.

Figure 7a illustrates that the curve in the scenario of $\Delta s_{\max}$ equal to 0.03 is overlapped with that in the unconstrained case (i.e., without considering any limitations on SWI), and the curves in the cases of $\Delta s_{\max}$ equal to 0.02 and 0.01 are only higher than that under the unconstrained case when Q_{p} is greater than 1400 m^3. It demonstrates that when the management problem is only constrained by Δs, $\Delta s_{\max}$ should be at least smaller than 0.02 to let the constraint work.

Figure 7b compares the Pareto fronts across four $\Delta SM_{\max}$ scenarios along with the unconstrained case. The Pareto front under the scenario of $\Delta SM_{\max}$ equal to 0.005 is the same as that in the unconstrained case, while the Pareto fronts in the cases of $\Delta SM_{\max}$ equal to 0.001, 0.0005 and 0.0001 are gradually higher than that under the unconstrained condition with Q_{p} increasing. That indicates if the formulated management problem is only constrained by ΔSM, $\Delta SM_{\max}$ should be defined by around 0.001 or smaller to ensure the constraint works.

Moreover, Figures 7a-b depict that Pareto fronts remain consistent across different scenarios in the low-Q_{p} region, but subsequently, with the demand for Q_{p} gradually rising, the Pareto fronts under stringent constraint conditions are gradually higher than the Pareto front in the unconstrained case. This demonstrates that the low-intensity groundwater pumping imposes negligible impacts on exacerbating SWI, and there exists the Q_{p}-related threshold for the constraint coming into effects, which is dependent on the specified constraint setting and goes larger with loosening constraints.

To gain a visual understanding of how constraint conditions impact optimal pumping patterns, Figure 8 presents the optimal pumping patterns under four scenarios of constraint setting and Q_p. In each subpanel, red columns represent the pumping well, the lengths of which denote the pumping depth, and bule boundaries represent the shoreline. The meanings of ***X*** and ***Y*** are the same as those in Figure 4a.

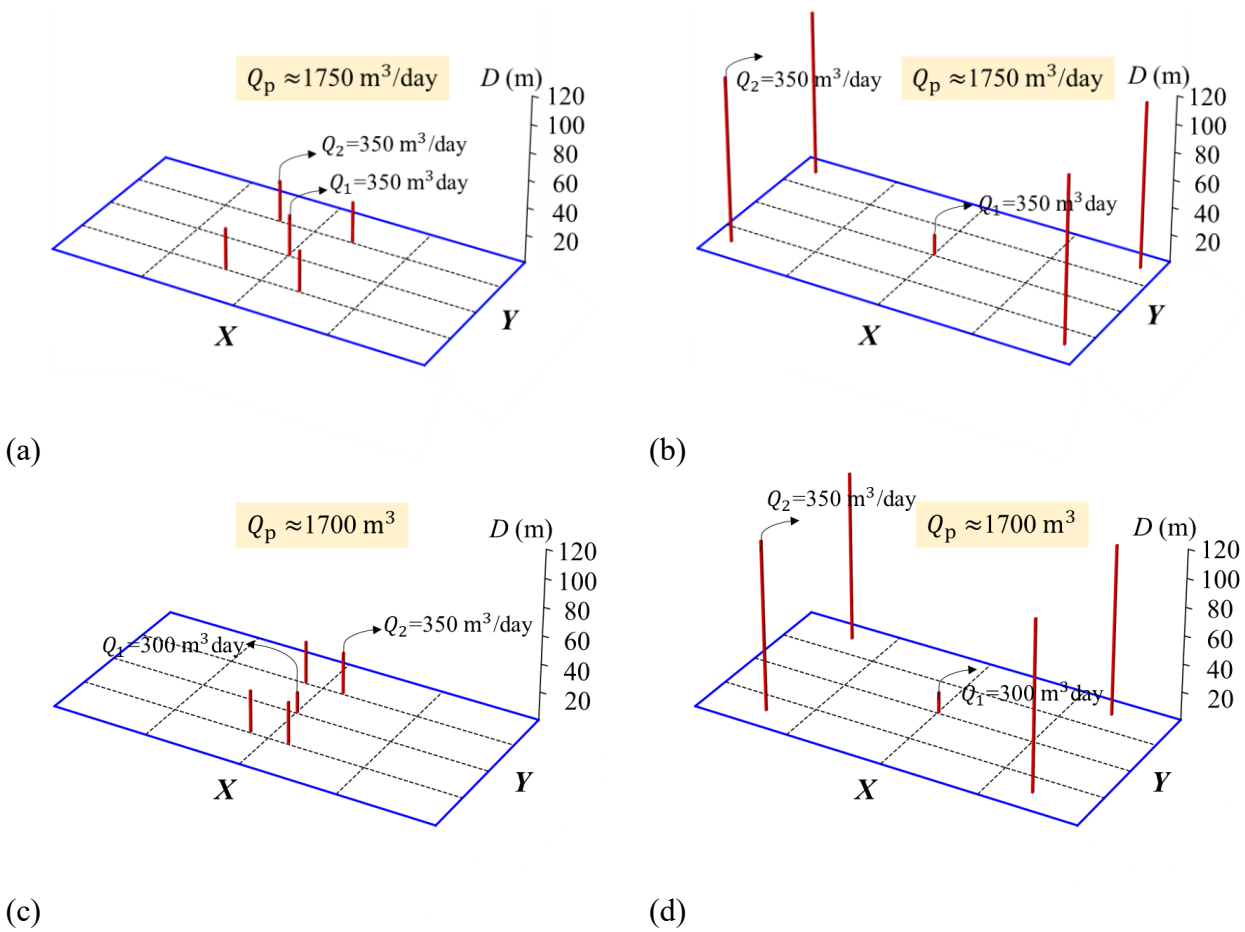

Figure 8. Optimal pumping patterns under various scenarios of constraint setting and Q_p, (a) unconstrained case, Q_p ≈1750 m³/day; (b) Δs_{max} = 0.01, Q_p ≈1750 m³/day; (c) unconstrained case, Q_p ≈1700 m³/day; (d) ΔSM_{max} = 0.0001, Q_p ≈1700 m³/day.

Figures 8a-b illustrate that for reaching Q_p approximately equal to 1750 m³/day, in the unconstrained case and Δs_{max} equal to 0.01, both the central well and four movable wells exploit groundwater with the intensity of 350 m³/day. However, compared to the unconstrained case (Figure 8a), when Δs_{max} is set to 0.01, four movable wells are distributed far away from the island centre and closer to the shoreline, and they pump groundwater from the deeper aquifer.

Figure 8c-d depict that for reaching Q_p approximately equal to 1700 m³/day, pumping intensities of all wells keep unchanged in the cases of both ΔSM_{max} equal to 0.0001 and unconstrained condition. Unlike four movable wells located near the island centre under

unconstrained conditions, applying a condition where $\Delta SM_{\max}$ equal to 0.0001 results in four movable wells being positioned farther from the island centre and nearer to the shoreline, and leads to the deeper groundwater extraction.

Overall, Figures 8a-d indicate that when the limitations on SWI become stricter, to obtain the same volume of Q_{p}, most of the groundwater extracted through the pumping system is from the regions, which are farther from the island centre, closer to the coastline and in the deeper aquifer. This aligns with the findings in **Chapter 2**, where it was found that with the SWI constraint conditions going stricter, optimal locations of the pumping well gradually move towards the shoreline or/and to the deeper aquifer.

3.3 Groundwater management under two SWI constraint conditions

This section explores the impact of incorporating two SWI constraints on Pareto-optimal pumping solutions and analyses the global sensitivity of optimal f_{OC} to different constraints. Figure 9 illustrates three Pareto fronts, each corresponding to the management problem being constrained by the single constraint $\Delta s_{\max}$ equal to 0.01, $\Delta SM_{\max}$ equal to 0.001 and combinations of these two constraints. All these Pareto fronts are produced by GP models that consume 450 training samples.

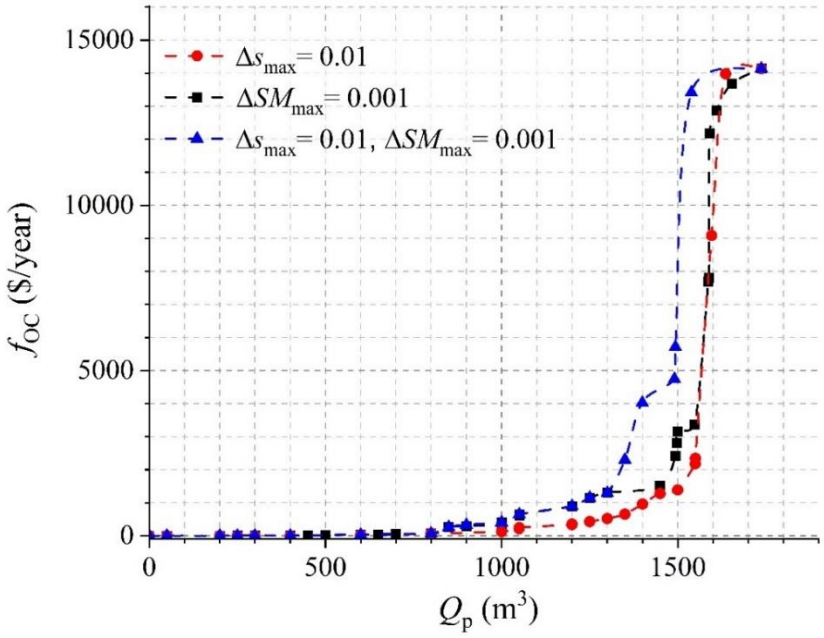

Figure 9. Pareto fronts under three different constraint scenarios, 1) $\Delta s_{\max}$=0.01; 2) $\Delta SM_{\max}$=0.001; 3) $\Delta s_{\max}$=0.01 and $\Delta SM_{\max}$=0.001.

Observing Figure 9, it can be found that when the management problem is separately constrained by $\Delta s_{\max}$ =0.01 and $\Delta SM_{\max}$ =0.001, the derived Pareto fronts are nearly overlapped across the range of Q_{p}. However, employing these two constraint scenarios simultaneously generates a higher Pareto front, obviously when Q_{p} ranging from around 1300

to 1600 m^3/day. It indicates that in that range of Q_p, the most cost-effective pumping strategies depend jointly on these two constraint scenarios, resulting in higher optimal f_{OC}, and demonstrates that constraint Δs and ΔSM do not exhibit a practical equivalence in terms of SWI control. This is also confirmed in **Chapter 2**.

To investigate the global sensitivity of optimal f_{OC} to the SWI constraints given in Equations 11 and 13, the first step is to define the range of Δs_{max} and ΔSM_{max}. It defines Δs_{max} varying between 0.001 and 0.01 while ΔSM_{max} ranging from 0.0001 to 0.001. This study selects three values of Q_p, including 300, 800 and 1,400 m^3/day, which almost distribute across the range of allowed Q_p. By employing the developed GP models to generate Pareto-optimal pumping solutions, values of μ^*, σ^* of the elementary effects of Δs, ΔSM in different cases of Q_p with respect to optimal f_{OC} in the global sensitivity analysis can be calculated according to Equations 28-30, which are shown in Figure 10. The value of *P* in Equations 29-30 is set to 10.

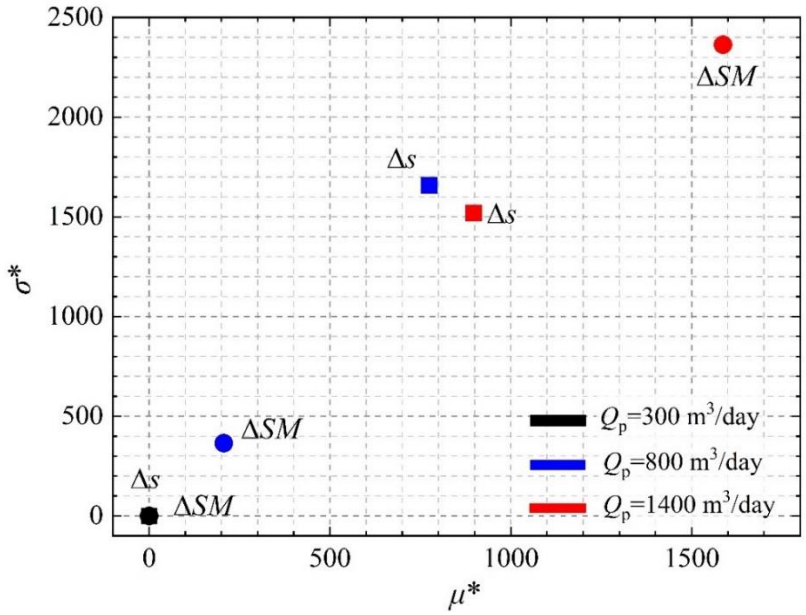

Figure 10. Values of μ^*, σ^* of the elementary effects of Δs, ΔSM in three cases of Q_p with respect to optimal f_{OC} in the global sensitivity analysis.

Figure 10 illustrates that 1) in the case of Q_p equal to 300 m^3/day, both the values of $\mu^*$and σ^* of variable Δs and ΔSM are nearly equal to zero. It indicates that when required Q_p is low, corresponding to low-intensity pumping, both the constraints Δs and ΔSM are non-influential factors to Pareto-optimal pumping solutions. 2) when required Q_p is set to 800 m^3/day, the values of $\mu^*$of constraint Δs and ΔSM become greater, suggesting that the constraint Δs, ΔSM are influential factors to derive optimal f_{OC}, but the constraint Δs has greater μ^* than ΔSM, exhibiting higher importance than the constraint ΔSM in determining optimal solutions. 3)

when required Q_{p} reaches 1,400 m^3/day, the values of $\mu^*$of constraint Δs and ΔSM continue to rise, suggesting the influence of the constraints Δs and ΔSM on optimal solutions strengthens. In this case, ΔSM is with a larger μ^* and it plays a predominant role in determining optimal solutions. The values of σ^* of constraint Δs and ΔSM are also high when Q_{p} reaches 800 and 1,400 m^3/day, suggesting that the constraints Δs and ΔSM have strong interactions, jointly determining optimal pumping solutions in these two conditions.

It should be noted that the importance of the constraints Δs and ΔSM in determining optimal solutions depends on the defined range of $\Delta s_{\max}$ and $\Delta SM_{\max}$. That means if give a larger range of $\Delta SM_{\max}$, such as varying between 0.005 and 0.01, the constraint ΔSM makes no difference to optimal solutions (according to Figure 7b) regardless of the changes in required Q_{p}. This main purpose at here is to investigate the efficiency of our proposed SSO framework in analysing the sensitivity of optimal f_{OC} to the different constraint when Q_{p} is specified.

4 Conclusions

This study proposed an efficient SSO framework for a sustainable coastal groundwater management problem, which focuses on a simplified 3D island aquifer created by hydrogeological conditions observed in San Salvador Island (Bahamas) and involves two conflicting objectives, minimizing f_{OC} and maximizing Q_{p}. It is subject to constraints on SWI control, as quantified by Δs and ΔSM. This management problem considers five pumping wells, one located at the island centre and the others movable and symmetric with each other relative to the island centre. The two groups of wells are respectively characterized by two and four DVs, resulting in a total of six DVs and producing 163,840 potential pumping patterns.

To efficiently obtain the optimal solutions by the SSO method, this study proposed a novel offline training algorithm to construct surrogate models, where an iterative process is introduced and sampling new points is based on the information of distance to the known points and gradients of estimates, along with adopted the coarse model resolution to develop SEAWAT models, generating training data. This work employed the GP modelling technique to construct surrogate models, and a total of five GP models are required to be built for respectively offering management objective and constraint values during the optimisation. Considering the inexpensiveness of the GP models, this study adopted the full enumeration method to derive the optimal solutions.

Before applying the developed SSO framework for island groundwater management, this study first evaluated its performance in producing optimal pumping solutions by the indicators, $\overline{PPO}$, *NRMSE* and *CCE*. Calculating the values of *NRMSE* and *CCE* are based on the simulated

values from high-resolution SEAWAT models. Investigations indicated that when the allowed maximum training sample size for the surrogate models reaches 450, developed GP models can provide reliable and trustable optimal pumping schemes.

After validation, GP models built by consuming 450 training samples were used to investigate the optimal pumping schemes under various scenarios of single SWI constraint conditions. Results showed that when the management problem is separately constrained by Δs or ΔSM, to ensure them work, $\Delta s_{\max}$ should be at least smaller than 0.02 while $\Delta SM_{\max}$ should be defined by around 0.001 or smaller. It also found that when the constraints of Δs or ΔSM strengthens, optimal pumping strategies are prone to extract most of the groundwater from the regions, which are farther from the island centre, closer to the coastline and in the deeper aquifer, which aligns with the findings in **Chapter 2**.

Then, it explored the impact of incorporating two SWI constraints on Pareto-optimal pumping solutions. Results showed that although the management problem separately constrained by $\Delta s_{\max}$ equal to 0.01 and $\Delta SM_{\max}$ equal to 0.001 leads to the quite similar Pareto fronts, the Pareto front in the case of considering these two constraint scenarios is higher. It demonstrates that employing these two constraints together caused more expensive optimal pumping schemes, suggesting the constraints Δs and ΔSM do not exhibit a practical equivalence in terms of SWI control, which has been confirmed in **Chapter 2**.

The authors also applied the developed GP models to analyse the global sensitivity of optimal f_{OC} to the constraint Δs and ΔSM in three cases of Q_{p}. It defines the range of $\Delta s_{\max}$ and $\Delta SM_{\max}$ are between 0.001 and 0.01, and between 0.0001 and 0.001, respectively. Investigations found that when required Q_{p} is low, both the constraints Δs and ΔSM are non-influential factors to Pareto-optimal pumping solutions. If required Q_{p} reaches high, such as 800 and 1,400 m^3/day, Δs and ΔSM impose important effects on optimal pumping schemes. The constraint Δs is more important than ΔSM in determining optimal pumping solutions in the case of Q_{p} equal to 800 m^3/day while the importance of ΔSM is greater than Δs under the condition of Q_{p} equal to 1,400 m^3/day. The results also highlighted that under the given range of $\Delta s_{\max}$ and $\Delta SM_{\max}$, the constraints Δs and ΔSM jointly impose the influence on optimal pumping schemes.

Overall, investigations demonstrated the proposed efficient SSO framework can efficiently provide reliable and trustable optimal pumping schemes regardless of the changes in constraint conditions and be used to conduct sensitivity analysis of optimal groundwater supply costs to constraint conditions.

APPENDIX A. Investigating the effects of model resolution on SWI extent simulation in the island aquifer.

Prior to simulating SWI in the three-dimensional island aquifer, selecting an appropriate model resolution becomes essential to strike a balance between computational expenses and simulation precision. The modelling domain of San Salvador Island has dimensions of 20,000 m in length (X-axis), 8,000 m in width (Y-axis), and 480 m in thickness (Z-axis). According to the distribution of freshwater lens, the model domain is vertically discretized into fifteen layers, with the top twelve layers being 15 m thick, and the bottom three layers being 100 m thick where there is all saltwater. The elevation of the model top is set as 7.5 m, and thus bottom elevation is -472.5 m. Figure 4 illustrates the 3D model domain and the discretization scheme applied in the vertical direction.

For the horizontal plane discretization, this study assumes Δx and Δy are the same. Table A1 presents five model resolution schemes, the total number of grids varying from 375,000 to 60,000.

Table A1. *A Summary of Five Model Resolution Scenarios*

Resolution scenario	Δx (m)	Δy (m)	Δz (m)	Number of rows	Number of columns	Number of layers	Number of grids
1	80	80	15 (top twelve layers), 100 (bottom three layers)	100	250	15	375,000
2	100	100		80	200	15	240,000
3	125	125		64	160	15	153,600
4	160	160		50	125	15	93,750
5	200	200		40	100	15	60,000

To comprehend the impact of model resolution on simulation results, this study first explores the subsurface freshwater volume (FV), aquifer salt mass (SM), and water table elevation at the island centre (H_c) at the initial state where no pumping occurs, under various resolution scenarios. Next, simulation results (e.g., FV, SM, H_c, f_{OC} and Q_p) and the computing time required to achieve a steady state when pumping is taken into account are investigated. The pumping case considered here is groundwater extraction at the island centre, with an intensity of $0.005\,RCH \cdot S$ and a depth of 75 m, where S denotes the surface area of the modelling domain. In the following, Tables A2 and A3 present the simulation results for various resolution scenarios in the initial state and in the case of pumping at the island centre, respectively, all of which are relative to the corresponding ones obtained from the model with the finest resolution.

Table A2. *Simulation Results at the Initial State for Various Resolution Scenarios, Relative to Those Obtained in the Case of the Finest Resolution.*

Resolution scenario	*FV*	*SM*	H_c
1	1.000	1.000	1.000
2	1.004	1.003	0.998
3	0.992	1.007	0.996
4	0.976	1.013	0.993
5	0.960	1.019	0.991

Table A3. *Simulation Results in the Pumping Case for Various Resolution Scenarios, Relative to Those Obtained in the Case of the Finest Resolution.*

Resolution scenario	*FV*	*SM*	H_c	*C*	f_{OC}	Q_p	Computing time for reaching the steady state
1	1.000	1.000	1.000	1.000	1.000	1.000	1.000
2	0.995	1.001	0.992	0.984	0.980	1.001	0.543
3	0.984	1.002	0.989	0.954	0.949	1.003	0.315
4	0.967	1.003	0.993	0.908	0.904	1.006	0.236
5	0.955	1.004	1.002	0.858	0.855	1.009	0.173

Table A2 shows that with the resolution going coarser, both *FV* and H_c at the initial state in general, decrease gradually, while *SM* has a gradual growth. The observed changes in *FV*, H_c and *SM* exhibit consistency, wherein a lower H_c can exacerbate SWI, leading to smaller *FV* and higher *SM*. Results indicate that the model with coarser resolution tends to slightly overestimate SWI extent in the initial state. However, it is important to highlight that these discrepancies across different model resolutions are relatively minor, suggesting that reducing the model resolution has an insignificant impact on the simulation results in the initial state.

Observing Table A3, it becomes apparent that as the model resolution decreases, $\Delta x \times \Delta y$ changing from 80 m ×80 m to 200 m ×200 m, there is a slight decrease in the *FV* and a slight increase in the *SM*. This trend aligns with the observations made in Table A2, indicating that the model with coarser resolution tends to slightly overestimate the SWI extent in response to pumping activities. The values of H_c for various model resolutions are found to be close to each other in the case of pumping. The changes in Q_p for various model resolution scenarios can also be ignored, but the difference in concentration of pumped groundwater (*C*) is noticeable, up to nearly fourteen percent between the resolution scheme 80 m ×80 m and 200 m ×200 m, consequently causing a similar distinction among f_{OC} across the different resolution scenarios. Another significant variation is observed in the required time for reaching the steady state, which can differ by approximately eighty-three percent from the model resolution scenario 1 to 5. This considerable difference in convergence times indicates that the computational effort to achieve a steady state varies significantly depending on the model resolution used.

In summary, the analysis reveals that reducing the model resolution tends to lead to a slight overestimation of aquifer salinity distribution in both non-pumping and pumping cases, but that affects *C* and the required time for reaching the steady state when considering the pumping. Overall, the differences caused by using different model resolutions in *FV*, *SM*, H_c, *C*, f_{OC} and Q_p are within the acceptable level. Therefore, attracted by the computing efficiency, this work adopts resolution scenario 5 to develop a 3D SWI simulation.

APPENDIX B. Energy consumption for water desalination by reverse-osmosis.

As reverse osmosis (RO) is the most popular technique for desalinating brackish water and seawater in coastal groundwater management (Abd-Elhamid & Javadi, 2011; Hussain et al., 2019) it is the method considered in this work to treat groundwater whose salt concentration exceeds accepted potability standards. The specific (per unit mass) energy consumption for desalination SEC [L^2T^{-2}] by RO is estimated as (Stillwell & Webber, 2016):

$$SEC(C) = \frac{R \cdot T_s}{M_w} \cdot \left\{ \frac{x_{sF} - x_{sP}}{x_{sB} - x_{sF}} \cdot \left[x_{sB} \cdot \ln\left(\frac{x_{sB}}{x_{sF}}\right) + x_{wB} \cdot \ln\left(\frac{x_{wB}}{x_{wF}}\right) \right] + \left[x_{sP} \cdot \ln\left(\frac{x_{sP}}{x_{sF}}\right) + x_{wP} \cdot \ln\left(\frac{x_{wP}}{x_{wF}}\right) \right] \right\} \quad \text{(B1)}$$

where *R* is the universal gas constant, T_s is the saturation absolute temperature [K], and M_w is the water molecular weight [e.g., M/mole]. The symbols *x* represents mole fractions [/], with the subscripts "*s*" and "*w*" referring to salt and water, respectively. The subscript F indicates the "feed", that is, the water abstracted that undergoes desalination; the subscript P stands for "permeate", that is, the water distributed to users after desalination; and the subscript B denotes "brine", that is, the by-product high salinity water produced by RO, which is typically disposed.

The salt mole fraction of the feed, x_{sF}, can be calculated from the feed water concentration C as (Avlonitis et al., 2012):

$$x_{sF} = \frac{C/M_s}{C/M_s + [\rho_w(C) - C]/M_w} \quad \text{(B2)}$$

where M_s is the salt molecular weight [M/mole]. The water mole fraction of the feed x_{wF} is:

$$x_{wF} = 1 - x_{sF} \quad \text{(B3)}$$

The mole fractions of the permeate, x_{sP} and x_{wP}, are obtained using Equations B2-B3 with C equal to the target concentration C_d in the permeate, assumed to be 1.0 g/l. Likewise, the mole fractions for the brine, x_{sB} and x_{wB}, are calculated using Equations B2-B3, with C equal to the brine concentration C_b, whose value varies depending on the adopted desalination system. If this is designed to provide a fixed recovery ratio r between the flow rate Q_d sent to water users and the feed flow rate Q ($r = Q_d/Q$), then the brine mole fractions can be derived

by combining the mass balance equations of water and salt for the treatment plant (Avlonitis et al., 2012):

$$x_{\mathrm{sB}} = \frac{x_{s\mathrm{F}} - r x_{s\mathrm{P}}}{1-r} \tag{B4}$$

$$x_{\mathrm{wB}} = \frac{1 - x_{s\mathrm{F}} - r x_{w\mathrm{P}}}{1-r} \tag{B5}$$

The resulting brine concentration can then be calculated as:

$$C_b = \frac{1}{1-r} \cdot C - \frac{r}{1-r} \cdot C_d \tag{B6}$$

Equation B6 shows that C_b may result in excessively large for high recovery ratios (e.g., $r >$ 0.8) and large feed concentrations C, which ultimately leads to cost-ineffective energy consumption (Squire, 2000). On the other hand, if the feed concentrations C is slightly above the target C_d, large quantities of brine with relatively low concentration are discarded, which may result in cost-ineffective as well.

If the desalination system is designed to achieve a fixed brine concentration C_b, Equations B2-B3 with C=C_b are still valid, but the recovery ratio r results in a function of the feed concentrations C, which is obtained from Equation B6 as:

$$r = \frac{C_b - C}{C_b - C_d} \tag{B7}$$

In this work, we adopt the latter approach, and select a fixed brine concentration value C_b of 150.0 g/l (Ahunbay, 2019; Azerrad et al., 2019). For $C_d = 1$ g/l, and C ranging from 1 to 35 g/l, r values vary between 0.77 and 1 (Equation B7).

APPENDIX C. Predicting management objective and constraint values for each Monte Carlo run.

For each Monte Carlo run, expressions for calculating predicted values of f_{OC}, Q_{p}, Δs_1, Δs_2 and ΔSM under the i-th pumping candidate, are given by:

$$\tilde{f}_{\mathrm{OC},i} = 10^{(\mu_{\mathrm{OC},i} + z_{\mathrm{OC}} \cdot \sigma_{\mathrm{OC},i})} \tag{C1}$$

$$\tilde{Q}_{\mathrm{p},i} = Q/(1 + 10^{-\mu_{\mathrm{p},i} + z_{\mathrm{p}} \cdot \sigma_{\mathrm{p},i}}) \tag{C2}$$

$$\Delta\tilde{s}_{1,i} = 10^{(\mu_{\Delta s_{1,i}} + z_{\Delta s_1} \cdot \sigma_{\Delta s_{1,i}})} \tag{C3}$$

$$\Delta\tilde{s}_{2,i} = 10^{(\mu_{\Delta s_{2,i}} + z_{\Delta s_2} \cdot \sigma_{\Delta s_{2,i}})} \tag{C4}$$

$$\Delta\widetilde{SM}_i = 10^{(\mu_{\Delta SM_i} + z_{\Delta SM} \cdot \sigma_{\Delta SM_i})} - 1 \tag{C5}$$

$\mu_{\mathrm{OC},i}$, $\mu_{\mathrm{p},i}$, $\mu_{\Delta s_{1,i}}$, $\mu_{\Delta s_{2,i}}$ and $\mu_{\Delta SM_i}$ are respectively the expected values of f_{OC}, Q_{p}, Δs_1, Δs_2 and ΔSM under the pumping scheme i, while $\sigma_{\mathrm{OC},i}$, $\sigma_{\mathrm{p},i}$, $\sigma_{\Delta s_{1,i}}$, $\sigma_{\Delta s_{2,i}}$ and $\sigma_{\Delta SM_i}$ are respectively the standard deviations of predicted f_{OC}, Q_{p}, Δs_1, Δs_2 and ΔSM at this input vector, all of

which are provided by the GP models. z_{OC}, z_{p}, $z_{\Delta s_1}$, $z_{\Delta s_2}$ and $z_{\Delta SM}$ are the random variables following the standard normal distribution, interpreted as a measure of uncertainty, quantifying the deviation of the estimate from the expected value. As both f_{OC} and Q_{p} are functions of pumping intensities, while Δs_1, Δs_2 and ΔSM are used to quantify the SWI extent, it is believed that f_{OC} and Q_{p}, Δs_1 and ΔSM, Δs_2 and ΔSM have certain correlations, indicating the values of z_{OC}, z_{p}, $z_{\Delta s_1}$, $z_{\Delta s_2}$ and $z_{\Delta SM}$ cannot be determined independently at each run and should consider the corresponding correlations. Generating values of z_{OC}, z_{p}, $z_{\Delta s_1}$, $z_{\Delta s_2}$ and $z_{\Delta SM}$ with considering the correlation can refer to the following general equations.

Given the correlation coefficient between two random variables, *X* and *Y*, data on them can be obtained by the following equations.

$$X = Z_1 \tag{C6}$$

$$Y = \vartheta Z_1 + \sqrt{1-\vartheta^2} Z_2 \tag{C7}$$

where Z_1 and Z_2 are two independent random variables, both of which follow the normal standard distribution. ϑ is the correlation coefficient between *X* and *Y*, and $\vartheta \in [-1,1]$.

Values of z_{OC}, z_{P}, $z_{\Delta s_1}$, $z_{\Delta s_2}$ and $z_{\Delta SM}$ in Equations C1-C5 can be determined by the above equations, and correlation coefficients between them are calculated by the training data.

Acknowledgements

The authors have no relevant financial or non-financial interests to declare that are relevant to the content of this article. This work was partially supported by the EPSRC grant no. EP/T018542/1, and the NSF under grant agreement CBET-EPSRC 2022278. The authors also would like to thank the editor and anonymous reviewers for their kind feedback and insightful comments, which helped improve the clarity of this paper.

References

Kishi, Y., & Fukuo, Y. (1977). Studies on salinization of groundwater, I: Theoretical consideration on the three-dimensional movement of the salt water interface caused by the pumpage of confined groundwater in fan-shaped alluvium. *Journal of Hydrology*, *35*(1), 1-29. https://doi.org/10.1016/0022-1694(77)90074-9

Davis, R. L. & Johnson, C. R. (1989). Karst Hydrology of San Salvador. In Mylroie, J.E. (Ed.), Proceedings of the Fourth Symposium on the Geology of the Bahamas. Bahamian Field Station, San Salvador Island, Bahamas, pp. 118–135.

Morris, M. D. (1991). Factorial sampling plans for preliminary computational experiments. *Technometrics*, *33*(2), 161-174. https://doi.org/10.1080/00401706.1991.10484804

Squire, D. (2000). Reverse osmosis concentrate disposal in the UK. *Desalination*, *132*(1), 47-54. https://doi.org/10.1016/S0011-9164(00)00134-X

Mayer, A. S., Kelley, C. T., & Miller, C. T. (2002). Optimal design for problems involving flow and transport phenomena in saturated subsurface systems. *Advances in Water Resources*, *25*(8), 1233–1256. https://doi.org/10.1016/S0309-1708(02)00054-4

Saltelli, A., Tarantola, S., Campolongo, F., & Ratto, M. (2004). Sensitivity Analysis in Practice: A Guide to Assessing Scientific Models. Wiley, New York, NY.

Campolongo, F., Cariboni, J., & Saltelli, A. (2007). An effective screening design for sensitivity analysis of large models. *Environmental Modelling & Software*, 22(10), 1509–1518. http://dx.doi.org/10.1016/j.envsoft.2006.10.004.

Langevin, C. D., Thorne, D. T., Jr., Dausman, A. M., Sukop, M. C., & Guo, W. (2008). *SEAWAT version 4: A computer program for simulation of multi-species solute and heat transport* (Rep. 2328-7055). Geological Survey (US).

Martin, J. B., & Moore, P. J. (2008). Sr concentrations and isotope ratios as tracers of groundwater circulation in carbonate platforms: Examples from San Salvador Island and Long Island, Bahamas. *Chemical Geology*, *249*(1), 52-65. https://doi.org/10.1016/j.chemgeo.2007.11.009

Moore, P. J. (2009). Controls on the generation of secondary porosity ineogenetic karst: examples from San Salvador Island, Bahamas and north-central Florida, USA, (Doctoral dissertation). Gainesville, FL: University of Florida.

McGee, D. K., Wynn, J. G., Onac, B. P., Harries, P. J., & Rothfus, E. A. (2010). Tracing groundwater geochemistry using $\delta^{13}C$ on San Salvador Island (southeastern Bahamas): implications for carbonate island hydrogeology and dissolution. *Carbonates Evaporites*, *25*(2), 91–105. https://doi.org/10.1007/s13146-010-0013-6

Papadopoulou, M. P., Nikolos, I. K., & Karatzas, G. P. (2010). Computational benefits using artificial intelligent methodologies for the solution of an environmental design problem: saltwater intrusion. *W*ater *S*cience & *T*echnology, *62*(7), 1479–1490. https://doi.org/10.2166/wst.2010.442

Abd-Elhamid, H. F., & Javadi, A. A. (2011). A cost-effective method to control seawater intrusion in coastal aquifers. *Water Resources Management*, *25*, 2755–2780. https://doi.org/10.1007/s11269-011-9837-7

Kourakos, G., & Mantoglou, A. (2011). Simulation and multi-Objective management of coastal aquifers in semi-arid regions. *W*ater *R*esources *M*anagement, *25*, 1063–1074. https://doi.org/10.1007/s11269-010-9677-x

Sreekanth, J., & Datta, B. (2011). Coupled simulation-optimisation model for coastal aquifer management using genetic programming-based ensemble surrogate models and

multiple-realization optimisation. *Water Resources Research*, *47*(4), W04516. https://doi.org/10.1029/2010WR009683

Avlonitis, S. A., Avlonitis, D. A., & Panagiotidis, Th. (2012). Experimental study of the specific energy consumption for brackish water desalination by reverse osmosis. *International Journal of Energy Research*, *36*, 36-45. https://doi.org/10.1002/er.1780

Herman, J. D., Kollat, J. B., Reed, P. M., & Wagener, T. (2013). Method of Morris effectively reduces the computational demands of global sensitivity analysis for distributed watershed models. *Hydrology and Earth System Sciences*, *17*(7), 2893–2903. https://doi.org/10.5194/hess-17-2893-2013

King, D. M., & Perera, B. J. C. (2013). Morris method of sensitivity analysis applied to assess the importance of input variables on urban water supply yield – A case study. *Journal of Hydrology*, *477*, 17-32. https://doi.org/10.1016/j.jhydrol.2012.10.017

Kourakos, G., & Mantoglou, A. (2013). Development of a multi-objective optimisation algorithm using surrogate models for coastal aquifer management. *Journal of Hydrology*, *479*, 13-23. https://doi.org/10.1016/j.jhydrol.2012.10.050

Ho, H. C., Mylroie, J. E., Infante, L. R., & Rodgers, J. C. (2014). Fuzzy-based spatial modeling approach to predict island karst distribution: a conceptual model. *Environmental Earth Sciences*, *71*(3), 1369–1377. https://doi.org/10.1007/s12665-013-2543-4

Morgan, L. K., & Werner, A. D. (2014). Seawater intrusion vulnerability indicators for freshwater lenses in strip islands. *Journal of Hydrology*, *508*, 322-327. https://doi.org/10.1016/j.jhydrol.2013.11.002

Vandenbohede, A., Mollema, P. N., Greggio, N., & Antonellini, M. (2014). Seasonal dynamic of a shallow freshwater lens due to irrigation in the coastal plain of Ravenna, Italy. *Hydrogeology Journal*, *22*, 893–909. https://doi.org/10.1007/s10040-014-1099-z

Holding, S., & Allen, D. M. (2015). From days to decades: numerical modelling of freshwater lens response to climate change stressors on small low-lying islands. *Hydrology and Earth System Sciences*, *19*(2), 933–949. https://doi.org/10.5194/hess-19-933-2015

Javadi, A., Hussain, M., Sherif, M., & Farmani, R. (2015). Multi-objective optimisation of different management scenarios to control seawater intrusion in coastal aquifers. *W*ater *R*esources *M*anagement, *29*, 1843–1857. https://doi.org/10.1007/s11269-015-0914-1

Ketabchi, H., & Ataie-Ashtiani B. (2015a). Evolutionary algorithms for the optimal management of coastal groundwater: A comparative study toward future challenges. *J*ournal of *H*ydrology, *520*, 193-213. https://doi.org/10.1016/j.jhydrol.2014.11.043

Ketabchi, H., & Ataie-Ashtiani B. (2015b). Assessment of a parallel evolutionary optimisation approach for efficient management of coastal aquifers. *E*nvironmental *M*odelling & *S*oftware, *74*, 21-38. https://doi.org/10.1016/j.envsoft.2015.09.002

Kourakos, G., & Mantoglou, A. (2015). An efficient simulation-optimisation coupling for management of coastal aquifers. *Hydrogeology Journal*, *23*, 1167–1179. https://doi.org/10.1007/s10040-015-1293-7

Zekri, S., Triki, C., Al-Maktoumi, A., & Bazargan-Lari, M. R. (2015). An optimisation-simulation approach for groundwater abstraction under recharge uncertainty. *W*ater *R*esources *M*anagement, *29*, 3681–3695. https://doi.org/10.1007/s11269-015-1023-x

Gulley, J. D., Mayer, A. S., Martin, J. B., & Bedekar, V. (2016). Sea level rise and inundation of island interiors: Assessingimpacts of lake formation and evaporationon water resources in arid climates. *Geophysical Research Letters*, *43*(18), 9712-9719. https://doi.org/10.1002/2016GL070667

Stillwell, A. S., & Webber, M. E. (2016). Predicting the specific energy consumption of reverse osmosis desalination. *Water*, *8*(12), 601. https://doi.org/10.3390/w8120601

Ge, Q., & Menendez, M. (2017). Extending Morris method for qualitative global sensitivity analysis of models with dependent inputs. *Reliability Engineering & System Safety*, *162*, 28-39. https://doi.org/10.1016/j.ress.2017.01.010

Gingerich, S. B., Voss, C. I., & Johnson, A. G. (2017). Seawater-flooding events and impact on freshwater lenses of low-lying islands: Controlling factors, basic management and mitigation. *Journal of Hydrology*, *551*, 676–688. https://doi.org/10.1016/j.jhydrol.2017.03.001

Rajabi, M. M., & Ketabchi, H. (2017). Uncertainty-based simulation-optimisation using Gaussian process emulation: Application to coastal groundwater management. *J*ournal of *H*ydrology, *555*, 518-534. https://doi.org/10.1016/j.jhydrol.2017.10.041

Song, J., Yang, Y., Wu, J., Wu, J., Sun, X., & Lin, J. (2018). Adaptive surrogate model based multiobjective optimisation for coastal aquifer management. *J*ournal of *H*ydrology, *561*, 98-111. https://doi.org/10.1016/j.jhydrol.2018.03.063

Xu, Z., Hu, B. X., & Ye, M. (2018). Numerical modeling and sensitivity analysis of seawater intrusion in a dual-permeability coastal karst aquifer with conduit networks. *Hydrology and Earth System Sciences*, *22*(1), 221–239. https://doi.org/10.5194/hess-22-221-2018

Ahunbay, M. G. (2019). Achieving high water recovery at low pressure in reverse osmosis processes for seawater desalination. *Desalination*, *465*, 58–68. https://doi.org/10.1016/j.desal.2019.04.023

Azerrad, S. P., Isaacs, M., & Dosoretz, C. G. (2019). Integrated treatment of reverse osmosis brines coupling electrocoagulation with advanced oxidation processes. *Chemical Engineering Journal*, *356*, 771–780. https://doi.org/10.1016/j.cej.2018.09.068

Christelis, V., Kopsiaftis, G., & Mantoglou, A. (2019). Performance comparison of multiple and single surrogate models for pumping optimisation of coastal aquifers. *H*ydrological *S*ciences *J*ournal, *64*(3), 336–349. https://doi.org/10.1080/02626667.2019.1584400

Hussain, M. S., Abd-Elhamid, H. F., Javadi, A. A., & Sherif, M. M. (2019). Management of seawater intrusion in coastal aquifers: a review. *Water*, *11*(12), 2467. https://doi.org/10.3390/w11122467

Roy, D. K., & Datta, B. (2019). Adaptive management of coastal aquifers using entropy-set pair analysis–based three-dimensional sequential monitoring network design. *Journal of Hydrologic Engineering*, *24*(3), 04018072. https://doi.org/10.1061/(ASCE)HE.1943-5584.000176

Yao, Y., Andrews, C., Zheng, Y., He, X., Babovic, V., & Zheng, C. (2019). Development of fresh groundwater lens in coastal reclaimed islands. *Journal of Hydrology*, *573*, 365–375. https://doi.org/10.1016/j.jhydrol.2019.03.062

Dey, S., & Prakash, O. (2020). Managing saltwater intrusion using conjugate sharp interface and density dependent models linked with pumping optimisation. *Groundwater for Sustainable Development*, *11*, 100446. https://doi.org/10.1016/j.gsd.2020.100446

Fan, Y., Lu, W., Miao, T., Li, J., & Lin, J. (2020). Multiobjective optimisation of the groundwater exploitation layout in coastal areas based on multiple surrogate models', *E*nvironmental *S*cience *and P*ollution *R*esearch, *27*, 19561–19576. https://doi.org/10.1007/s11356-020-08367-2

Han, Z., Lu, W., Fan, Y., Lin, J., & Yuan, Q. (2020). A surrogate-based simulation–optimisation approach for coastal aquifer management. *W*ater *S*upply, *20*(8), 3404–3418. https://doi.org/10.2166/ws.2020.259

Jasechko, S., Perrone, D., Seybold, H., Fan, Y., & Kirchner, J. W. (2020). Groundwater level observations in 250,000 coastal US wells reveal scope of potential seawater intrusion. *Nature Communications*, *11*, 3229. https://doi.org/10.1038/s41467-020-17038-2

Mostafaei-Avandari, M., & Ketabchi, H. (2020). Coastal groundwater management by an uncertainty-based parallel decision model. *Journal of Water Resources Planning and Management*, *146*(6), 04020036. https://doi.org/10.1061/(ASCE)WR.1943-5452.0001227

Ranjbar, A., & Mahjouri, N. (2020). Multi-objective freshwater management in coastal aquifers under uncertainty in hydraulic parameters. *N*atural *R*esources *R*esearch, *29*(4), 2347–2368. https://doi.org/10.1007/s11053-019-09585-3

Yin, J., Pham, H. V., & Tsai, F. T. C. (2020). Multiobjective spatial pumping optimisation for groundwater management in a multiaquifer system. *J*ournal of *W*ater *R*esources *P*lanning *and M*anagement, *146*(4), 04020013. https://doi.org/10.1061/(ASCE)WR.1943-5452.0001180

Agoubi, B. (2021). A review: saltwater intrusion in North Africa's coastal areas-current state and future challenges. *Environmental Science and Pollution Research*, *8*(14), 17029-17043. https://doi.org/10.1007/s11356-021-12741-z.

Al-Maktoumi, A., Rajabi, M. M., Zekri, S., & Triki, C. (2021). A probabilistic multiperiod simulation–optimisation approach for dynamic coastal aquifer management. *W*ater *R*esources *M*anagement, *35*, 3447–3462. https://doi.org/10.1007/s11269-021-02828-0

Crouch, M. L., Jacobs, H. E., & Speight, V. L. (2021). Defining domestic water consumption based on personal water use activities. *Aqua Water Infrastructure, Ecosystems and Society*, *70*(7), 1002-1011. https://doi.org/10.2166/aqua.2021.056.

Han, Z., Lu, W., Fan, Y., Xu, J., & Lin, J. (2021). Surrogate-based stochastic multiobjective optimisation for coastal aquifer management under parameter uncertainty. *W*ater *R*esources *M*anagement, *35*, 1479–1497. https://doi.org/10.1007/s11269-021-02796-5

Yang, Y., Song, J., Simmons, C. T., Ataie-Ashtiani, B., Wu, J., Wang, J., & Wu, J. (2021). A conjunctive management framework for the optimal design of pumping and injection strategies to mitigate seawater intrusion. *J*ournal of *E*nvironmental *M*anagement, *282*, 111964. https://doi.org/10.1016/j.jenvman.2021.111964

Coulon, C., Lemieux, J. M., Pryet, A., Bayer, P., Young, N. L., & Molson, J. (2022). Pumping optimisation under uncertainty in an island freshwater lens using a sharp-interface seawater intrusion model. *W*ater *R*esources *R*esearch, *58*, e2021WR031793. https://doi.org/10.1029/2021WR031793

Jamal, M. S., Awotunde, A. A., & Patil, S. (2022). Management of saltwater intrusion in coastal Karstic aquifers under geological uncertainties associated with shapes and locations of cave networks. *J*ournal *of W*ater *R*esources *P*lanning and *M*anagement, *148*(11), 04022053. https://doi.org/10.1061/(ASCE)WR.1943-5452.0001603

Wang, Z., Yang, Y., Wu, J., Sun, X., Lin, J., & Wu, J. (2022). Multi-objective optimisation of the coastal groundwater abstraction for striking the balance among conflicts of resource-environment-economy in Longkou City, China. *W*ater *R*esearch, *211*, 118045. https://doi.org/10.1016/j.watres.2022.118045

Yin, J., Tsai, F. T. C., & Lu, C. (2022). Bi-objective extraction-injection optimisation modeling for saltwater intrusion control considering surrogate model uncertainty. *W*ater *R*esources *M*anagement, *36*, 6017–6042. https://doi.org/10.1007/s11269-022-03340-9

Chapter 5

Summary and Conclusions

5.1 Summary of the thesis

The research background of this study was elucidated in Chapter 1, in which the strategy of coastal groundwater management is commonly used to strike a balance between cost, sustainability, and environmental impact and the SO method serves as a popular alternative to derive optimal pumping schemes. However, the SO method involves repeated calls of SWI simulators during the optimisation, and it would be computationally intractable when the number of SWI simulations is substantial and/or each SWI simulation is time-consuming. A feasible option to address that computational issue is to replace the SWI simulator with the surrogate models during the optimisation, constituting an SSO framework where surrogate models offer aquifer response under the pumping in the optimisation stage.

Two typical types of surrogate models are used in the SSO framework, including the offline and online-trained surrogate models. The former completes development before the optimisation, while the latter continuously adapts and improves with new data added during the optimisation. In coastal groundwater management, the traditional training ways to build offline and online-trained surrogate models for solving multi-objective management problems are inefficient. Moreover, despite the support of the SSO framework, solving multi-objective management problems remains a time-consuming task, particularly when they comprise many DVs and are formulated within a 3D aquifer that is discretized by numerous cells in the simulation model, causing substantial computational expenses for each simulation run.

In view of these challenges, this PhD research aimed to explore the efficient approaches for offline and online training surrogate models, and to develop an efficient SSO framework for multi-objective groundwater management within the 3D coastal aquifer. According to the research aim, five objectives were formed.

The first objective was to develop a preliminary insight into the effects of pumping patterns on the SWI extent and optimal operation cost of abstracting groundwater, along with the effects of choice of SWI constraint conditions on optimal pumping schemes. It was addressed and discussed in Chapter 2. In this chapter, a one-well management problem was formulated within a simplified 2D aquifer created by the hydrogeological conditions observed on the San Salvador Island aquifer (Bahamas), aiming at minimizing f_{OC}, subject to constraints on SWI control, as quantified by Δs, ΔFV, or ΔSM in the aquifer. Each pumping pattern was

characterized by three DVs, including WL, D and Q. A total of 224 pumping patterns were designed to distribute across the decision variable space, and the SEAWAT model was employed to generate the aquifer response under these pumping schemes. According to the simulation results, the effects of WL, D and Q on Δs, ΔFV, and ΔSM were studied and the interplay between management costs and these three types of constraints, both individually and in combination was analysed.

The second objective was to assess the performance of proposed offline training algorithms relative to traditional offline training strategy and to identify the most appropriate algorithm for offline training GP models in multi-objective groundwater management problems. It was addressed and studied in Chapter 3. In this chapter, a two-objective pumping optimisation problem, aiming at minimizing f_{OC} and maximizing Q_{p}, was formulated within a simplified 2D aquifer created by the hydrogeological conditions observed on San Salvador Island (Bahamas). It was still a one-well problem and includes three DVs, including WL, D and Q. This study introduced the iterative process to the development of offline-trained GP models and proposed a total of three offline training algorithms. Their performance was evaluated and analysed by CC and $\overline{PPO}$.

The third objective was to assess the performance of proposed online training algorithms and to identify the most efficient approaches for online training GP models in multi-objective coastal groundwater management problems. It was addressed and discussed in Chapter 3. This study proposed a total of four online training algorithms to solve the same two-objective management problems described in the second objective. Their performance in deriving optimal pumping solutions was evaluated and analysed by CC and $\overline{PPO}$.

The fourth objective was to investigate the advantages and disadvantages of respectively employing offline and online-trained surrogate models in the realm of coastal groundwater management. It was addressed and discussed in Chapter 3 based on the findings from the second and third research objectives by comparing the performance of identified the most appropriate offline and online training algorithms in obtaining optimal pumping solutions.

The fifth objective was to develop an efficient SSO framework based on the findings from the previous objectives for sustainable groundwater management within a 3D island aquifer model. It was addressed and discussed in Chapter 4. As offline-trained surrogate models are independent of the changes in the constraint conditions, this chapter developed an efficient SSO framework, which adopted a coarse model resolution to create SEAWAT models to generate training data and employed the most appropriate offline training algorithm to build

GP models, for solving a two-objective management problem. This management problem had the same objectives and constraints as in the second objective, but it had more DVs, up to six, which generated 163,840 pumping candidates. The proposed SSO framework was first validated by $\overline{PPO}$, *NRMSE* and *CCE*, and then applied to investigate the optimal pumping solutions under various single-constraint and two-constraint scenarios.

5.2 Key research findings

The achievement of the research objectives discussed earlier unfolds the following key findings of the research.

The achievement of the first objective revealed that,

(1) Pumping with the shallow aquifer or/and near the island centre is prone to extract freshwater without a desalination process, leading to a lower f_{OC}. However, the formulated SWI indicators show that pumping in proximity of the island centre has a negative impact on the availability of freshwater resources in the aquifer, when compared to the effect of "decentralized" pumping strategies. This highlights an inherent conflict between SWI control and the economic cost of groundwater supply.

(2) The impact of the constraint on Δs on cost-optimal pumping strategies is quite different than that of constraints on ΔFV and ΔSM. Constraints on Δs are observed to lead to selecting deeper pumping systems located towards the island centre, whereas both the constraints on ΔFV and ΔSM favour the choice of shallower pumping systems closer to the shoreline. Therefore, the pumping strategies under Δs constraints result generally more expensive than those under ΔFV and ΔSM constraints, as they involve extraction of groundwater with higher salinity that require more intense desalination treatment.

(3) Our analysis has shown also that constraints on ΔFV and ΔSM exhibit a practical equivalence in terms of SWI control, and to reduce the complexity of management problems, they should not be adopted simultaneously in the optimisation formulation of the groundwater management problem.

The achievement of the second objective revealed that,

(4) Compared with traditional offline training, introducing the iterative procedure can improve the computing efficiency and reliability of the resulting Pareto front.

(5) The strategy, integrating information about the gradient of estimate values and the distance to the closest training point to determine training points at each iteration, is proved as the most appropriate and efficient offline training approach. It outperforms the strategies considering them separately in terms of global prediction accuracy and reliability of derived

Pareto front. Furthermore, when aiming to attain a Pareto front with moderate reliability, applying this strategy can achieve a reduction of over 50% in computational expenses compared to the traditional offline training approach.

The achievement of the third objective revealed that,

(6) Discretizing the objective space into equal sub-regions based on the obtained Pareto front and then selecting sampling points within these sub-regions can facilitate the convergence of GP models with low computational costs.

(7) Findings demonstrated that among the proposed online training strategies for building GP models, the efficient ones for identifying new sampling points at each iteration rely on information about either the distance between Pareto-optimal solutions and the ideal point within the objective space, or the distance between Pareto-optimal solutions and their sub-region centre within the objective space. The latter slightly outperforms the former.

The achievement of the fourth objective revealed that,

(8) In view of the performance of applying efficient offline and online approaches for training GP models in solving bi-objective groundwater management problem, it can be concluded that given limitations on SWI control, employing online-trained GP models can produce more reliable, cost-effective Pareto front with higher computing efficiency compared to adopting offline-trained GP models. However, offline-trained GP models can provide considerably trustworthy predictions over the entire input space and are independent of changes in SWI constraint conditions.

The achievement of the fifth objective revealed that,

(9) When the proposed efficient SSO framework consumes 450 training samples, it can provide reliable and trustable optimal pumping solutions to the formulated management problem. Applying this SSO system investigates the optimal pumping solutions under various single-constraint and two-constraint scenarios, and it obtains findings that are consistent with those achieved in the first objective. It demonstrates that the proposed SSO framework exhibits substantial efficiency and reliability in solving multi-objective coastal pumping optimisation problems within the 3D aquifer.

5.3 Significance of research findings

The significance of research findings in this PhD research mainly has three aspects:

(1) Help researchers understand the influence of pumping patterns on the SWI extent and operation cost of pumping groundwater, and to know the impact of different constraint indicators on cost-optimal pumping strategies.

(2) The novel offline and online training algorithms that have been confirmed efficient and reliable in this study can make up the research gap with respect to efficiently employing offline and online-trained surrogate models in multi-objective coastal groundwater management.

(3) The proposed efficient SSO framework, which has been validated as reliable and trustable to solve multi-objective management problems within a 3D aquifer, can be promoted to address many computationally intractable issues in coastal groundwater management. For example, it can be utilized for performing sensitivity and uncertainty analyses on optimal pumping solutions concerning the constraint conditions involved in the management problem or the parameters related to the aquifer (e.g., recharge intensity).

5.4 Limitations and recommendations for future research

Limitations of this PhD research include two main aspects,

(1) All the SWI models created in this thesis are assumed homogeneous and isotropic, not aligning with the realistic case.

(2) Coastal groundwater management problems involved in this thesis include few DVs, three or six, far away from the practical applications.

Based on the research limitations stated above and motivated by the performance of the proposed SSO framework in multi-objective groundwater management, the following recommendations and plans for future research can be made:

(1) Investigate the effects of pumping patterns on the SWI extent by considering the aquifer heterogeneity. This investigation involves numerous SWI simulations under the various conditions of hydrogeological parameters and thus huge computational costs. To mitigate this computational burden, machine learning proves to be an effective tool. Therefore, the findings about training surrogate models in this study can be employed to study the influence of aquifer heterogeneity on the SWI extent during pumping activities.

(2) Promote the application of the proposed efficient SSO method in Chapter 4 to high-dimensional coastal groundwater management problems, where the number of DVs is more than six. To be specific, the proposed SSO method is applied to solve the more complex pumping optimisation problems where the number of pumping wells, the well locations, the pump depth of each well, the pumping rate of each well and the pumping duration of each well are all unknown, or/and where precipitation changes and sea-level rise are considered and treated as DVs. In these cases, the number of pumping candidates would be significantly numerous, and there is a need to choose an optimisation algorithm to incorporate into the SSO

framework rather than simply depending on the surrogate estimates of objectives and constraints to efficiently identify optimal pumping schemes.

(3) Apply the proposed SSO framework to efficiently identify optimal pumping strategies for comprehensively addressing various coastal environmental concerns related to groundwater abstraction, such as SWI, land subsidence, and aquifer depletion. These hydrogeological issues can be treated as either management objectives or constraint conditions, and all of them are predicted by the surrogate models. Assisted by the proposed SSO method, it is possible to realize the sustainable utilization of coastal groundwater, striking a balance between economic costs, sustainability, and environmental impact.

(4) Continue to improve the offline and online training algorithms, recognised as the most efficient in this study, to achieve optimal solutions for multi-objective coastal groundwater management problems. For example, it can investigate the effects of initial training samples (e.g., their size and distribution across the input space), and the choice of kernel functions in the GP modelling technique on the optimal solutions generated by the SSO method. According to the findings, combining the identified offline, and online training algorithms with a suitable initial training sample design and kernel function in the GP modelling technique efficiently produces more reliable and accurate optimal pumping solutions.

(5) Investigate the effects of the behaviour of the objective and constraint functions on the choice of efficient offline and online training algorithms. The objective and constraint functions across the input space can take on linear, convex, concave or other highly non-linear forms. Developing insight into that is helpful for researchers to adopt appropriate training algorithms, achieving trustworthy results given by the SSO method.

(6) Assess and compare the performance of offline and online-trained surrogate models in addressing pumping optimisation problems with various-scale pumping candidates and develop a general guide for selecting the surrogate models when the number of pumping candidates is known.